



Universiteit  
Leiden  
The Netherlands

## **Intricacies of alpha-synuclein aggregation**

Mucibabic, M.

### **Citation**

Mucibabic, M. (2016, December 14). *Intricacies of alpha-synuclein aggregation*. *Casimir PhD Series*. Retrieved from <https://hdl.handle.net/1887/44785>

Version: Not Applicable (or Unknown)

License: [Licence agreement concerning inclusion of doctoral thesis in the Institutional Repository of the University of Leiden](#)

Downloaded from: <https://hdl.handle.net/1887/44785>

**Note:** To cite this publication please use the final published version (if applicable).

Cover Page



Universiteit Leiden



The handle <http://hdl.handle.net/1887/44785> holds various files of this Leiden University dissertation.

**Author:** Mucibabic, M.

**Title:** Intricacies of alpha-synuclein aggregation

**Issue Date:** 2016-12-14

# INTRICACIES OF ALPHA-SYNUCLEIN AGGREGATION

Proefschrift

ter verkrijging van  
de graad van Doctor aan de Universiteit Leiden,  
op gezag van Rector Magnificus prof.mr. C.J.J.M. Stolker,  
volgens besluit van het College voor Promoties  
te verdedigen op woensdag 14 december 2016  
klokke 12.30 uur

door

**Marija Mučibabić**

geboren te Kruševac, Servië  
in 1983

Promotoren: Prof. Dr. T. J. Aartsma (Universiteit Leiden)  
Prof. Dr. G. W. Canters (Universiteit Leiden)

Promotiecommissie: Prof. Dr. E. R. Eliel (Universiteit Leiden)  
Prof. Dr. T. Schmidt (Universiteit Leiden)  
Prof. Dr. V. Subramaniam (Vrije Universiteit)  
Prof. Dr. M. M. A. E. Claessens (Universiteit Twente)  
Dr. M. Huber (Universiteit Leiden)  
Dr. S. Semrau (Universiteit Leiden)

Casimir PhD Series, Delft-Leiden 2016-34

ISBN: 978-90-8593-280-2

This work was performed in the research program entitled “A Single Molecule View on Protein Aggregation”, supported by the Foundation for Fundamental Research on Matter (FOM, project number 10SMPA06), which is part of the Netherlands Organization for Scientific Research (NWO).



*" The important thing is not to stop questioning. Curiosity has its own reason for existing."*

*Albert Einstein*

*To my mother Dragana and my father Spasoje*



## Contents

<b>1</b>	<b>Introduction</b>	<b>1</b>
1.1	Neuropathology of Parkinson's disease	1
1.2	Proteins and protein folding	2
1.3	Protein misfolding and disease	2
1.4	Parkinson's disease and $\alpha$ -synuclein	3
1.5	The mechanism and molecular basis of $\alpha$ -synuclein aggregation	4
1.6	The methods to determine kinetics of $\alpha$ -synuclein aggregation	6
1.7	The factors influencing $\alpha$ -synuclein aggregation	7
1.8	Thesis outline	8
1.9	References	10
<b>2</b>	<b>The effect of fluorescent labeling on <math>\alpha</math>-synuclein fibril morphology</b>	<b>15</b>
2.1	Introduction	16
2.2	Materials and Methods	18
2.3	Results	21
2.4	Discussion	27
2.5	Conclusion	32
2.6	References	34
2.7	Supporting Information	37
<b>3</b>	<b>Early events in <math>\alpha</math>-synuclein aggregation</b>	<b>41</b>
3.1	Introduction	42
3.2	Materials and Methods	43
3.3	Results	47
3.4	Discussion	56
3.5	Conclusion	60
3.6	References	61
3.7	Supporting Information	64
<b>4</b>	<b>Influence of solution conditions on <math>\alpha</math>-synuclein aggregation kinetics</b>	<b>65</b>
4.1	Introduction	66
4.2	Materials and Methods	67
4.3	Results	70
4.4	Discussion	71
4.5	Conclusion	74
4.6	References	75
<b>5</b>	<b>Intermittent growth of <math>\alpha</math>-synuclein fibrils</b>	<b>79</b>
5.1	Introduction	80
5.2	Materials and Methods	81

5.3	Results and Discussion	85
5.4	Conclusion	93
5.5	References	95
5.6	Supporting Information	96
<b>6</b>	<b>Substrate surface affects <math>\alpha</math>-synuclein aggregate morphology</b>	<b>97</b>
6.1	Introduction	98
6.2	Materials and Methods	99
6.3	Results	103
6.4	Discussion	110
6.5	Conclusion	113
6.6	References	114
<b>7</b>	<b>Summary and Prospects</b>	<b>119</b>
	<b>Samenvatting</b>	<b>125</b>
	<b>Zaključak</b>	<b>131</b>
	<b>Curriculum Vitae</b>	<b>137</b>
	<b>List of publications</b>	<b>139</b>
	<b>Acknowledgements</b>	<b>141</b>

## Introduction<sup>1</sup>

### 1.1. Neuropathology of Parkinson's disease

Almost two centuries ago James Parkinson first described the manifestation of shaking palsy and the disease was named after him as Parkinson's disease (PD). Presently, PD takes second place on the list of the most common neurodegenerative disorders of the human brain [1] affecting approximately 6.3 million people around the world. Symptoms like tremor, rigidity, bradykinesia, speaking difficulties and postural instability are characteristic for PD that ultimately may lead to total disability followed by death. The disease develops not only in the central, but also in the peripheral (PNS) and the enteric nervous system [2]. When the disease is diagnosed, approximately 70% of the striatum dopamine has already been depleted and it advances in time [3]. In advanced PD most of the dopaminergic neurons are lost, suggesting significant cell death during the process [4]. Moreover, choline neurons present in the dorsal vagal nucleus degenerate too [5].

It took a full century from the time of Parkinson's discovery until Fritz Heinrich Lewy identified the abnormal inclusions in nerve cell bodies to be a hallmark of the disease. They were named Lewy bodies (LBs) after him. LBs and Lewy neurites (LNs) are not unique to PD, they are also found, for example, in the PNS of patients with pure autonomic failure [6]. Electron microscopy helped in finding out that LBs and LNs are largely composed of 200-600 nm long  $\alpha$ -synuclein ( $\alpha$ -syn) filaments [7].  $\alpha$ -Syn is a protein that is mostly present in the human brain, but also found in the heart and muscles. This thesis focuses on the properties of  $\alpha$ -syn and on its propensity to form aggregates. We will briefly describe the properties of proteins in general and of  $\alpha$ -syn in particular.

---

<sup>1</sup> This chapter is partially based on M. Mućibabić, G. Canters, T. Aartsma, Parkinson's disease – the hardship at old age, *Vojnosanit Pregl* 2016; 73(4): 303–305.

## 1.2. Proteins and protein folding

Protein molecules are made of building blocks - amino acids - connected into linear chains through covalent peptide bonds [8]. Although only 20 amino acids are considered to be involved in building proteins, there are nearly 100,000 different proteins in the human body [9]. The majority of the proteins have to be folded properly into a unique 3-dimensional (3D) structure in order to function correctly [10]. Synthesized proteins usually adopt their unique structure through the folding process on ribosomes. It is well-known, however, that folding also takes place in the cytoplasm after their release from ribosomes, mitochondria or the endoplasmic reticulum [11]. The folding process itself is strongly influenced by the specific environmental conditions under which it takes place. It is also widely known that the basic principles of folding are common. Sometimes the folding process goes wrong and it needs to be supported by molecular chaperones and folding catalysts in order to prevent such behavior [11,12]. If the assistance of molecular chaperones and folding catalysts also fails, the cell then tends to degrade the misfolded protein, *e.g.*, *via* the ubiquitin-proteasome system [13].

## 1.3. Protein misfolding and disease

A large number of proteins, however, do not adopt a well-defined 3D structure, although they are functional and biologically active [14,15]. They are called intrinsically disordered or natively unfolded proteins (IDPs). Some IDPs are associated with neurodegenerative diseases, clinging together to form aggregates [9,16]. Others are very quick in reacting to changes in their surroundings and tend to involve themselves in numerous signaling, regulation and recognition processes, often modulating and controlling their binding partners [17]. IDPs biological activities are controlled *via* posttranslational modifications [15] and alternative splicing [18,19]. While IDPs can operate as hubs (one-to-many signaling), they also can bind to hubs [20–23] (many-to-one signaling). When interacting with different binding partners, IDPs can fold in a different fashion [24,25].

Protein misfolding and aggregation play a key role in numerous human diseases such are Parkinson's, Alzheimer's, Huntington's disease, type II (late-onset) diabetes, Amyotrophic Lateral Sclerosis and prion disease [26] (Table 1.1). These diseases all correlate with the formation of inter- and intracellular inclusions consisting of insoluble amyloid fibrillar aggregates. The structure of amyloids is very similar, although they may be composed of proteins with very different original function. Amyloids are fibrillar aggregates with a length

of up to a few microns, which exhibit a characteristic cross- $\beta$  structure which plays a key role in the interaction and binding of adjacent, individual proteins within the fibrils [27].

**Table 1.1: Intrinsically disordered proteins associated with human diseases.**

Protein/peptide	Disease(s)	Polypeptide length (number of amino acid residues)	Protein/peptide structure
$\alpha$ -synuclein	Parkinson's disease Synucleopathies Dementia with Lewy body  Multiple system atrophy  Lewy body variant of Alzheimer's disease	140	Intrinsically disordered
Amyloid- $\beta$ peptide	Alzheimer's disease	37-43	Intrinsically disordered
Huntingtin fragments	Huntington's disease	Variable	Mostly intrinsically disordered
Amylin	Type II diabetes	37	Intrinsically disordered
TDP43	Amyotrophic lateral sclerosis	414	Intrinsically disordered
Prion protein	Prion disease  Creutzfeld-Jacob disease  Bovine spongiform encephalopathy	231	Intrinsically disordered and $\alpha$ -helical

#### 1.4. Parkinson's disease and $\alpha$ -synuclein

In 1997 two breakthrough discoveries shed light onto the molecular basis of PD. The first one connected the rare, familiar form of PD to a missense mutation in the gene that codes for a small, relatively unknown protein,  $\alpha$ -syn, consisting of 140 amino acid residues [28] (SNCA).

The second one brought to light that LBs and neurites of PD patients were immunoreactive for  $\alpha$ -syn [7]. After the first identified missense mutation (Ala53Thr) appeared to be associated with dominantly inherited PD with Lewy pathology, two other missense mutations, Glu46Lys [29] and Ala30Pro [30], were found to cause PD or dementia with LBs. The abovementioned mutations are positioned in the  $\alpha$ -syn region made of seven 11-amino-acid repeats with a common KTKEGV sequence [31]. Residues 1-60 (Figure 1.1) make up the positively charged amino-terminal domain of  $\alpha$ -syn, which contains 5 repeats of this sequence [31]. The central domain of  $\alpha$ -syn, *i.e.*, residues 61-95, is described as the “non-amyloid-beta-component” (NAC) of Alzheimer’s disease plaques [32], and is now identified as the hydrophobic part that is responsible for  $\alpha$ -syn aggregation involving  $\beta$ -sheet formation [33,34]. The carboxyl-terminus of  $\alpha$ -syn is rich in acidic residues, especially glutamic acid [31]. It has been suggested that particularly the negatively charged amino acids 104, 105, 114, 115 at the carboxylic-terminus reduce the  $\alpha$ -syn aggregation propensity [35].

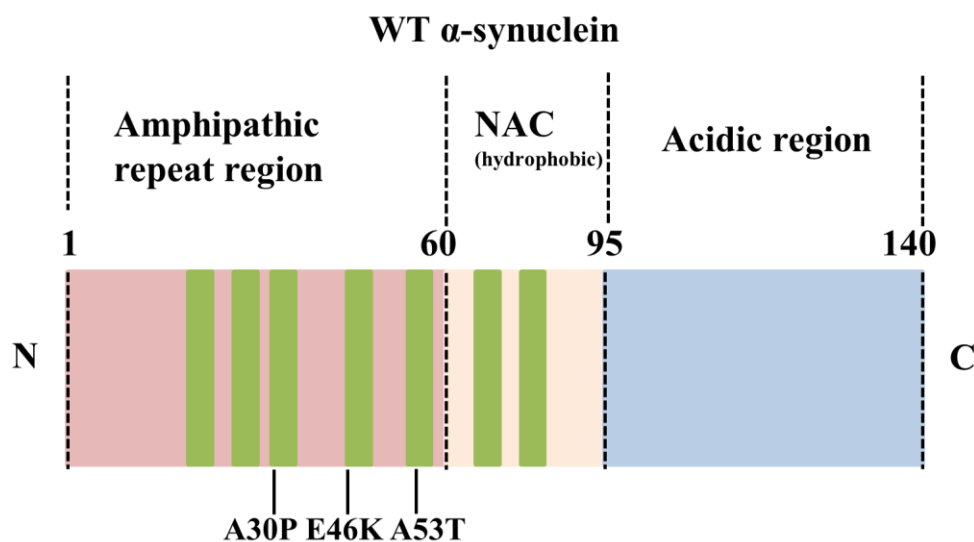


**Figure 1.1:** Primary structure of WT  $\alpha$ -syn. The main domains: N (amphipathic), C-terminus (acidic) and NAC (hydrophobic) regions are indicated. The green marked regions are KTKEGV repeats.

### 1.5. The mechanism and molecular basis of $\alpha$ -synuclein aggregation

The aggregation of  $\alpha$ -syn is thought to be a key aspect of the pathology of Parkinson's disease. The protein aggregation process is represented in a simplified way in Figure 1.2. Oligomers are intermediate species between the monomeric and the fibrillar form of the protein, and believed to be toxic, possibly by destructing the cell membranes [36–38]. The



oligomer formation is a rather obscure state of  $\alpha$ -syn aggregation. It is still challenging to follow the dynamics of oligomer formation experimentally, due to their transient nature and their low concentration in the sample solution. It also remains unclear how the oligomers transform into fibrils and whether all oligomers have the same ability to do so. The oligomers that are involved in fibril formation are referred to as the on-pathway species (Figure 1.2).

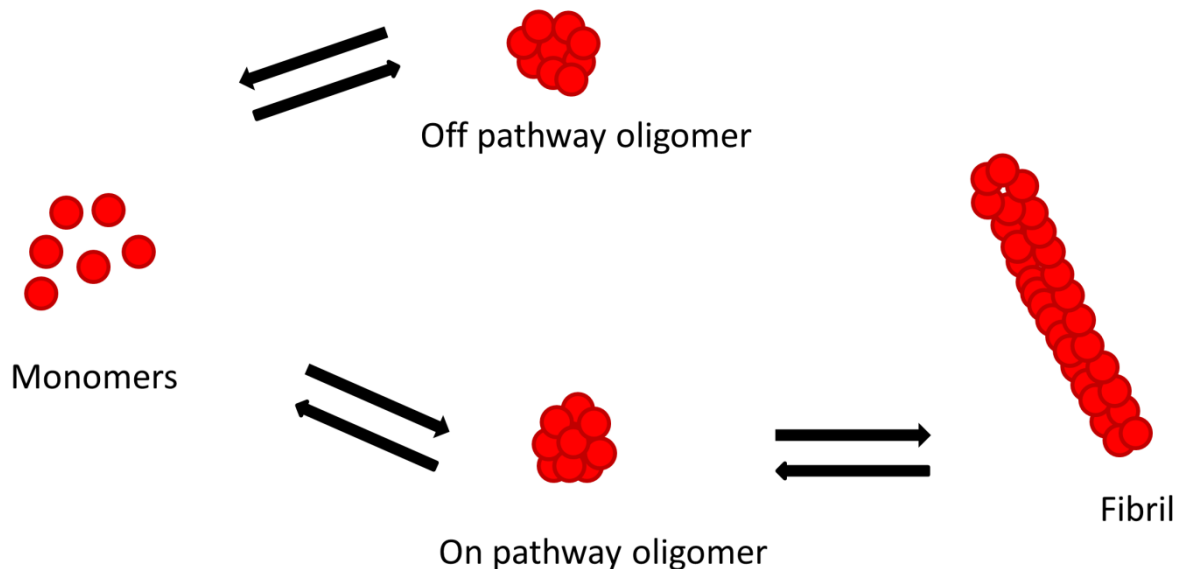


**Figure 1.2: Simplified representation of the protein aggregation.**

We can identify three stages in the process of  $\alpha$ -syn aggregation, starting from a solution of  $\alpha$ -syn monomers. The first stage is the nucleation phase with the (relatively slow) formation of small oligomers that eventually become precursors for fibril formation. Once these precursors are formed the aggregation process is dominated by fibril elongation and secondary nucleation. The latter mechanism involves, for example, fibril breaking, which is also the reason why the rate of fibrillar growth of  $\alpha$ -syn in solution is enhanced by shaking the sample. Ultimately, equilibrium is achieved between monomer binding to and dissociation from the fibril ends.

Kinetic studies on fibril growth found a first-order dependence on monomer and fibril concentration [39]. Early  $\alpha$ -syn aggregates formed through nucleation processes seem to elongate by addition of monomer to the existing fibrils ends [40,41]. There has been much speculation, and recently increasing evidence, that growth may also occur through oligomer addition [42], although it has been shown that the concentration of oligomers does not depend linearly on monomer concentration.

In bulk studies of  $\alpha$ -syn elongation, a fluorescent assay based on Thioflavin T (ThT) is often used to detect the presence of aggregates. Recently, single fibril growth measurements of fluorescently labeled  $\alpha$ -syn, using total internal reflection (TIRF) microscopy [43] and two-color direct stochastic optical reconstruction microscopy [41,44] (dSTORM), have provided deeper insight into  $\alpha$ -syn elongation kinetics.

## 1.6. Methods to determine kinetics of $\alpha$ -synuclein aggregation

### 1.6.1. Thioflavin T fluorescent assay

A widely used method to establish and detect the formation of amyloid aggregates, including  $\alpha$ -syn, uses the fluorogenic dye ThT. In general, when ThT binds to  $\beta$ -sheet secondary structures such as those in amyloid aggregates, its fluorescence intensity is enhanced and the emission spectrum is red shifted.  $\alpha$ -Syn aggregation can be monitored by measuring the increase of ThT fluorescence intensity as a function of time. A typical aggregation curve shows a sigmoidal increase of ThT fluorescence intensity described by the initial, so-called lag phase, followed by the exponential-like growth phase and the plateau or saturation phase. A typical example of such an aggregation curve is shown in Figure 1.3. The lag phase is associated with the primary nucleation, and its duration varies strongly from sample to sample because of the highly stochastic character of the nucleation and initial elongation processes which occur more or less simultaneously [45]. The elongation rate is often determined as the maximal slope of the sigmoidal curve [45].

### 1.6.2. TIRF microscopy

Although a huge leap in elucidating the  $\alpha$ -syn aggregation kinetics was made by bulk kinetic experiments, the information at the single-fibril level was missing until recently. To better understand  $\alpha$ -syn aggregation at the molecular level, high resolution imaging methods proved to be essential. Ban et al. showed the use of ThT staining and TIRF in monitoring elongation of amyloid proteins such as amyloid beta [46], glucagon [47], amylin [48,49] and  $\beta_2$ -microglobulin [50]. Wördenhoff et al. [43] applied TIRF microscopy using ThT fluorescence to follow  $\alpha$ -syn growth and reported its elongation rate to be  $8.6 \times 10^3 \text{ M}^{-1}\text{s}^{-1}$ . The experimentally determined elongation rate of  $\alpha$ -syn is lower than that of other amyloid proteins. The lower elongation rate of  $\alpha$ -syn might be related to its size, as it is longer compared to other amyloid proteins and its incorporation into the fibril core may take more time [51].

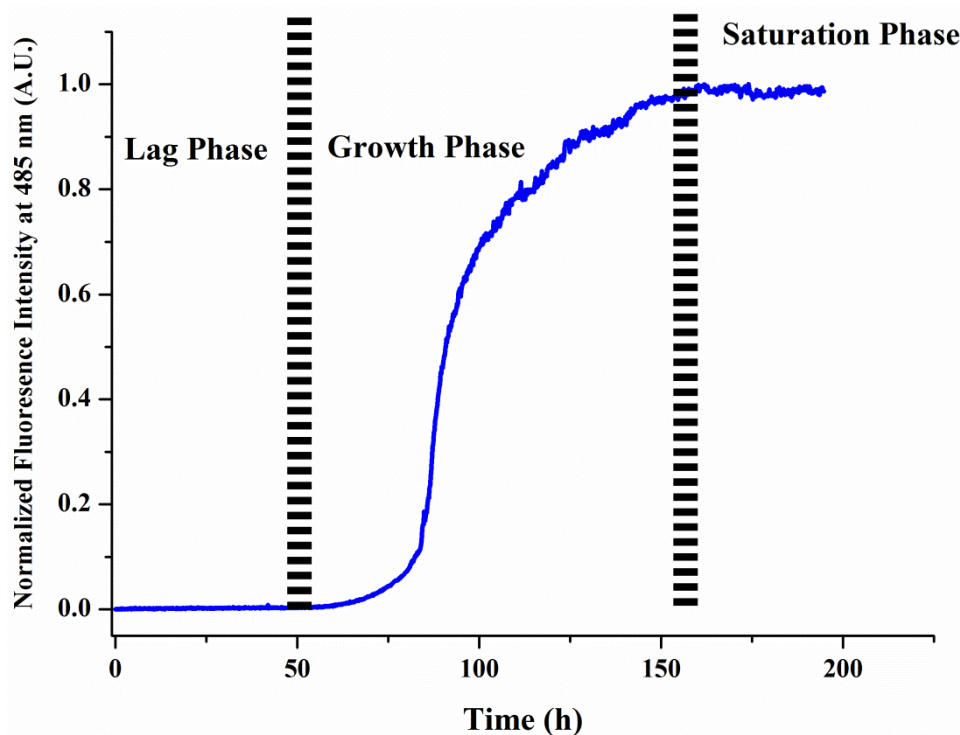


Figure 1.3: A typical aggregation curve monitored using ThT fluorescence intensity, showing lag, growth and saturation phases. The aggregation of 100  $\mu\text{M}$  WT  $\alpha$ -syn was performed in 6 mM sodium phosphate buffer at pH 7.4 with 0.1 mM EDTA, 1,000 rpm, and 37°C. Fluorescence spectra of ThT in solution were subtracted from each  $\alpha$ -syn sample measurement.

### 1.7. The factors influencing $\alpha$ -synuclein aggregation

A large number of studies have reported extrinsic factors that markedly influence  $\alpha$ -syn aggregation kinetics. Membranes [52], salts, pH, metal ions, temperature and shaking are just a few of them. Although intrinsic properties of the protein determine to a large extent the reaction rate, for example the net charge of  $\alpha$ -syn, tuning the solution conditions, like pH or ionic strength [53], will modulate the effective charges of the protein and influence the screening of self-repulsion. Hoyer et al. [54] provided details on the differences in morphology of  $\alpha$ -syn aggregates formed under different pH and NaCl concentrations by atomic force microscopy (AFM). Later on, the detailed study by Buell et al. [53] addressed similar solution conditions using bulk kinetic measurements and provided accurate rate constants for the process. An important question relates to the effect that membranes have on the  $\alpha$ -syn aggregation process. Numerous recent studies have suggested their impact on the primary nucleation process [52] as well as the morphology of  $\alpha$ -syn aggregates [55].

## 1.8. Thesis outline

In this thesis we describe the results of our study on  $\alpha$ -syn aggregation *in vitro* with the help of several experimental approaches. As optical techniques were our main tool, the first step was the fluorescent labeling of  $\alpha$ -syn.

**Chapter 2** is dedicated to the influence that fluorescent dyes have on the morphology of  $\alpha$ -syn fibrils. AFM images of wild type (WT) and the A140C  $\alpha$ -syn mutant mature fibrils show a twisted, ribbon-like appearance with a pitch at 127 nm and an average height of 9.4 nm. The effect of fluorescent labels on the  $\alpha$ -syn fibril morphology is remarkable, especially with increasing fractions of the labeled  $\alpha$ -syn, affecting mostly the length of fibrils and their general architecture. The reason for significantly reduced fibril length with increasing fractions of labeled  $\alpha$ -syn is most probably due to a change of the affinity of monomers to the fibril ends, while the short-range interactions between dyes attached to the C-terminus of the protein presumably plays an important role in the disappearance of the twisted morphology of the  $\alpha$ -syn fibrils.

**Chapter 3** focuses on the isolation of early aggregates in  $\alpha$ -syn aggregation. We succeeded in detecting dimers and tetramers using fluorescence-based imaging of gels and confirmed the presence of small species with additional methods. The results of diffusion time measurements by fluorescence correlation spectroscopy in the electrophoresed gels confirm the difference in molecular weight between isolated species. The intensities of the bands in electrophoresed gels allow the assessment of the time profile of species accumulation and disappearance during the aggregation process.

**Chapter 4** describes a systematic study on the relationship between  $\alpha$ -syn aggregation kinetics, ionic strength and pH. We use bulk kinetic measurements in a plate reader to elucidate this important phenomenon. Since the initial elongation rate decreases significantly with increasing ionic strength (more than 30 mM NaCl), we assign an important role to electrostatic interactions in the  $\alpha$ -syn aggregation process.

Real-time TIRF imaging was performed to monitor fibril elongation in order to determine the rate of monomer binding to fibril ends, and, subsequently, to establish the average fibril length in time. Surprisingly, our findings reported in **Chapter 5** show that it is not possible to describe the evolution of fibril growth according to the existing 3-step amyloid formation model. In fact, our results suggest that, in time, many  $\alpha$ -syn fibrils tend to lose their ability for

binding additional monomers. For this reason, we introduced quenching rate constant ( $k_q$ ) in the kinetic model to analyze our results.

**Chapter 6** addresses the impact of the substrate surface on the morphology of  $\alpha$ -syn aggregates. When studying the aggregation process in real-time by TIRF, significant differences appeared between the species formed on a charged surface and on a zwitterionic supported lipid bilayer. The morphology of aggregates formed on the charged surface displayed the greater heterogeneity compared to the ones formed on neutral surface, suggesting a significant effect of substrate surface properties on the morphology of  $\alpha$ -syn aggregates.

In the closing **Chapter 7** we summarize the work done in this thesis with highlighting the most important findings, and present prospects for future work.

## 1.9. References

- [1] L.M.L. de Lau, M.M.B. Breteler, Epidemiology of Parkinson's disease., *Lancet Neurol.* 5 (2006) 525–35. doi:10.1016/S1474-4422(06)70471-9.
- [2] H. Braak, K. Del Tredici, Invited Article: Nervous system pathology in sporadic Parkinson disease, *Neurology.* 70 (2008) 1916–1925. doi:10.1212/01.wnl.0000312279.49272.9f.
- [3] D.J. Brooks, The Early Diagnosis of Parkinson's Disease, (1998) 10–18.
- [4] M.R. Cookson,  $\alpha$ -Synuclein and neuronal cell death, *Mol. Neurodegener.* 4 (2009) 9. doi:10.1186/1750-1326-4-9.
- [5] W.P. Gai, P.C. Blumbergs, L.B. Geffen, W.W. Blessing, Age-related loss of dorsal vagal neurons in Parkinson's disease., *Neurology.* 42 (1992) 2106–2111. doi:10.1212/WNL.42.11.2106.
- [6] M. Goedert, Alpha-synuclein and neurodegenerative diseases., *Nat. Rev. Neurosci.* 2 (2001) 492–501. doi:10.1038/35081564.
- [7] M.G. Spillantini, R.A. Crowther, R. Jakes, M. Hasegawa, M. Goedert,  $\alpha$ -Synuclein in filamentous inclusions of Lewy bodies from Parkinson's disease and dementia with Lewy bodies, *Proc. Natl. Acad. Sci.* 95 (1998) 6469–6473. doi:10.1073/pnas.95.11.6469.
- [8] C.M. Dobson, Principles of protein folding, misfolding and aggregation, *Semin. Cell Dev. Biol.* 15 (2004) 3–16. doi:10.1016/j.semcdb.2003.12.008.
- [9] C.M. Dobson, Protein misfolding, evolution and disease, *Trends Biochem. Sci.* 24 (1999) 329–332. doi:10.1016/S0968-0004(99)01445-0.
- [10] F.U. Hartl, A. Bracher, M. Hayer-Hartl, Molecular chaperones in protein folding and proteostasis., *Nature.* 475 (2011) 324–332. doi:10.1038/nature10317.
- [11] B. Bukau, A.L. Horwich, The Hsp70 and Hsp60 Chaperone Machines, *Cell.* 92 (1998) 351–366. doi:10.1016/S0092-8674(00)80928-9.
- [12] J.C. Young, V.R. Agashe, K. Siegers, F.U. Hartl, Pathways of chaperone-mediated protein folding in the cytosol, *Nat. Rev. Mol. Cell Biol.* 5 (2004) 781–791. doi:10.1038/nrm1492.
- [13] A. Ciechanover, P. Brundin, The ubiquitin proteasome system in neurodegenerative diseases: Sometimes the chicken, sometimes the egg, *Neuron.* 40 (2003) 427–446. doi:10.1016/S0896-6273(03)00606-8.
- [14] M.M. Babu, R. van der Lee, N.S. de Groot, J. Gsponer, Intrinsically disordered proteins: regulation and disease, *Curr. Opin. Struct. Biol.* 21 (2011) 432–440. doi:10.1016/j.sbi.2011.03.011.
- [15] V.N. Uversky, Intrinsically disordered proteins and their (disordered) proteomes in neurodegenerative disorders, *Front. Aging Neurosci.* 7 (2015) 1–6. doi:10.3389/fnagi.2015.00018.
- [16] D. Eisenberg, M. Jucker, The Amyloid State of Proteins in Human Diseases, *Cell.* 148 (2012) 1188–1203. doi:10.1016/j.cell.2012.02.022.
- [17] V.N. Uversky, A.K. Dunker, Understanding protein non-folding, *Biochim. Biophys. Acta - Proteins Proteomics.* 1804 (2010) 1231–1264. doi:10.1016/j.bbapap.2010.01.017.

- [18] M. Buljan, G. Chalancon, A.K. Dunker, A. Bateman, S. Balaji, M. Fuxreiter, M.M. Babu, Alternative splicing of intrinsically disordered regions and rewiring of protein interactions, *Curr. Opin. Struct. Biol.* 23 (2013) 443–450. doi:10.1016/j.sbi.2013.03.006.
- [19] V.N. Uversky, Wrecked regulation of intrinsically disordered proteins in diseases: pathogenicity of deregulated regulators, *Front. Mol. Biosci.* 1 (2014) 1–24. doi:10.3389/fmolb.2014.00006.
- [20] A.K. Dunker, M.S. Cortese, P. Romero, L.M. Iakoucheva, V.N. Uversky, Flexible nets. The roles of intrinsic disorder in protein interaction networks, *FEBS J.* 272 (2005) 5129–5148. doi:10.1111/j.1742-4658.2005.04948.x.
- [21] V.N. Uversky, C.J. Oldfield, A.K. Dunker, Showing your ID: Intrinsic disorder as an ID for recognition, regulation and cell signaling, *J. Mol. Recognit.* 18 (2005) 343–384. doi:10.1002/jmr.747.
- [22] C.J. Oldfield, J. Meng, J.Y. Yang, M.Q. Yang, V.N. Uversky, A.K. Dunker, Flexible nets: disorder and induced fit in the associations of p53 and 14-3-3 with their partners, *BMC Genomics.* 9 (2008) S1. doi:10.1186/1471-2164-9-S1-S1.
- [23] V.N. Uversky, C.J. Oldfield, A.K. Dunker, Intrinsically Disordered Proteins in Human Diseases: Introducing the D<sup>2</sup> Concept, *Annu. Rev. Biophys.* 37 (2008) 215–246. doi:10.1146/annurev.biophys.37.032807.125924.
- [24] W.L. Hsu, C.J. Oldfield, B. Xue, J. Meng, F. Huang, P. Romero, V.N. Uversky, A.K. Dunker, Exploring the binding diversity of intrinsically disordered proteins involved in one-to-many binding, *Protein Sci.* 22 (2013) 258–273. doi:10.1002/pro.2207.
- [25] H.J. Dyson, P.E. Wright, Intrinsically unstructured proteins and their functions., *Nat. Rev. Mol. Cell Biol.* 6 (2005) 197–208. doi:10.1038/nrm1589.
- [26] F. Chiti, C.M. Dobson, Protein misfolding, functional amyloid, and human disease., *Annu. Rev. Biochem.* 75 (2006) 333–366. doi:10.1146/annurev.biochem.75.101304.123901.
- [27] R. Nelson, M.R. Sawaya, M. Balbirnie, A.Ø. Madsen, C. Riek, R. Grothe, D. Eisenberg, Structure of the cross-beta spine of amyloid-like fibrils., *Nature.* 435 (2005) 773–778. doi:10.1038/nature03680.
- [28] M.H. Polymeropoulos, C. Lavedan, E. Leroy, S.E. Ide, A. Dehejia, A. Dutra, B. Pike, H. Root, J. Rubenstein, R. Boyer, E.S. Stenroos, S. Chandrasekharappa, A. Athanassiadou, T. Papapetropoulos, W.G. Johnson, A.M. Lazzarini, R.C. Duvoisin, G. Di Iorio, L.I. Golbe, R.L. Nussbaum, Mutation in the  $\alpha$ -Synuclein Gene Identified in Families with Parkinson's Disease, *Science* (80-. ). 276 (1997) 2045–2047. doi:10.1126/science.276.5321.2045.
- [29] J.J. Zarranz, J. Alegre, J.C. Gómez-Esteban, E. Lezcano, R. Ros, I. Ampuero, L. Vidal, J. Hoenicka, O. Rodriguez, B. Atarés, V. Llorens, E. Gomez Tortosa, T. Del Ser, D.G. Muñoz, J.G. De Yebenes, The New Mutation, E46K, of  $\alpha$ -Synuclein Causes Parkinson and Lewy Body Dementia, *Ann. Neurol.* 55 (2004) 164–173. doi:10.1002/ana.10795.
- [30] R. Krüger, W. Kuhn, T. Müller, D. Voitalla, M. Graeber, S. Kösel, H. Przuntek, J.T. Epplen, L. Schöls, O. Riess, Ala30Pro mutation in the gene encoding alpha-synuclein in Parkinson's disease., *Nat. Genet.* 18 (1998) 106–108. doi:10.1038/ng0298-106.
- [31] J.M. George, H. Jin, W.S. Woods, D.F. Clayton, Characterization of a novel protein regulated during the critical period for song learning in the zebra finch, *Neuron.* 15

- (1995) 361–372. doi:10.1016/0896-6273(95)90040-3.
- [32] A. Takeda, M. Mallory, M. Sundsmo, W. Honer, L. Hansen, E. Masliah, Abnormal accumulation of NACP/alpha-synuclein in neurodegenerative disorders., *Am. J. Pathol.* 152 (1998) 367–72.
- [33] A.M.A. Bodles, D.D.J.S. Guthrie, B. Greer, G. Brent Irvine, Identification of the region of non-Abeta component (NAC) of Alzheimer’s disease amyloid responsible for its aggregation and toxicity., *J. Neurochem.* 78 (2001) 384–395. doi:10.1046/j.1471-4159.2001.00408.x.
- [34] B.I. Giasson, I.V.J. Murray, J.Q. Trojanowski, V.M.Y. Lee, A Hydrophobic Stretch of 12 Amino Acid Residues in the Middle of  $\alpha$ -Synuclein Is Essential for Filament Assembly, *J. Biol. Chem.* 276 (2001) 2380–2386. doi:10.1074/jbc.M008919200.
- [35] I.V.J. Murray, B.I. Giasson, S.M. Quinn, V. Koppaka, P.H. Axelsen, H. Ischiropoulos, J.Q. Trojanowski, V.M.-Y. Lee, Role of alpha-synuclein carboxy-terminus on fibril formation in vitro., *Biochemistry.* 42 (2003) 8530–8540. doi:10.1021/bi027363r.
- [36] M.J. Volles, P.T. Lansbury, Zeroing in on the pathogenic form of  $\alpha$ -synuclein and its mechanism of neurotoxicity in Parkinson’s disease, *Biochemistry.* 42 (2003) 7871–7878. doi:10.1021/bi030086j.
- [37] D. Snead, D. Eliezer, Alpha-synuclein function and dysfunction on cellular membranes., *Exp. Neurobiol.* 23 (2014) 292–313. doi:10.5607/en.2014.23.4.292.
- [38] C. Haass, D.J. Selkoe, Soluble protein oligomers in neurodegeneration: lessons from the Alzheimer’s amyloid beta-peptide., *Nat. Rev. Mol. Cell Biol.* 8 (2007) 101–12. doi:10.1038/nrm2101.
- [39] S.R. Collins, A. Douglass, R.D. Vale, J.S. Weissman, Mechanism of prion propagation: Amyloid growth occurs by monomer addition, *PLoS Biol.* 2 (2004). doi:10.1371/journal.pbio.0020321.
- [40] V.V. Shvadchak, M.M.A.E. Claessens, V. Subramaniam, Fibril Breaking Accelerates  $\alpha$ -Synuclein Fibrillization, *J. Phys. Chem. B.* 119 (2015) 1912–1918. doi:10.1021/jp5111604.
- [41] D. Pinotsi, A.K. Buell, C. Galvagnion, C.M. Dobson, G.S. Kaminski Schierle, C.F. Kaminski, Direct observation of heterogeneous amyloid fibril growth kinetics via two-color super-resolution microscopy, *Nano Lett.* 14 (2014) 339–345. doi:10.1021/nl4041093.
- [42] A.T. Sabareesan, J.B. Udgaonkar, Amyloid fibril formation by the chain B subunit of monellin occurs by a nucleation-dependent polymerization mechanism., *Biochemistry.* 53 (2014) 1206–17. doi:10.1021/bi401467p.
- [43] M.M. Wördehoff, O. Bannach, H. Shaykhalishahi, A. Kulawik, S. Schiefer, D. Willbold, W. Hoyer, E. Birkmann, Single Fibril Growth Kinetics of  $\alpha$ -Synuclein, *J. Mol. Biol.* 427 (2015) 1428–1435. doi:10.1016/j.jmb.2015.01.020.
- [44] D. Pinotsi, C.H. Michel, A.K. Buell, R.F. Laine, P. Mahou, C.M. Dobson, C.F. Kaminski, G.S.K. Schierle, Nanoscopic insights into seeding mechanisms and toxicity of  $\alpha$ -synuclein species in neurons, *Proc Natl Acad Sci U S A.* 1 (2016) 1–5. doi:10.1073/pnas.1516546113.
- [45] T.P.J. Knowles, C.A. Waudby, G.L. Devlin, S.I.A. Cohen, A. Aguzzi, M. Vendruscolo, E.M. Terentjev, M.E. Welland, C.M. Dobson, An analytical solution to the kinetics of breakable filament assembly., *Science.* 326 (2009) 1533–1537.



- doi:10.1126/science.1178250.
- [46] T. Ban, M. Hoshino, S. Takahashi, D. Hamada, K. Hasegawa, H. Naiki, Y. Goto, Direct observation of A $\beta$  amyloid fibril growth and inhibition, *J. Mol. Biol.* 344 (2004) 757–767. doi:10.1016/j.jmb.2004.09.078.
- [47] C.B. Andersen, H. Yagi, M. Manno, V. Martorana, T. Ban, G. Christiansen, D.E. Otzen, Y. Goto, C. Rischel, Branching in Amyloid Fibril Growth, *Biophys. J.* 96 (2009) 1529–1536. doi:10.1016/j.bpj.2008.11.024.
- [48] C. Goldsbury, J. Kistler, U. Aebi, T. Arvinte, G.J. Cooper, Watching amyloid fibrils grow by time-lapse atomic force microscopy., *J. Mol. Biol.* 285 (1999) 33–39. doi:10.1006/jmbi.1998.2299.
- [49] S.M. Patil, A. Mehta, S. Jha, A.T. Alexandrescu, Heterogeneous Amylin Fibril Growth Mechanisms Imaged by Total Internal Reflection Fluorescence Microscopy, *Biochemistry.* 50 (2011) 2808–2819. doi:10.1021/bi101908m.
- [50] T. Ban, D. Hamada, K. Hasegawa, H. Naiki, Y. Goto, Direct observation of amyloid fibril growth monitored by thioflavin T fluorescence, *J. Biol. Chem.* 278 (2003) 16462–16465. doi:10.1074/jbc.C300049200.
- [51] M. Vilar, H.-T. Chou, T. Lührs, S.K. Maji, D. Riek-Loher, R. Verel, G. Manning, H. Stahlberg, R. Riek, The fold of alpha-synuclein fibrils., *Proc. Natl. Acad. Sci. U. S. A.* 105 (2008) 8637–8642. doi:10.1073/pnas.0712179105.
- [52] C. Galvagnion, A.K. Buell, G. Meisl, T.C.T. Michaels, M. Vendruscolo, T.P.J. Knowles, C.M. Dobson, Lipid vesicles trigger  $\alpha$ -synuclein aggregation by stimulating primary nucleation, *Nat. Chem. Biol.* 11 (2015) 229–234. doi:10.1038/nchembio.1750.
- [53] A.K. Buell, C. Galvagnion, R. Gaspar, E. Sparr, M. Vendruscolo, T.P.J. Knowles, S. Linse, C.M. Dobson, Solution conditions determine the relative importance of nucleation and growth processes in  $\alpha$ -synuclein aggregation., *Proc. Natl. Acad. Sci. U. S. A.* 111 (2014) 7671–7676. doi:10.1073/pnas.1315346111.
- [54] W. Hoyer, T. Antony, D. Cherny, G. Heim, T.M. Jovin, V. Subramaniam, Dependence of  $\alpha$ -synuclein aggregate morphology on solution conditions, *J. Mol. Biol.* 322 (2002) 383–393. doi:10.1016/S0022-2836(02)00775-1.
- [55] A. Iyer, N.O. Petersen, M.M.A.E. Claessens, V. Subramaniam, Amyloids of alpha-synuclein affect the structure and dynamics of supported lipid bilayers, *Biophys. J.* 106 (2014) 2585–2594. doi:10.1016/j.bpj.2014.05.001.



# The effect of fluorescent labeling on $\alpha$ -synuclein fibril morphology<sup>1</sup>

### Abstract

The misfolding and aggregation of a small, natively unfolded protein  $\alpha$ -synuclein ( $\alpha$ -syn) is presumably an important factor in the development of Parkinson's disease. However, the mechanism of  $\alpha$ -syn aggregation into amyloid fibrils and their morphology are not well understood. To elucidate the aggregation kinetics and the morphology of aggregates by the use of fluorescent techniques the protein needs to be suitably labeled. In this study, using atomic force microscopy, we demonstrate a significant effect of fluorescent labels on the end stage of the  $\alpha$ -syn fibrillization process. We studied in detail the morphology of  $\alpha$ -syn aggregates as a function of the composition of mixtures of labeled and wild type (WT)  $\alpha$ -syn in solution using different types of fluorescent dyes. Although the overall charge of the fluorophores we used and their chemical structure varied significantly, the morphology of  $\alpha$ -syn fibrils changed in a similar way in all cases. The increase in the fraction of labeled  $\alpha$ -syn in solution led to shortening of the fibrils as compared to those from WT-only  $\alpha$ -syn, whereas the height of the fibrils remained mainly unaffected. The twisted fibril morphology observed in the WT and A140C  $\alpha$ -syn mutant completely disappeared when the A140C  $\alpha$ -syn mutant was 100% fluorescently labeled.

---

<sup>1</sup>This chapter is based on: M. Mučibabić, M.M. Apetri, G.W. Canters, T.J. Aartsma, The effect of fluorescent labeling on  $\alpha$ -synuclein fibril morphology, *Biochim. Biophys. Acta Proteins Proteomics*. (2016). doi:10.1016/j.bbapap.2016.07.007.

## 2.1. Introduction

The mechanism of the conversion of soluble proteins into amyloid fibrils has been an important and active field of research. The high interest in the properties of amyloid fibrils comes from the fact that they are associated with approximately 50 different health disorders [1–3]. Among the diseases that are presumably affected by protein misfolding and aggregation are Alzheimer’s disease, Parkinson’s disease (PD), type II diabetes, and Huntington’s disease, to mention just a few. Research on the properties of amyloid fibrils spreads over a large spectrum of scientific disciplines, aimed at resolving their structural properties, the mechanisms and dynamics of their formation, and the functional and pathological role in their native environment. In addition to the great importance of amyloids in the context of the disease and the development of potential therapeutics [4], the properties of such protein filaments are also considered to be of interest for the development of nanostructured materials [5,6].

Efforts aimed at understanding the molecular details of amyloid fibrils are challenged by factors such as their size, low solubility, and variable morphology [7]. The typical diameter of these fibrils ranges from 6 to 10 nm and their length up to several micrometers [8]. They are composed of thousands of the constituent monomeric proteins [9]. Typical fibrils are known to have a bundled appearance in negatively stained transmission electron microscope (EM) images [10] composed of several so-called protofibrils. Amyloid fibrils share a common ordered cross  $\beta$ -sheet structure, with  $\beta$ -strands oriented perpendicular to the fibril axis [11,12].

The main role in PD development is thought to be played by a small, natively unfolded protein,  $\alpha$ -syn with a significant propensity for the formation of amyloid fibrils.  $\alpha$ -syn aggregation into amyloid fibrils is considered to be a nucleation-dependent polymerization process [13]. A common method to establish and detect the formation of amyloid aggregates uses the dye thioflavin T (ThT). In general, upon ThT binding to  $\beta$ -sheet secondary structures, such as those in amyloid aggregates, its fluorescence intensity is strongly enhanced and the emission spectrum is red shifted. The aggregation process of  $\alpha$ -syn can be monitored by measuring the increase of the ThT fluorescent intensity as a function of time. A typical aggregation curve shows a sigmoidal increase of ThT fluorescent intensity described by the initial, so-called lag phase, followed by an exponential growth phase and the equilibrium or plateau phase (see Supporting Information (SI) Figure S.2.1 at the end of this

chapter). The early lag phase of aggregation appears to be very complex [14]. The aggregation kinetics of  $\alpha$ -syn is a highly sensitive process dependent on the solution conditions [15] such as ionic strength, pH [16], temperature, metal ions, and protein concentration [17]. It is known that  $\alpha$ -syn aggregates much faster under shaking as compared to quiescent conditions [18].

Morphological heterogeneity among  $\alpha$ -syn aggregates has been shown by the use of AFM and EM in a number of studies.  $\alpha$ -syn fibrillization *in vitro* involves intermediate oligomeric species and only at a later stage protofilaments and mature fibrils [19] are formed. The majority of the observed oligomers have spherical shape [20–24], still annular forms [20,25,26] and chains of spheres [21] were also described in the literature. The height of observed spherical oligomers varies between 2 and 10 nm [20,21], whereas using different preparation protocols it can increase up to 30 nm [27].  $\alpha$ -syn fibrils display a smaller variation in their morphology [21] which is similar to that of other amyloid fibrils as amyloid  $\beta$  [28,29], ovalbumin [30], immunoglobulin light chain [29] and  $\beta$ -lactoglobulin [31].

In recent years, optical techniques [32–35] have been applied to study the aggregation of  $\alpha$ -syn. Fluorescent labeling is often achieved by replacing one of the residues of  $\alpha$ -syn with a cysteine. The reaction of a cysteine thiol with maleimide-functionalized dyes is commonly used for labeling of biomolecules, including proteins and peptides<sup>2</sup>. By fluorescence correlation spectroscopy and fluorescence resonance energy transfer, the gradual disappearance of  $\alpha$ -syn monomers and the formation of a transient population of early aggregates have been detected in solution during the aggregation process [32]. Using single-molecule photobleaching in combination with substoichiometric fluorescent labeling techniques, the molecular composition of *in vitro* prepared oligomers was precisely determined [33]. Recently, two independent studies have reported the bidirectional growth of the single  $\alpha$ -syn fibril by two-color direct stochastic optical reconstruction microscopy [34] and real-time total internal reflection fluorescence microscopy [35]. Most of these studies were performed using a small fraction (up to 30%) of fluorescently labeled protein.

Fluorescent labeling of biomolecules facilitates detailed detection of numerous features of their role and function *in vitro* and *in vivo* with high sensitivity. In principle, fluorescent labeling of  $\alpha$ -syn could be a very effective tool not only for the observation of the very onset of the aggregation *in vitro*, *e.g.*, by single-molecule techniques, but also to follow the role of

---

<sup>2</sup> The maleimide functional group is an electrophilic molecular structure that specifically binds to thiols.

aggregation process in live cells. It is crucial, however to preserve the functionality of  $\alpha$ -syn after attaching a fluorescent probe. A possible effect that the attachment of a dye molecule might have on the aggregation propensity and the species formed during the process still remains largely unknown. In general, fluorescent probes have to be used with caution [36]. Here we show that fluorescent labeling of  $\alpha$ -syn interferes with its aggregation.

In the present study, we probed various fluorescent dyes and varied the fraction of fluorescently labeled  $\alpha$ -syn in solution to determine to what extent fluorescent labeling interferes with the end stage of the fibrillization process, and the effect that it has on the morphology of the mature fibrils. We investigated in detail the effect of various, commonly used fluorescent dyes, covalently bound, on  $\alpha$ -syn aggregation. Using atomic force microscopy (AFM) we followed the distribution of  $\alpha$ -syn fibrils characteristics such as fibrillar height, length and twisting when the protein is labeled with different fluorophores. The impact of fluorescent labeling on  $\alpha$ -syn aggregation is important in order to assess the viability of applying labeling techniques in the investigation of amyloid aggregation mechanisms.

## 2.2. Materials and Methods

### 2.2.1. $\alpha$ -syn expression and purification

$\alpha$ -syn preparation and purification was done as described earlier [37,38]. Both WT and A140C  $\alpha$ -syn mutant were used within this study. Expression of protein was performed in *E.coli* B121 (DE3) transformed with the pT7-7 plasmid carrying the  $\alpha$ -syn gene. Culturing was done in lysogeny broth medium with 100  $\mu$ g/ml ampicillin. After isopropylthio- $\beta$ -galactoside induction (1 mM, 4 h) bacterial cell pellets were harvested by centrifugation (6,000  $\times$  g, 10 min) and resuspended in 10 mM Tris-HCl, pH 8.0, 1 mM ethylenediaminetetraacetic acid (EDTA) and 1 mM phenylmethylsulfonyl fluoride (10% of the culture volume) and stirred for 1 h at 4°C. Cells were lysed by sonication for 2 min and centrifuged (10,000  $\times$  g, 20 min, 4°C). DNA was precipitated by adding streptomycin sulfate (1%, 15 min, 4°C) and removed by centrifugation at 13,500  $\times$  g for 30 min. Then  $\alpha$ -syn was salted out from the solution by slow addition of 0.295 g/ml of ammonium sulfate and mild stirring for 1 h at 4°C. Precipitated protein was collected by centrifugation (13,500  $\times$  g, 30 min, 4°C). The pellet was gently resuspended in 10 mM Tris-HCl, pH 7.4 (5% of the culture volume) and filtered through a 0.22  $\mu$ m filter. The solution was purified on a 6 ml ResourceQ

column using the Akta Purifier system (GE Healthcare). The protein was eluted using a linear gradient of NaCl (0–500 mM) in 10 mM Tris–HCl, pH 7.4 at the flow rate of 3 ml/min. Collected fractions were checked for  $\alpha$ -syn using sodium dodecyl sulfate polyacrylamide gel electrophoresis (SDS-PAGE). Fractions containing  $\alpha$ -syn were pooled and concentrated (Vivaspin-20, 10 kD; GE Healthcare). The sample was desalted with a PD-10 column (GE Healthcare) using 10 mM Tris–HCl pH 7.4 and diluted with Tris–HCl, pH 7.4 to the concentration of 250  $\mu$ M. Aliquots of 0.5 ml were stored at  $-80^{\circ}\text{C}$ . The A140C  $\alpha$ -syn mutant construct was generated by site directed mutagenesis using a QuikChange II Site-Directed Mutagenesis Kit (Stratgene). A140C  $\alpha$ -syn was expressed and purified using the same protocol as WT  $\alpha$ -syn, with additional inclusion of 1 mM dithiothreitol (DTT) in all buffers. The protein concentration was determined by tyrosine absorption at 275 nm using the extinction coefficient of  $5,600 \text{ M}^{-1}\text{cm}^{-1}$  for WT and  $5,745 \text{ M}^{-1}\text{cm}^{-1}$  for A140C  $\alpha$ -syn.

### 2.2.2. $\alpha$ -syn fluorescent labeling

A140C  $\alpha$ -syn was stored in a 10 mM phosphate buffer pH 7.4, 1 mM DTT at  $-80^{\circ}\text{C}$ . The first step in sample preparation was buffer exchange using 10 kD cut-off filters (Amicon Ultra 0.5 ml centrifugal filters) for 5 min at  $16,000 \times g$  to remove DTT and exclude any potential degradation products. To remove possible preexisting fibrillar species, the samples were passed through a 100 kD cut-off filter (Amicon Ultra 0.5 ml centrifugal filters) for 10 min at  $16,000 \times g$ . The sample concentration commonly used in labeling experiments was around 140  $\mu$ M (2 mg/ml) of protein. A140C  $\alpha$ -syn was incubated overnight at  $4^{\circ}\text{C}$  with 2-fold molar excess of Alexa 488 maleimide, Alexa 532 maleimide or Alexa 647 maleimide or 4-fold molar excess of ATTO 655 maleimide, resulting in A140C-Alexa 488, A140C-Alexa 532, A140C-Alexa 647, and A140C-ATTO 655 respectively. Afterwards, labeled samples were passed through a Zeba desalting column (Zeba Spin Desalting Columns, 7 K MWCO, 2 ml) two times at  $1,000 \times g$  for 2 min to remove the free dye. The labeling ratio was higher than 95%, confirmed by mass spectrometry (MS) and SDS-PAGE, and then calculated from the absorbance of the labeled sample. Labeled samples were concentrated and stored at  $-80^{\circ}\text{C}$ .

### 2.2.3. The process of fibrillization

The buffer of 6 mM phosphate, pH 7.4, used for the aggregation experiments contained in addition 9 mM sodium azide ( $\text{NaN}_3$ ), 0.1 mM EDTA and (only in case of A140C  $\alpha$ -syn

mutant) 1 mM DTT. The total protein concentration was 70  $\mu$ M. All reactions were performed in 200  $\mu$ l solutions contained in 1.5 ml Protein Low Binding Tubes (Sigma-Aldrich) by incubation at 37°C and 1,000 rpm in a Termomixer Comfort (Eppendorf), until ThT fluorescent signal reached plateau.

#### **2.2.4. Thioflavin T assay**

The fluorescence increase of ThT upon binding to the  $\beta$ -sheet secondary structure was used as an indicator of the protein aggregation state. A stock solution of 1 mM ThT was prepared in 6 mM phosphate buffer pH 7.4 and filtered using a 0.22  $\mu$ m syringe filter. A total of 4  $\mu$ l aliquots of aggregated mixture were added to 996  $\mu$ l of a 10  $\mu$ M ThT solution in 6 mM phosphate buffer pH 7.4.

The probe was excited at 446 nm in a fluorescence spectrophotometer (Cary Eclipse, Varian Inc, Palo Alto, CA, USA), and emission spectra were recorded from 400 to 600 nm using slit widths of 10 nm. Fluorescence spectra of ThT in solution were subtracted from each  $\alpha$ -syn sample measurement. ThT fluorescence detected aggregation curves were made by plotting the emission signals at 485 nm on y-axis vs the aggregation time on x-axis. All measurements were performed in triplicate.

#### **2.2.5. Atomic force microscopy – The morphology of aggregates**

Samples for AFM were prepared as follows: 10  $\mu$ l of  $\alpha$ -syn sample, 5 to 10 times diluted in a 6 mM phosphate buffer pH 7.4, was placed on unmodified freshly cleaved mica and allowed to adsorb for 2 min. Unbound protein was gently washed off with 5  $\times$  50  $\mu$ l of HPLC grade water and dried using a gentle stream of nitrogen gas. The sample was then mounted on the AFM stage. AFM images were acquired using a NanoscopeIIIa controller (Digital Instruments, Santa Barbara, CA) with a multimode scanning probe microscope equipped with an E-scanner. All measurements were carried out in tapping mode under ambient conditions using single-beam silicon cantilever probes with the force constant of 22 to 41 N/m. All AFM images were captured with the resolution of 512 samples/line at a scan rate of 1 Hz, with scan sizes of either 10  $\mu$ m  $\times$  10  $\mu$ m or 4  $\mu$ m  $\times$  4  $\mu$ m. The typical scan speed was 10  $\mu$ m/s. For each sample condition approximately 100 fibrils were analyzed using Nanoscope analysis software with quantitative determination of height and periodicity parameters. Fibril lengths were measured in ImageJ (Plugins-Segmentation-Single Neurite Tracer).



## 2.3. Results

### 2.3.1. Morphological analysis of WT and A140C fibrils

A binding site for fluorescent labels was introduced by replacing the alanine residue 140 of  $\alpha$ -syn with cysteine. It is assumed that this modification at the C-terminus of the  $\alpha$ -syn molecules does not affect its aggregation properties. To verify that this was indeed the case, we used AFM imaging in tapping mode under ambient conditions to examine fibrillar features of both WT and the mutated  $\alpha$ -syn at the end phase of the aggregation reaction (120–144 h). Figure 2.1 shows AFM images of unlabeled A140C and WT  $\alpha$ -syn fibrils at the end of the aggregation process. Height, length, and periodicity are the three most important parameters that are commonly used to describe twisted amyloid fibrils [39]. They can readily be obtained from AFM measurements. In contrast to height measurements, the lateral width of the fibrils cannot accurately be determined by this method because the observed width is convoluted with the (relatively large) radius of curvature of the AFM tip. It is clear, especially from the higher-resolution images in Figure 2.2, that the height along the A140C and WT  $\alpha$ -syn fibrils is not uniform. In fact, the fibrils have the appearance of a twisted ribbon which results in troughs (blue line, Figure 2.2A, and the graph in blue color, Figure 2.2B) and peaks (red line, Figure 2.2A and the graph in red color, Figure 2.2B) in the height profiles of the analyzed fibrils. This trough and peak pattern is a hallmark of twisted fibrillar morphology.

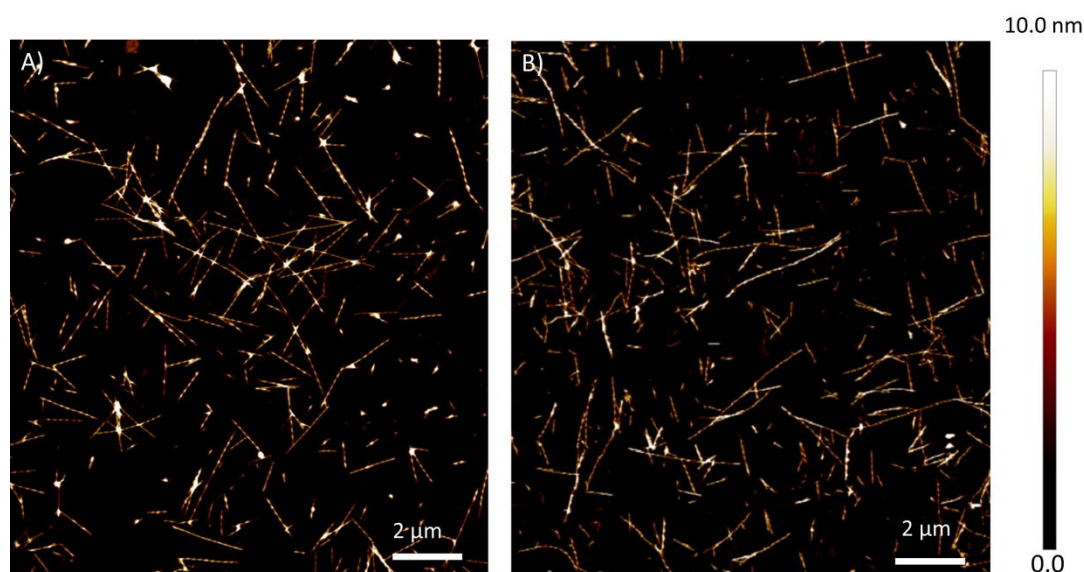


**Figure 2.1:** Representative AFM images of WT  $\alpha$ -syn (A) and A140C  $\alpha$ -syn (B) fibrils. WT and A140C  $\alpha$ -syn fibrils were prepared in 6 mM phosphate buffer at pH 7.4 with 0.1 mM EDTA, 1 mM DTT (only in case of A140C  $\alpha$ -syn) 1,000 rpm, 37°C, 120-144 h. AFM scan size: 10  $\mu$ m x 10  $\mu$ m.

We examined approximately 100 fibrils for a quantitative analysis of the height, periodicity and length of WT and A140C  $\alpha$ -syn fibrils. The periodic pitch of the fibrils was calculated as the average distance between adjacent peaks in the lengthwise height profile of the fibril (Figure 2.2C).

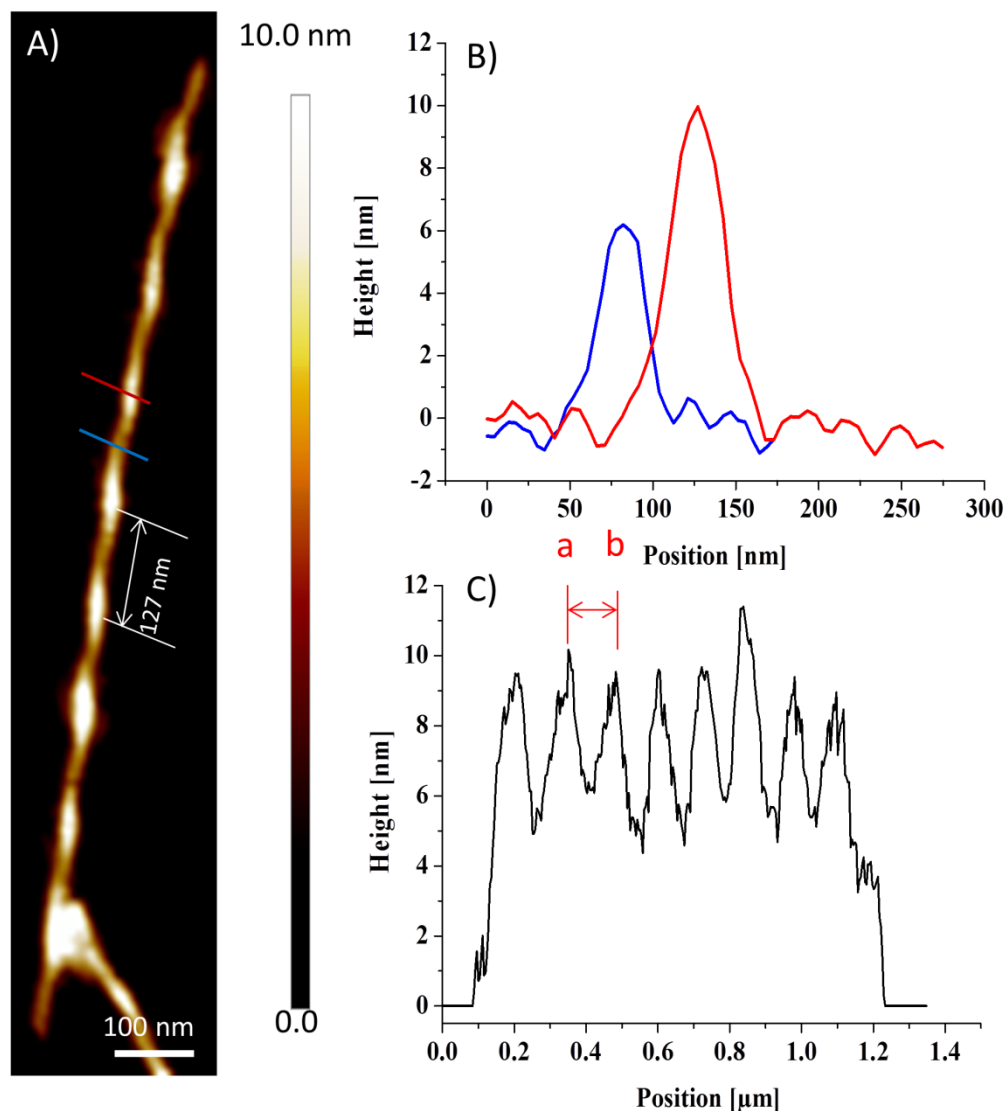


**Figure 2.2:** (A) High resolution AFM image of a typical WT  $\alpha$ -syn fibril. (B) Height profiles of trough (in blue) and peak (in red) of the WT  $\alpha$ -syn fibril. (C) Height profiles along the WT  $\alpha$ -syn fibril. The periodicity of the fibril height is calculated as the average distance between the fibril peaks (*e.g.*, a and b).

We found that the average length of WT  $\alpha$ -syn fibrils was  $2.2 \pm 0.7 \mu\text{m}$ , while A140C  $\alpha$ -syn fibrils, prepared under the very same conditions as WT, were on the average  $1.5 \pm 0.6 \mu\text{m}$  long (see Table 2.1). The length distribution is very similar in the two cases, as shown in Figure S.2.2 (see SI at the end of this chapter). The average pitch of the twist of, both, A140C and WT  $\alpha$ -syn fibrils was identical at 127 nm (Figure 2.2, Table 2.1). The measured fibril heights for WT and A140C  $\alpha$ -syn in both trough and peak positions were almost equal. The

trough height of WT  $\alpha$ -syn was  $6.9 \pm 0.7$  nm, and  $6.7 \pm 0.7$  nm for A140C  $\alpha$ -syn (Table 2.1). The peak height followed the same trend:  $9.4 \pm 0.6$  nm for WT  $\alpha$ -syn and  $9.0 \pm 0.8$  nm for A140C  $\alpha$ -syn (Table 2.1). These results on the fibrillar morphology are in good agreement with an earlier study performed on WT and A140C under similar conditions using AFM [38].

From this set of AFM experiments we conclude that the distributions of height, periodicity and fibril length are very similar between WT and A140C  $\alpha$ -syn. It confirms that the alanine mutation to cysteine in the carboxyl terminal domain of the protein does not interfere with the  $\alpha$ -syn aggregation process and that the end of the carboxyl terminus of the protein can be used as a suitable position for fluorescent labeling.

### 2.3.2. The effect of ATTO 655 on the $\alpha$ -syn fibril morphology

After showing that the A140C point mutation did not affect  $\alpha$ -syn aggregation and fibril morphology, we specifically labeled the A140C  $\alpha$ -syn mutant protein with an ATTO 655 maleimide fluorophore to follow the aging of labeled  $\alpha$ -syn samples. This dye is routinely used as a fluorescent probe for imaging. So far it has not been reported in the literature to interfere with  $\alpha$ -syn aggregation. It is an oxazine-type fluorophore with an overall charge of zero. Before fluorescent labeling, the A140C  $\alpha$ -syn sample was purified to remove possible oligomers and aggregates, and subsequently checked by MS. From the mass spectrum, shown in Figure S.2.3A (see SI), we concluded that the A140C  $\alpha$ -syn sample was fully in monomeric form. We then proceeded with the fluorescent labeling step. Prior to the subsequent aggregation process, the fluorescently labeled A140C  $\alpha$ -syn was also checked by MS (see SI, Figure S.2.3C). The A140C  $\alpha$ -syn was completely fluorescently labeled and the sample did not contain dimers or larger aggregates. The observed and calculated mass of labeled A140C  $\alpha$ -syn samples were in agreement.

By using constant agitation of 1,000 rpm and 37°C we prepared a series of WT  $\alpha$ -syn samples mixed, respectively, with 10, 25, and 50% A140C-ATTO 655, in parallel, respectively, with unlabeled samples of A140C, WT and with 100% A140C-ATTO 655-labeled  $\alpha$ -syn. The samples were aged for 120–144 h. Representative AFM images of mature fibrils adsorbed on freshly cleaved mica are shown in Figure 2.3. The fibrils in the images appear to become shorter and locally more clustered with increasing concentration compared to WT samples. This is particularly evident in the images with 50% and 100% labeled A140C  $\alpha$ -syn. For each sample we analyzed height, periodicity and fibril length of about 100 fibrils.

The measured trough fibril heights were very similar in samples with various ratios of labeled and unlabeled  $\alpha$ -syn (Table 2.1). The samples with 10–50% A140C-ATTO 655  $\alpha$ -syn had an average pitch between 115–120 nm (Table 2.1). There was no twisted pattern observed for 100% ATTO 655 labeled  $\alpha$ -syn fibrils (Figure 2.4). The height along the fibrils of 100% A140C-ATTO 655  $\alpha$ -syn was homogeneous (Figure 2.4F). Thus, the twisted morphology and length distribution appear to be sensitive to the presence of ATTO 655 fluorescent dye when more than 50% of the  $\alpha$ -syn is labeled, but not the height of  $\alpha$ -syn fibrils.

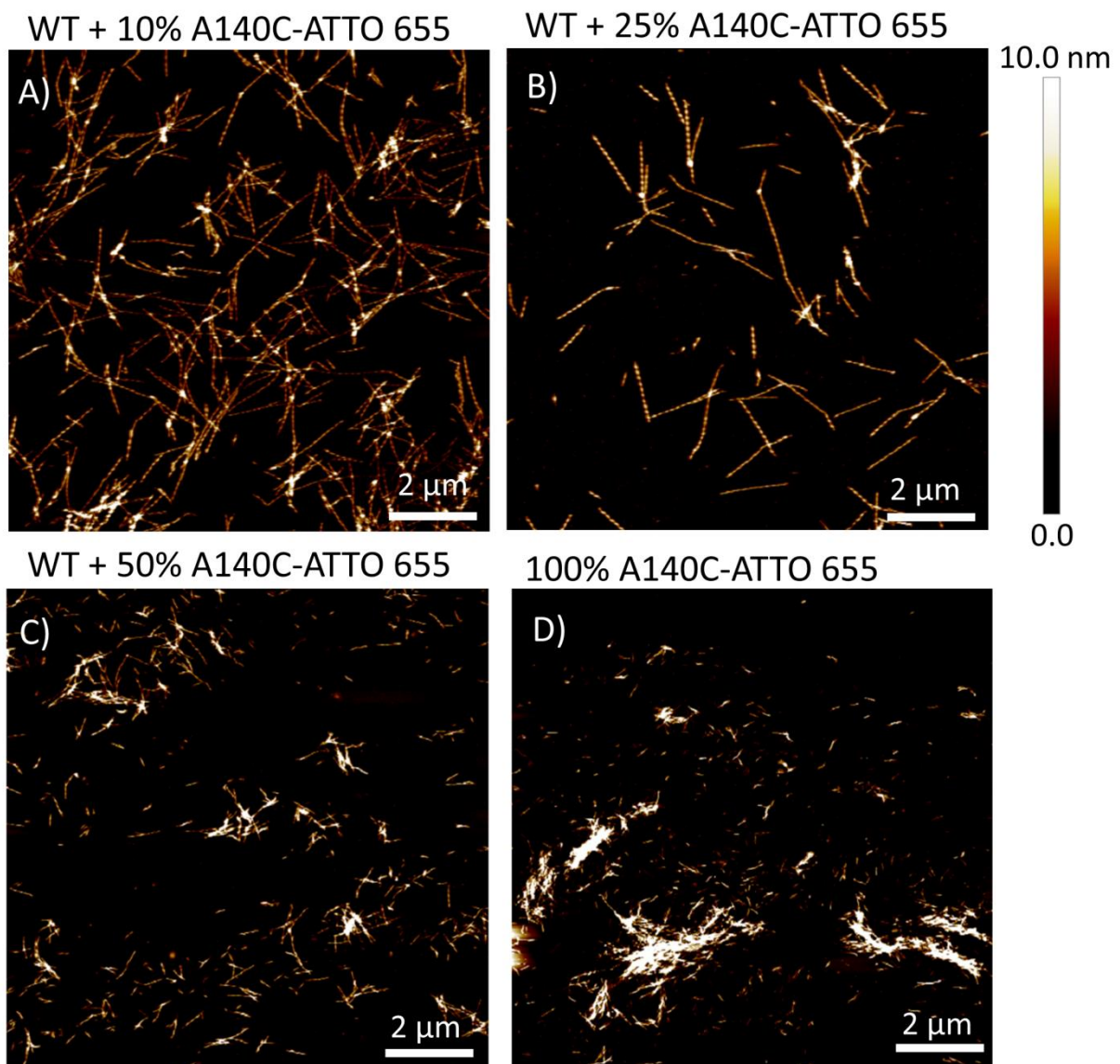


**Figure 2.3:** Effect of ATTO 655 fluorescent dye on  $\alpha$ -syn fibrillar morphology, showing fractions of 10% (A), 25% (B), 50% (C), 100% (D) A140C-ATTO 655. A140C  $\alpha$ -syn fibrils labeled with ATTO 655 were prepared in 6 mM phosphate buffer at pH 7.4 with 0.1 mM EDTA, 1,000 rpm, 37°C, 120-144 h. AFM scan size: 10  $\mu$ m x 10  $\mu$ m.

The results of the length analyses of aggregated  $\alpha$ -syn, fractionally labeled with ATTO 655, show a pronounced decrease in length with increasing fraction of labeled  $\alpha$ -syn (Figure 2.7

and Table 2.1). The average fibrillar length drops from 2.2  $\mu\text{m}$  for unlabeled fibrils to 0.4  $\mu\text{m}$  in the case of fully labeled  $\alpha$ -syn. The height of the analyzed labeled fibrils under the above mentioned conditions was almost identical. The fibrillar length is discussed further in the results section.

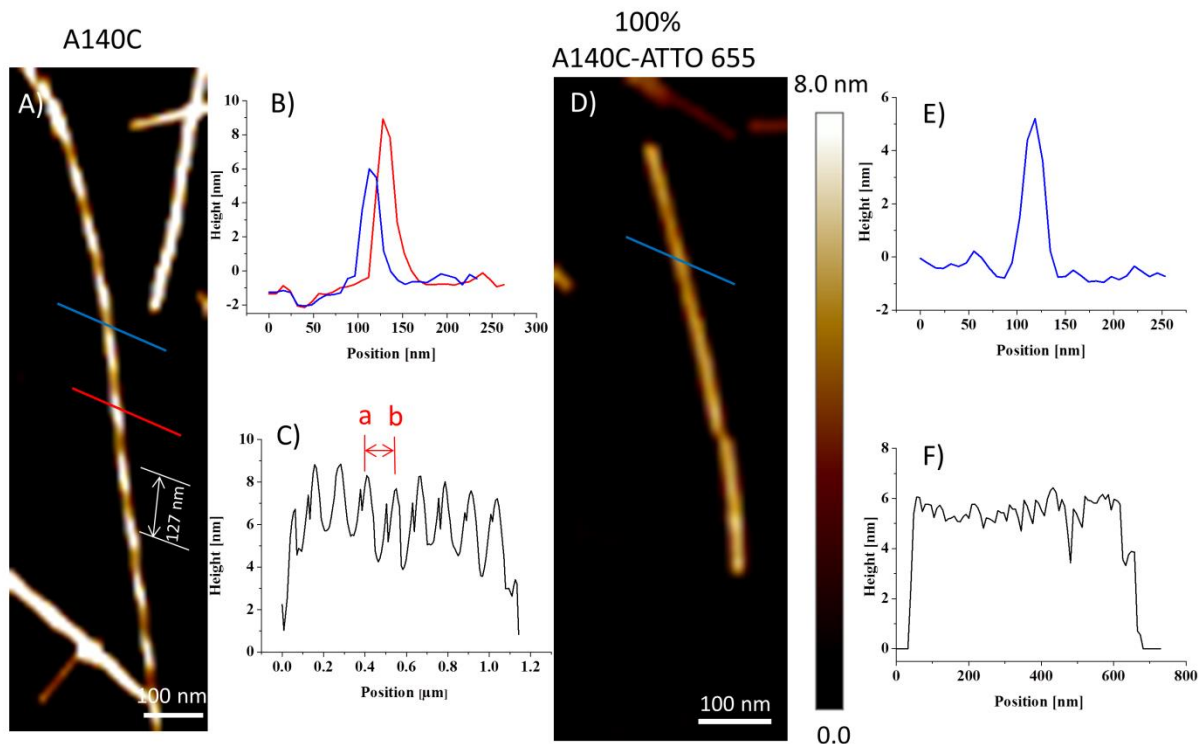


**Figure 2.4:** High resolution AFM image of a typical unlabeled A140C  $\alpha$ -syn fibril (A) and 100% labeled A140C-ATTO 655 fibril (D). (B, E) Height profiles of trough (in blue) and peak (in red) of the unlabeled A140C  $\alpha$ -syn fibril and 100% A140C-ATTO 655 fibril. (C, F) Height profiles along the A140C  $\alpha$ -syn fibril and 100% A140C-ATTO 655 fibril. The periodicity of the fibril height is calculated as the average distance between the two fibril peaks (a and b).

### 2.3.3. Comparison of the effect of four fluorescent dyes on the $\alpha$ -syn fibril morphology

To study the effect of the chemical structure of the fluorescent probe on the morphology of  $\alpha$ -syn fibrils, we selected three additional fluorophores with a different chemical structure and overall charge. Two of the chosen fluorophores were rhodamines, Alexa 488 with the overall charge of  $-2$  and Alexa 532 carrying the overall of charge  $-1$ . Alexa 647 belongs to the group of cyanine dyes and has the overall charge of  $-3$ , while ATTO 655 is an oxazine-type fluorophore with the overall charge zero.

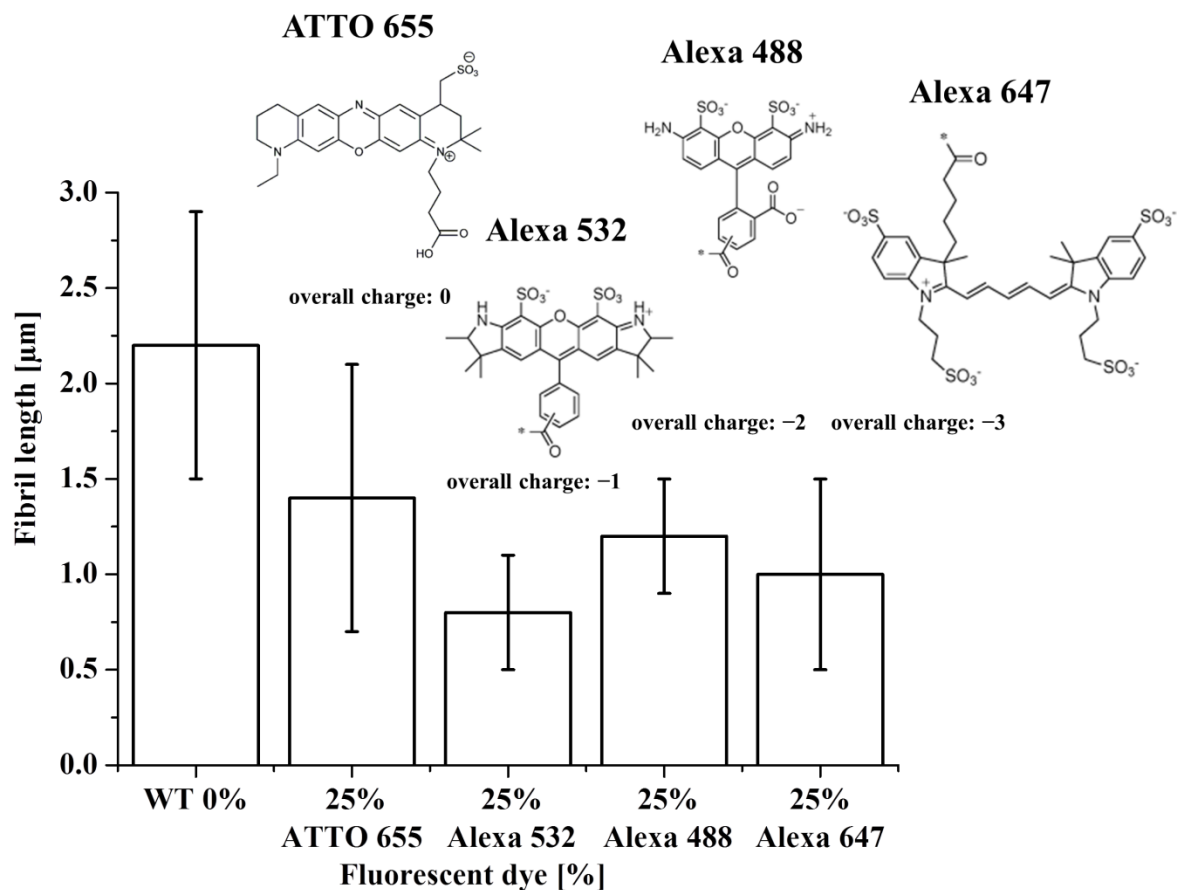


**Figure 2.5:** Dependence of  $\alpha$ -syn fibril length at 25% labeling with various fluorescent dyes. In each case the graph shows the average length of approximately 100 fibrils. The vertical bars represent the standard deviation of the average fibrillar length.

We focused on comparing results of fibrillization experiments with 25% labeled A140C  $\alpha$ -syn with, respectively, ATTO 655, Alexa 647, Alexa 488 and Alexa 532 – mixed with WT- under constant shaking at 1,000 rpm and 37°C for 120–144 h and otherwise identical conditions. AFM in tapping mode was done on samples at the end phase of the fibrillization experiment. Using the AFM images of the aged samples we measured the fibrillar length, height and twisting, and compared the measured fibrillar features. Interestingly, we found similar fibrillar heights in all tested samples, together with conserved fibrillar twists (Table 2.1). Measured fibrillar lengths in our study were not remarkably different among the 25% variantly labeled  $\alpha$ -syn samples, but they were significantly shorter than WT  $\alpha$ -syn. The results are summarized in Figure 2.5, where the vertical bars represent the standard deviation of the average fibrillar length. The size of the error bars are determined by the large spread in the fibrillar lengths which is typical for  $\alpha$ -syn. The average fibrillar length was the least affected by ATTO 655, with an overall charge 0 and the most with Alexa 532 with the overall



charge  $-1$ . This result suggests that the labeling of  $\alpha$ -syn with a dye molecule leads to a significant decrease in the fibrillar length when 25% of  $\alpha$ -syn is labeled.

#### 2.3.4. The effect of Alexa 647 on the $\alpha$ -syn fibril morphology

In A140C-ATTO 655 labeled  $\alpha$ -syn fibrils we observed significant changes in the morphology, especially concerning the fibrillar length and twisted appearance of fibrils. It was not clear whether the change in morphology was limited to the use of the specific dye, ATTO 655. Therefore we expanded our study to compare these results with Alexa 647. This is a cyanine-type fluorophore, which has not only a very different chemical structure than ATTO 655, but also a distinct overall charge of  $-3$  (Figure 2.5). We set up the same aggregation experiment for, both, Alexa 647 and ATTO 655 labeled  $\alpha$ -syn as a function of the fraction of labeled vs unlabeled monomer. Figure 2.6 shows the summary of representative AFM images on mica surface at the end aggregation stage using Alexa 647-labelled  $\alpha$ -syn. Fibril height, trough and peak heights of Alexa 647 labeled samples were almost the same as for ATTO 655 labeled samples (Table 2.1). The twisting of  $\alpha$ -syn fibrils was observed in all samples with up to 50% labeled  $\alpha$ -syn, but it was not observed in 100% labeled  $\alpha$ -syn sample (Table 2.1). The significant clustering of the fibrils was seen in samples with the 50% and 100% fraction of labeled samples (Figure 2.3 and Figure 2.6).

It is important to notice that the length of the fibrils was clearly affected by the presence of fluorophores (Figure 2.7). The average fibril length decreased as the labeled sample percentage increased in the reaction mix. The trend of fibrillar length decrease as a function of the fraction of ATTO 655 and Alexa 647 labeled  $\alpha$ -syn was very similar. Already at 10% of labeled sample in both cases the fibrillar length decreased significantly (Figure 2.7).

#### 2.4. Discussion

The AFM images show that mature fibrils of unlabeled, WT and A140C  $\alpha$ -syn have a ribbon-like, twisted appearance with a pitch of 127 nm, a maximum height of about 9.4 nm and an apparent height of 6.9 nm at the troughs. Presumably, at the trough position the ribbon stands off from the surface [40], and in that case its actual thickness at that point is 4.4 nm, determined by the width of the protofibril according to the model shown in Figure 2.8. This implies that the width to thickness ratio is about 2:1. Not only are these dimensional parameters constant along the length of the fibrils, they are also common features of virtually all fibrils in the image (Figure 2.1). Hence, apart from the variation in length, the morphology

of mature, unlabeled fibrils is rather homogeneous under the set of conditions in these experiments. Notably, only mature fibrils were observed at the conditions in our experiments.

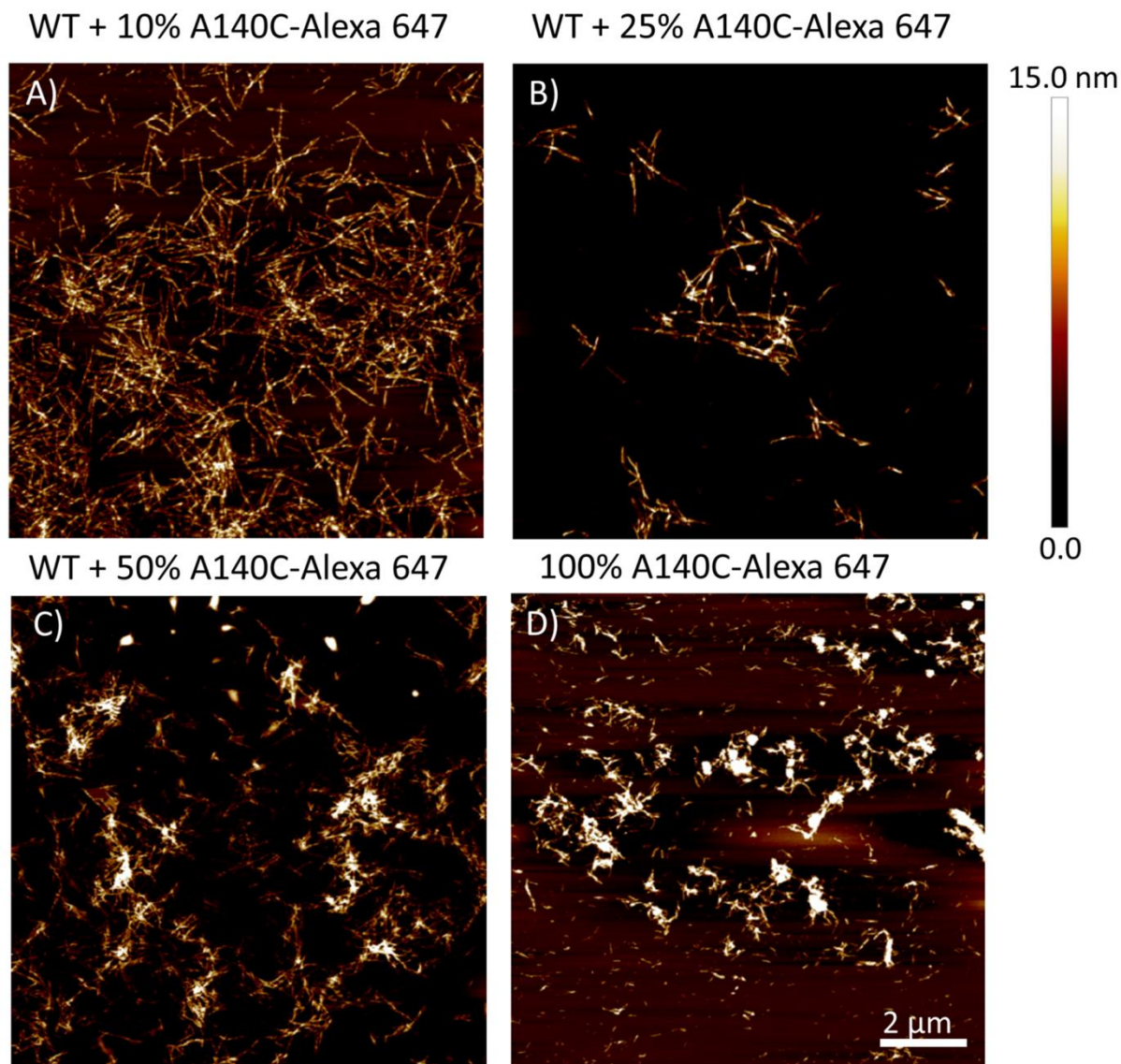


**Figure 2.6:** Effect of Alexa 647 fluorescent dye on the aggregation of  $\alpha$ -syn, where fractions of 10% (A), 25% (B), 50% (C), 100% (D) A140C-Alexa 647 are shown. A140C  $\alpha$ -syn fibrils labeled with Alexa 647 were prepared in 6 mM phosphate buffer at pH 7.4 with 0.1 mM EDTA, 1,000 rpm, 37°C, 120-144 h. AFM scan size: 10  $\mu$ m x 10  $\mu$ m.

We have performed experiments that consisted of labeling  $\alpha$ -syn fibrils after assembly [41]. The morphology of these fibrils was identical to those formed from  $\alpha$ -syn monomers of which a small fraction was fluorescently labeled. We conclude that the morphology of labeled  $\alpha$ -syn fibrils is not affected by the interaction with the surface.

The twisted appearance of  $\alpha$ -syn fibrils is consistent with earlier reports in the literature, with very similar values for height and width parameters of the mature fibrils [8,38,40,42]. We note that the morphology of  $\alpha$ -syn fibrils depends on growth conditions, and that there is not



a unique morphology of unlabeled  $\alpha$ -syn fibrils. For example, Bousset et al. [43] reported a different morphology of fibrils depending on the presence of KCl and EDTA in the solution. Under no-salt conditions a ribbon-like structure is observed, while 150 mM KCl results in a tubular shape of the fibrils, and 150 mM KCl plus 2.5 mM EDTA again results in ribbon-like fibrils. These fibrils appear to differ in stability as well as toxicity when applied to neuronal cell cultures. Sidhu et al. [38] similarly show that, depending on solvent conditions, A140C mutant and WT  $\alpha$ -syn can be directed to reproducibly form homogeneous populations of ribbon-like structures exhibiting regular periodicity. The conditions in the present work were chosen such that the ribbon-like structure prevailed.

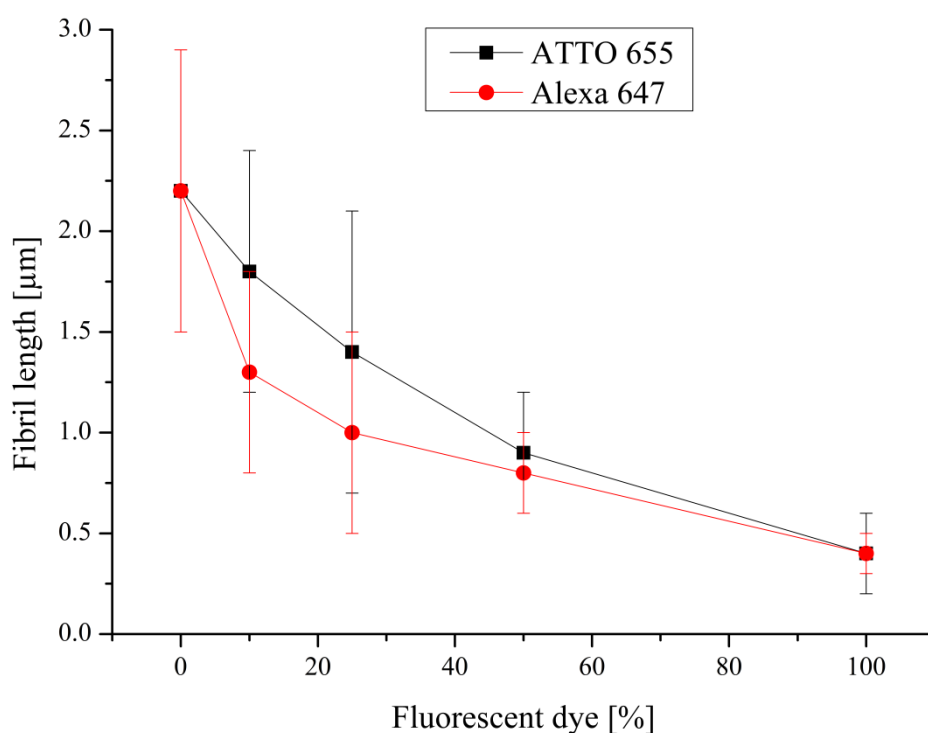


**Figure 2.7:** The dependence of fibril length on the fraction of ATTO 655 (in black) and Alexa 647 (in red) in the reaction mix measured for approximately 100 fibrils.

The measurements indicate that the intrinsic pitch of WT  $\alpha$ -syn and the A140C mutant are very similar (Table 2.1). In some cases the standard error in Table 2.1 is very large which could indicate a local change of fibrillar morphology. It has been shown [43,38] that once fibrils are formed those with different morphologies do not interconvert from one to the other. Moreover, the morphology is preserved when seeds obtained after sonication of mature fibrils are allowed to grow. Therefore we think that it is unlikely that the large standard error in some cases reflects the presence of a second class of pitch. Rather, we attribute the large standard error in these cases to heterogeneity of the pitch along the length of the fibril. The

standard error appears to be correlated with the charge of the fluorescent label, which is largest for Alexa 647. It is likely that variation of the label density along the fibril will affect the local pitch especially in the case of strong electrostatic interaction between dye-molecules. Measurement of the pitch is also less accurate with shorter fibrils, as is the case for Alexa 488 and Alexa 647 labeled samples when the fraction of labeled protein is high.

Contrary to Khurana et al. [42] we did not observe the appearance of protofilaments and protofibrils, neither in the plateau phase nor at earlier stages of aggregation. Presumably, this is due to different aggregation conditions, but also the history of the sample should be taken into account. In our case we verified that aggregation was started with strictly monomeric  $\alpha$ -syn. The coexistence of protofilaments, protofibrils and mature fibrils was the reason for Khurana et al. [42] to propose the hierarchical assembly model for  $\alpha$ -syn aggregation with a step-wise assembly of mature fibrils: protofilaments  $\rightarrow$  protofibrils  $\rightarrow$  mature fibrils. Our results are also not consistent with other predictions of this model [42]. Thus, we suggest that fibrils are fully capable of growing *via* monomer addition to the fibril ends that already have the mature morphology, and it is likely the primary mechanism of elongation.

Presumably the mature fibril morphology is the stable fibrillar, ribbon-like structure in the case of  $\alpha$ -syn. There is an agreement on the fact that this morphology arises from the intertwining of two protofibrils, each of which contains two intertwined protofilaments. This model is consistent with the 2:1 ratio of width and thickness of the fibrillar ribbon. The diameter of the protofibrils then is 4.4 nm, based on our AFM results (Figure 2.8).

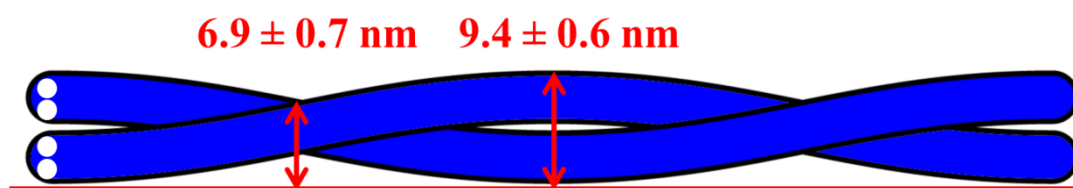


**Figure 2.8:** A model of mature WT  $\alpha$ -syn fibrils according to the reference 42. Two protofilaments (shown in white) form a protofibril (shown in blue). Two protofibrils intertwine and form a mature fibril. Samples were imaged on a mica surface (shown in red) where 9.4 nm represents the actual distance of the mature  $\alpha$ -syn fibril from the surface at the highest point (peak height) and 6.9 nm at the lowest (trough) position.

So far, the key factors that have been considered in the formation of amyloid fibrils are electrostatic interactions, hydrophobicity and hydrogen bonds [44,45]. It has been suggested that fibrillar twists are associated with a fine balance between electrostatic interactions and elastic energy [39]. In other amyloid forming proteins, like  $\beta$ -lactoglobulin, it has been claimed that the low ionic strength of the solution is crucial for twisting [39]. In the latter

case the periodic pitch of the fibrils changes when the ionic strength of the solution varies, presumably due to charge screening.

Incorporation of fluorescently labeled  $\alpha$ -syn has a pronounced effect on the morphology of mature fibrils. First of all we observed a significant decrease of the average fibril length with increasing fraction of labeled  $\alpha$ -syn, concomitant with an increasing number of disorganized clusters of entangled  $\alpha$ -syn fibrils. In addition, the twisted appearance of the fibrillar structure is lost when the fraction of labeled  $\alpha$ -syn exceeds 50%. Except for the latter, the AFM-measured height parameters of the fibrils were identical in all cases. The ionic strength of the reaction buffer was the same in all experiments, but the overall charge of the used dyes varied from  $-3$  to  $0$ . In particular, ATTO 655 and Alexa 647 have an overall charge of  $0$  and  $-3$ , respectively. Since, there was no clear difference in fibrillar length and morphology between the samples labeled with ATTO 655 and Alexa 647 fluorophore, it appears that the electrostatic effects of fluorescent probes on the morphology of  $\alpha$ -syn fibrils is not significant at the conditions used in the present work.

A possible explanation for fibrils shortening with the increase in the fraction of labeled  $\alpha$ -syn is the effect of the fluorescent label on the affinity of  $\alpha$ -syn monomer binding to the fibril end. The dye molecule is covalently attached to the end position at the C-terminus of the  $\alpha$ -syn protein. Being an intrinsically disordered protein,  $\alpha$ -syn can adopt different conformations in solution with varying affinity to fibril ends. It is very well possible that the attachment of the fluorescent label changes the conformational distribution of  $\alpha$ -syn in solution as compared to the unlabeled protein, and its affinity the fibril ends may change then, too. In principle the affinity for monomer binding to the  $\alpha$ -syn fibril ends can be measured by determining  $k_d$  of the binding/unbinding equilibrium. However, reproducible results for  $k_d$  are very difficult to obtain starting from a monomer solution because of the stochastic nature of  $\alpha$ -syn aggregation. Even in seeding experiments the extended time scale of aggregation with lowering the monomer concentration made it difficult to get reliable results beyond an order of magnitude estimate of  $k_d$  which is a few  $\mu\text{M}$ .

The stability of  $\alpha$ -syn fibrils is also affected by the influence of fluorescent probes on the fibril packing. Solid-state NMR data from amyloid fibrils by Vilar et al. indicate that the core of  $\alpha$ -syn filaments consists of 5 parallel  $\beta$ -sheets [46]. Moreover, these authors also show that a truncated form of  $\alpha$ -syn, in which only the 30-100 residues are retained, is still capable of forming fibrils with similar dimensions as the native form. This implies that the C- and N-

terminal domains are not essential for the assembly of the typical  $\alpha$ -syn fibrils with two protofilaments. This is not consistent with results reported by Qin et al. [45] who claim that the C-terminal domain plays a role in the interaction between the two protofibrils in the structure. Both reports agree, however, that the C-terminus is exposed to the solvent, which means that it is presumably not involved as part of the regular secondary fibril structure. We thus conclude that the fluorescent label, attached to the residue 140 of the flexible C-terminus of  $\alpha$ -syn, is solvent exposed as a peripheral decoration of the  $\alpha$ -syn fibril.

Based on this conclusion, together with the fact that the C-terminal domain is already negatively charged it can be reasonably expected that an additional, negatively charged label at the C-terminus does not inhibit aggregation. Indeed, facile aggregation is observed when the fraction of labeled  $\alpha$ -syn is low. However, our results clearly show that the stability of  $\alpha$ -syn fibrils decreases when the fraction of labeled  $\alpha$ -syn increases. Ultimately, the twisted morphology is lost, most likely due to the close proximity of the labels. The low sensitivity of fibril formation for the overall charge of the dye-labels suggests that steric and /or structural effects are the most important factors that contribute to the destabilization of  $\alpha$ -syn fibrils. It is very likely that this effect is exacerbated upon labeling residues in the  $\beta$  sheet-forming domains, or residues that are involved in the interaction between protofilaments or protofibrils.

Labeling at the C-terminus is probably least disruptive, but our results show that even this case imposes a significant limitation on the use of fluorescent labeling techniques in the study of  $\alpha$ -syn aggregation, both, *in vivo* and *in vitro*, by restrictions on the fraction of labeled  $\alpha$ -syn. This limitation may be prohibitive, for example, for the application of super resolution methods for fluorescence imaging of  $\alpha$ -syn aggregates since they require high labeling densities in order to reconstruct a high-resolution image.

## 2.5. Conclusion

The results obtained in this study clearly confirm that fluorescent dyes do exert an effect on the morphology of  $\alpha$ -syn aggregates. It is evident that the length of fibrils decreases significantly with the increase in the fraction of the labeled protein. We propose the explanation for the decrease of the fibrillar length by the changed kinetic properties, namely affinity of  $\alpha$ -syn monomer to fibril end. Morphological analysis by atomic force microscopy shows that more than 50% of fluorescently labeled  $\alpha$ -syn fibrils lose their distinct twisted

appearance, periodicity, while regular twists persist to be the significant characteristic of unlabeled and partially labeled  $\alpha$ -syn fibrils. We suspect that the original twisted appearance of the fibrils is lost when more than half of labeled  $\alpha$ -syn molecules are incorporated into it, due to short-range interactions between dye molecules. The obtained results also show that the height of  $\alpha$ -syn fibrils remains unaffected.

### Acknowledgements

We thank Ms. N. Schilderink from University of Twente for  $\alpha$ -synuclein expression and purification. We are grateful to Prof. Dr. V. Subramaniam for fruitful discussions and comments. This work was performed in the framework of the research program ‘‘A Single Molecule View on Protein Aggregation’’, supported by the Foundation for Fundamental Research on Matter (FOM), which is part of the Netherlands Organization for Scientific Research (NWO).

**Table 2.1:** Quantitative comparison of  $\alpha$ -syn fibril morphology performed on approximately 100 fibrils

Protein sample	Typical trough height (nm)	Typical peak height (nm)	Length ( $\mu\text{m}$ )	Pitch of fibrillar twist (nm)
WT $\alpha$ -syn	$6.9 \pm 0.7$	$9.4 \pm 0.6$	$2.2 \pm 0.7$	$127 \pm 12$
A140C $\alpha$ -syn	$6.7 \pm 0.7$	$9.0 \pm 0.8$	$1.5 \pm 0.6$	$127 \pm 11$
WT + 10% A140C-ATTO 655	$7.0 \pm 1.0$	$9.5 \pm 0.5$	$1.8 \pm 0.6$	$113 \pm 12$
WT + 25% A140C-ATTO 655	$7.2 \pm 0.8$	$9.4 \pm 0.3$	$1.4 \pm 0.7$	$122 \pm 14$
WT + 50% A140C-ATTO 655	$7.1 \pm 1.0$	$9.7 \pm 0.6$	$0.9 \pm 0.3$	$114 \pm 17$
100% A140C-ATTO 655	$6.6 \pm 1.4$	N.A	$0.4 \pm 0.2$	N.A
WT + 10 % A140C-Alexa 647	$6.9 \pm 1.1$	$9.7 \pm 0.6$	$1.3 \pm 0.5$	$107 \pm 39$
WT + 25% A140C-Alexa 647	$6.7 \pm 1.3$	$10.4 \pm 0.9$	$1.0 \pm 0.5$	$88 \pm 52$
WT + 50% A140C-Alexa 647	$7.3 \pm 1.4$	$10.8 \pm 1.2$	$0.8 \pm 0.2$	$128 \pm 32$
100% A140C-Alexa 647	$6.6 \pm 1.3$	N.A	$0.4 \pm 0.1$	N.A
WT + 1% A140C-Alexa 488	$7.0 \pm 0.7$	$8.7 \pm 0.9$	$1.9 \pm 1.0$	$86 \pm 22$
WT + 5 % A140C-Alexa 488	$7.1 \pm 0.9$	$9.0 \pm 0.7$	$1.4 \pm 0.5$	$89 \pm 29$
WT + 25 % A140C-Alexa 488	$6.9 \pm 0.9$	$9.7 \pm 0.8$	$1.2 \pm 0.3$	$126 \pm 22$
WT + 25 % A140C-Alexa 532	$6.8 \pm 1.0$	$9.0 \pm 0.8$	$0.8 \pm 0.3$	$108 \pm 17$

## 2.6. References

- [1] T.P.J. Knowles, M. Vendruscolo, C.M. Dobson, The amyloid state and its association with protein misfolding diseases, *Nat. Rev. Mol. Cell Biol.* 15 (2014) 384–96. doi:10.1038/nrm3810.
- [2] R.N. Rambaran, L.C. Serpell, Amyloid fibrils: abnormal protein assembly, *Prion.* 2 (2008) 112–117. doi:10.4161/pri.2.3.7488.
- [3] F. Chiti, C.M. Dobson, Protein misfolding, functional amyloid, and human disease, *Annu. Rev. Biochem.* 75 (2006) 333–366. doi:10.1146/annurev.biochem.75.101304.123901.
- [4] D.J. Selkoe, Folding proteins in fatal ways, *Nature.* 426 (2003) 900–904. doi:10.1038/nature02477.
- [5] S. Mankar, A. Anoop, S. Sen, S.K. Maji, Nanomaterials: amyloids reflect their brighter side, *Nano Rev.* 2 (2011) 1–12. doi:10.3402/nano.v2i0.6032.
- [6] I. Cherny, E. Gazit, Amyloids: Not only pathological agents but also ordered nanomaterials, *Angew. Chemie - Int. Ed.* 47 (2008) 4062–4069. doi:10.1002/anie.200703133.
- [7] E. Herczenik, M.F.B.G. Gebbink, Molecular and cellular aspects of protein misfolding and disease, *FASEB J.* 22 (2008) 2115–2133. doi:10.1096/fj.07-099671.
- [8] M.E. van Raaij, J. van Gestel, I.M.J. Segers-Nolten, S.W. de Leeuw, V. Subramaniam, Concentration dependence of alpha-synuclein fibril length assessed by quantitative atomic force microscopy and statistical-mechanical theory, *Biophys. J.* 95 (2008) 4871–4878. doi:10.1529/biophysj.107.127464.
- [9] J.D. Schmit, K. Ghosh, K. Dill, What drives amyloid molecules to assemble into oligomers and fibrils?, *Biophys. J.* 100 (2011) 450–458. doi:10.1016/j.bpj.2010.11.041.
- [10] S.B. Malinchik, H. Inouye, K.E. Szumowski, D.A. Kirschner, Structural analysis of Alzheimer's beta(1-40) amyloid: protofilament assembly of tubular fibrils, *Biophys. J.* 74 (1998) 537–545. doi:10.1016/S0006-3495(98)77812-9.
- [11] R. Nelson, M.R. Sawaya, M. Balbirnie, A.Ø. Madsen, C. Riek, R. Grothe, et al., Structure of the cross-beta spine of amyloid-like fibrils, *Nature.* 435 (2005) 773–778. doi:10.1038/nature03680.
- [12] K.C. Stein, H.L. True, Prion Strains and Amyloid Polymorphism Influence Phenotypic Variation, *PLoS Pathog.* 10 (2014) e1004328. doi:10.1371/journal.ppat.1004328.
- [13] S.J. Wood, J. Wypych, S. Steavenson, J. Louis, M. Citron, A.L. Biere,  $\alpha$ -Synuclein Fibrillogenesis is Nucleation-dependent, *Biochemistry.* (1999) 19509–19512.
- [14] T.P.J. Knowles, C.A. Waudby, G.L. Devlin, S.I.A. Cohen, A. Aguzzi, M. Vendruscolo, et al., An analytical solution to the kinetics of breakable filament assembly, *Science.* 326 (2009) 1533–1537. doi:10.1126/science.1178250.
- [15] A.K. Buell, C. Galvagnion, R. Gaspar, E. Sparr, M. Vendruscolo, T.P.J. Knowles, et al., Solution conditions determine the relative importance of nucleation and growth processes in  $\alpha$ -synuclein aggregation, *Proc. Natl. Acad. Sci. U. S. A.* 111 (2014) 7671–7676. doi:10.1073/pnas.1315346111.
- [16] W. Hoyer, T. Antony, D. Cherny, G. Heim, T.M. Jovin, V. Subramaniam, Dependence

- of  $\alpha$ -synuclein aggregate morphology on solution conditions, *J. Mol. Biol.* 322 (2002) 383–393. doi:10.1016/S0022-2836(02)00775-1.
- [17] M.E. van Raaij, I.M.J. Segers-Nolten, V. Subramaniam, Quantitative morphological analysis reveals ultrastructural diversity of amyloid fibrils from alpha-synuclein mutants, *Biophys. J.* 91 (2006) L96–L98. doi:10.1529/biophysj.106.090449.
- [18] L. Giehm, D.E. Otzen, Strategies to increase the reproducibility of protein fibrillization in plate reader assays, *Anal. Biochem.* 400 (2010) 270–281. doi:10.1016/j.ab.2010.02.001.
- [19] H. Heise, W. Hoyer, S. Becker, O.C. Andronesi, D. Riedel, M. Baldus, Molecular-level secondary structure, polymorphism, and dynamics of full-length alpha-synuclein fibrils studied by solid-state NMR, *Proc. Natl. Acad. Sci. U. S. A.* 102 (2005) 15871–15876. doi:10.1073/pnas.0506109102.
- [20] K.M. Danzer, D. Haasen, A.R. Karow, S. Moussaud, M. Habeck, A. Giese, et al., Different species of alpha-synuclein oligomers induce calcium influx and seeding, *J. Neurosci.* 27 (2007) 9220–9232. doi:10.1523/JNEUROSCI.2617-07.2007.
- [21] K.A. Conway, S.J. Lee, J.C. Rochet, T.T. Ding, R.E. Williamson, P.T. Lansbury, Acceleration of oligomerization, not fibrillization, is a shared property of both alpha-synuclein mutations linked to early-onset Parkinson's disease: implications for pathogenesis and therapy, *Proc. Natl. Acad. Sci. U. S. A.* 97 (2000) 571–576. doi:10.1073/pnas.97.2.571.
- [22] K.A. Conway, S.J. Lee, J.C. Rochet, T.T. Ding, J.D. Harper, R.E. Williamson, et al., Accelerated oligomerization by Parkinson's disease linked alpha-synuclein mutants, *Ann. N. Y. Acad. Sci.* 920 (2000) 42–45.
- [23] M.M. Apetri, N.C. Maiti, M.G. Zagorski, P.R. Carey, V.E. Anderson, Secondary Structure of  $\alpha$ -Synuclein Oligomers: Characterization by Raman and Atomic Force Microscopy, *J. Mol. Biol.* 355 (2006) 63–71. doi:10.1016/j.jmb.2005.10.071.
- [24] W. Hoyer, D. Cherny, V. Subramaniam, T.M. Jovin, Impact of the acidic C-terminal region comprising amino acids 109-140 on  $\alpha$ -synuclein aggregation in vitro, *Biochemistry.* 43 (2004) 16233–16242. doi:10.1021/bi048453u.
- [25] H.A. Lashuel, B.M. Petre, J. Wall, M. Simon, R.J. Nowak, T. Walz, et al.,  $\alpha$ -Synuclein, Especially the Parkinson's Disease-Associated Mutants, Forms Pore-Like Annular and Tubular Protofibrils, *J. Mol. Biol.* 322 (2002) 1089–1102. doi:10.1016/S0022-2836(02)00735-0.
- [26] A. Quist, I. Doudevski, H. Lin, R. Azimova, D. Ng, B. Frangione, et al., Amyloid ion channels: a common structural link for protein-misfolding disease, *Proc. Natl. Acad. Sci. U. S. A.* 102 (2005) 10427–10432. doi:10.1073/pnas.0502066102.
- [27] H.-Y. Kim, M.-K. Cho, A. Kumar, E. Maier, C. Siebenhaar, S. Becker, et al., Structural Properties of Pore-Forming Oligomers of alpha-Synuclein, *J. Amer. Chem. Soc.* 131 (2009) 17482–17489.
- [28] M. Fändrich, J. Meinhardt, N. Grigorieff, Structural polymorphism of Alzheimer Abeta and other amyloid fibrils, *Prion.* 3 (2009) 89–93. doi:8859.
- [29] C. Goldsbury, P. Frey, V. Olivieri, U. Aebi, S. A. Müller, Multiple assembly pathways underlie amyloid- $\beta$  fibril polymorphisms, *J. Mol. Biol.* 352 (2005) 282–298. doi:10.1016/j.jmb.2005.07.029.
- [30] C. Lara, S. Gourdin-Bertin, J. Adamcik, S. Bolisetty, R. Mezzenga, Self-assembly of

- ovalbumin into amyloid and non-amyloid fibrils, *Biomacromolecules*. 13 (2012) 4213–4221. doi:10.1021/bm301481v.
- [31] S. Assenza, J. Adamcik, R. Mezzenga, P. De Los Rios, Universal Behavior in the Mesoscale Properties of Amyloid Fibrils, *Phys. Rev. Lett.* 113 (2014) 268103. doi:10.1103/PhysRevLett.113.268103.
- [32] S. Nath, J. Meunier, J. Hendrix, S.A. Carl, Y. Engelborghs, Early aggregation steps in  $\alpha$ -synuclein as measured by FCS and FRET: Evidence for a contagious conformational change, *Biophys. J.* 98 (2010) 1302–1311. doi:10.1016/j.bpj.2009.12.4290.
- [33] N. Zijlstra, C. Blum, I.M.J. Segers-Nolten, M.M.A.E. Claessens, V. Subramaniam, Molecular composition of sub-stoichiometrically labeled  $\alpha$ -synuclein oligomers determined by single-molecule photobleaching, *Angew. Chemie - Int. Ed.* 51 (2012) 8821–8824. doi:10.1002/anie.201200813.
- [34] D. Pinotsi, A.K. Buell, C. Galvagnion, C.M. Dobson, G.S. Kaminski Schierle, C.F. Kaminski, Direct observation of heterogeneous amyloid fibril growth kinetics via two-color super-resolution microscopy, *Nano Lett.* 14 (2014) 339–345. doi:10.1021/nl4041093.
- [35] M.M. Wördehoff, O. Bannach, H. Shaykhalishahi, A. Kulawik, S. Schiefer, D. Willbold, et al., Single Fibril Growth Kinetics of  $\alpha$ -Synuclein, *J. Mol. Biol.* 427 (2015) 1428–1435. doi:10.1016/j.jmb.2015.01.020.
- [36] L.D. Hughes, R.J. Rawle, S.G. Boxer, Choose your label wisely: Water-soluble fluorophores often interact with lipid bilayers, *PLoS One*. (2014). doi:10.1371/journal.pone.0087649.
- [37] V.V. Shvadchak, M.M.A.E. Claessens, V. Subramaniam, Fibril Breaking Accelerates  $\alpha$ -Synuclein Fibrillization, *J. Phys. Chem. B.* 119 (2015) 1912–1918. doi:10.1021/jp5111604.
- [38] A. Sidhu, I. Segers-Nolten, V. Subramaniam, Solution conditions define morphological homogeneity of  $\alpha$ -synuclein fibrils, *Biochim. Biophys. Acta.* 1844 (2014) 2127–2134. doi:10.1016/j.bbapap.2014.09.007.
- [39] J. Adamcik, R. Mezzenga, Adjustable twisting periodic pitch of amyloid fibrils, *Soft Matter*. 7 (2011) 5437. doi:10.1039/c1sm05382e.
- [40] J.C. Rochet, K.A. Conway, P.T. Lansbury, Inhibition of fibrillization and accumulation of prefibrillar oligomers in mixtures of human and mouse  $\alpha$ -synuclein, *Biochemistry*. 39 (2000) 10619–10626. doi:10.1021/bi001315u.
- [41] M.M. Apetri, R. Harkes, V. Subramaniam, G.W. Canters, T. Schmidt, T.J. Aartsma, Direct Observation of  $\alpha$ -Synuclein Amyloid Aggregates in Endocytic Vesicles of Neuroblastoma Cells, *PLoS One*. 11 (2016) e0153020. doi:10.1371/journal.pone.0153020.
- [42] R. Khurana, C. Ionescu-Zanetti, M. Pope, et al., A general model for amyloid fibril assembly based on morphological studies using atomic force microscopy, *Biophys. J.* 85 (2003) 1135–44. doi:10.1016/S0006-3495(03)74550-0.
- [43] L. Bousset, L. Pieri, G. Ruiz-Arlandis, J. Gath, P.H. Jensen, B. Habenstein, et al., Structural and functional characterization of two  $\alpha$ -synuclein strains, *Nat. Commun.* 4 (2013) 2575. doi:10.1038/ncomms3575.
- [44] L. Nielsen, S. Frokjaer, J. Brange, V.N. Uversky, A. L. Fink, Probing the mechanism of insulin fibril formation with insulin mutants, *Biochemistry*. 40 (2001) 8397–8409.



doi:10.1021/bi0105983.

- [45] Z. Qin, D. Hu, S. Han, D.-P. Hong, A.L. Fink, Role of different regions of alpha-synuclein in the assembly of fibrils, *Biochemistry*. 46 (2007) 13322–13330. doi:10.1021/bi7014053.
- [46] M. Vilar, H.-T. Chou, T. Lührs, S.K. Maji, D. Riek-Loher, R. Verel, et al., The fold of alpha-synuclein fibrils, *Proc. Natl. Acad. Sci. U. S. A.* 105 (2008) 8637–8642. doi:10.1073/pnas.0712179105.

## 2.7. Supporting information

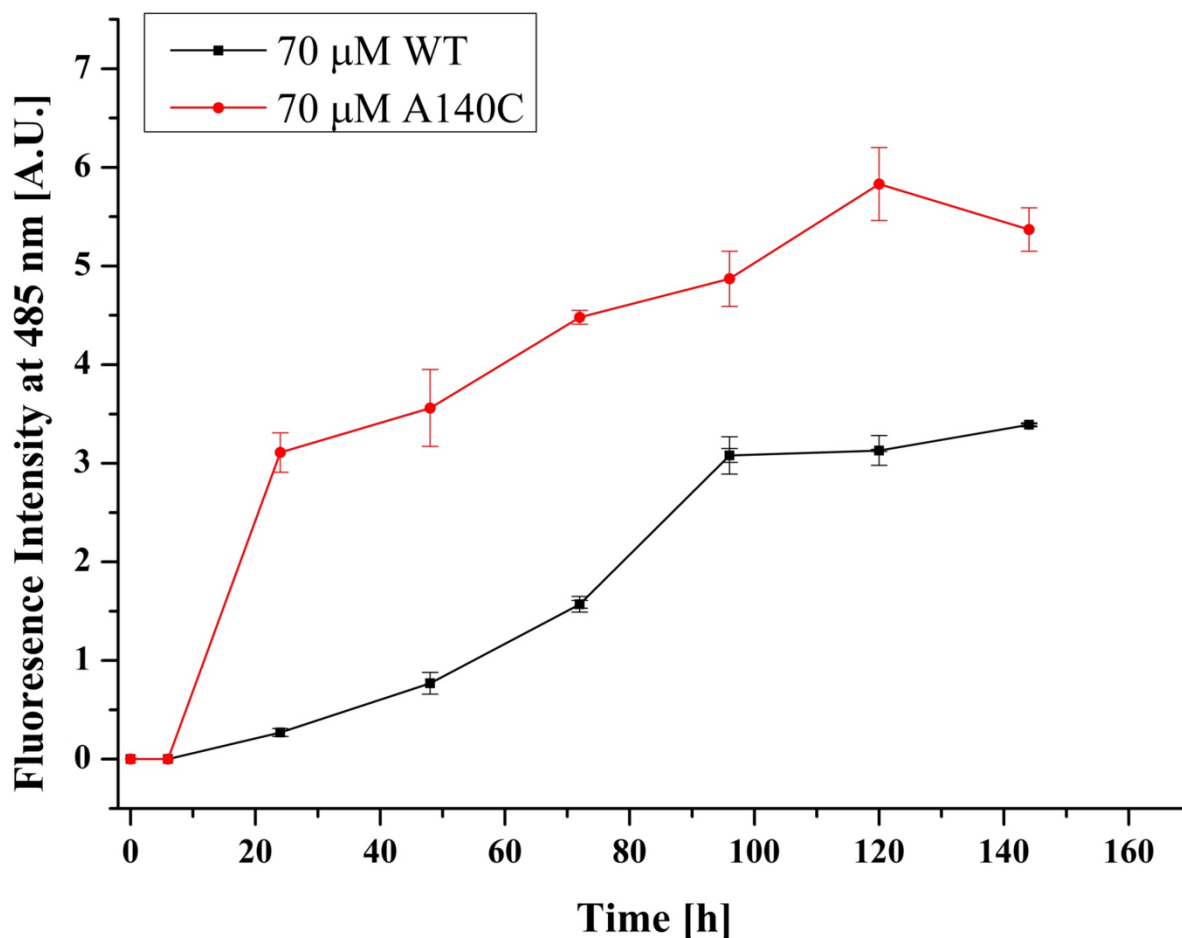


Figure S.2.1: Typical kinetics of WT  $\alpha$ -syn (in black) and A140C  $\alpha$ -syn (in red) aggregation measured by ThT fluorescence. 70  $\mu$ M WT and A140C  $\alpha$ -syn samples were aged in 6 mM phosphate buffer at pH 7.4 with 0.1 mM EDTA, 1 mM DTT (only in case of A140C  $\alpha$ -syn) under constant shaking of 1,000 rpm, 37°C, for 120-144 h. The red and black lines are guide for the eyes. Error bars denote standard deviation between triplicates.

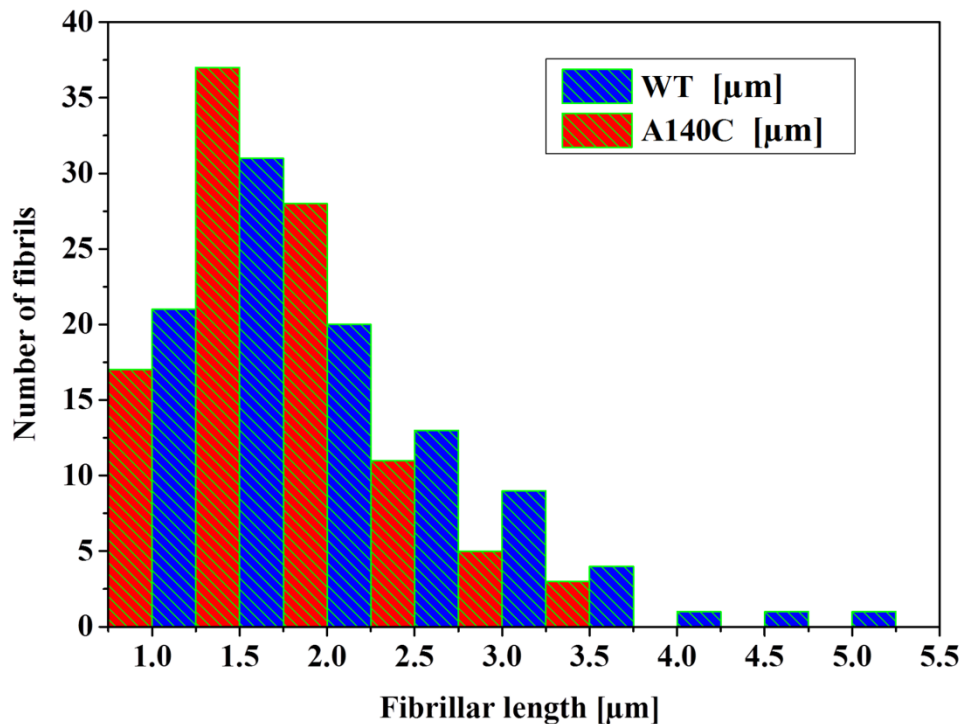
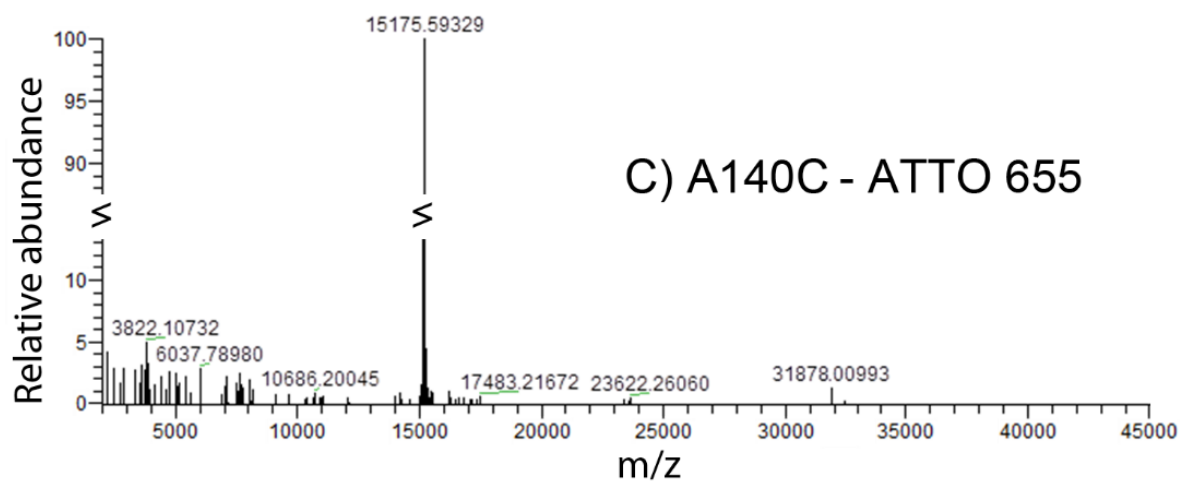
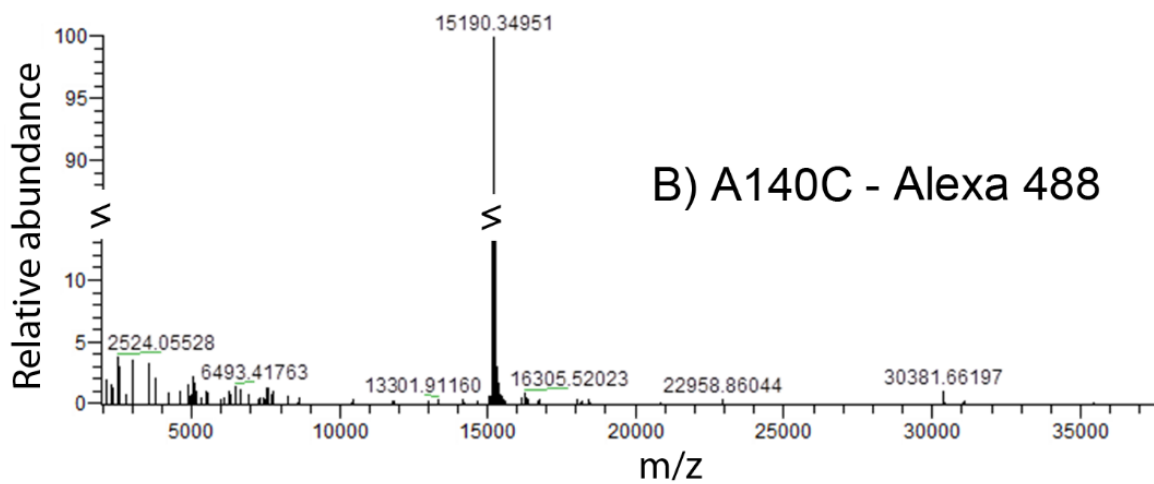
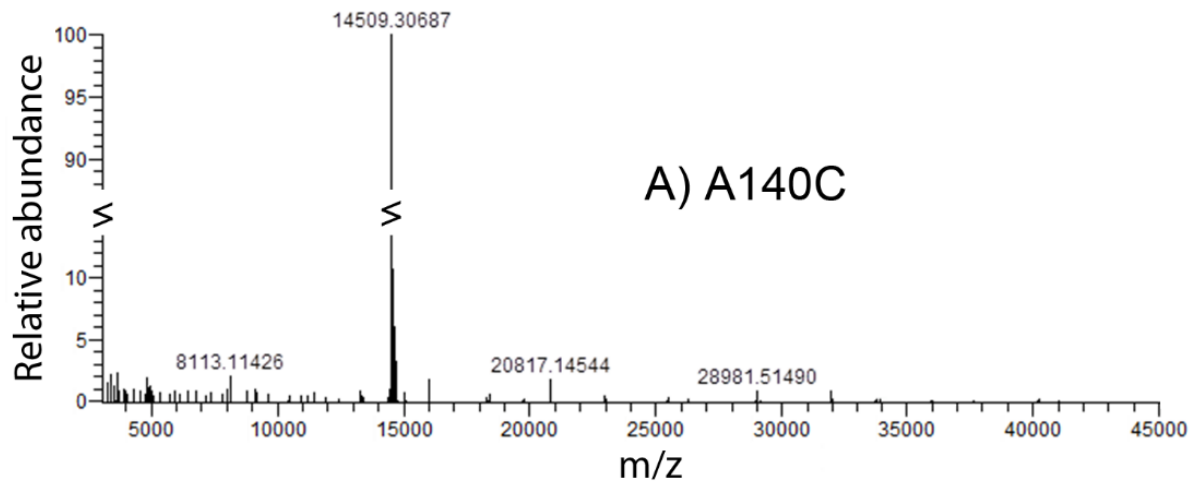


Figure S.2.2: Histogram of the WT (in blue) and A140C (in red)  $\alpha$ -syn fibrillar length distribution on approximately 100 fibrils. 70  $\mu\text{M}$  WT and A140C  $\alpha$ -syn fibrils were prepared in 6 mM phosphate buffer at pH 7.4 with 0.1 mM EDTA, 1 mM DTT (only in case of A140C  $\alpha$ -syn) under constant shaking of 1,000 rpm, 37°C, for 120-144 h. Samples were imaged by tapping mode AFM and for fibril length estimate ImageJ (Plugins-Segmentation-Single Neurite Tracer) was used.

**Mass spectrometry data for various  $\alpha$ -synuclein moieties:**

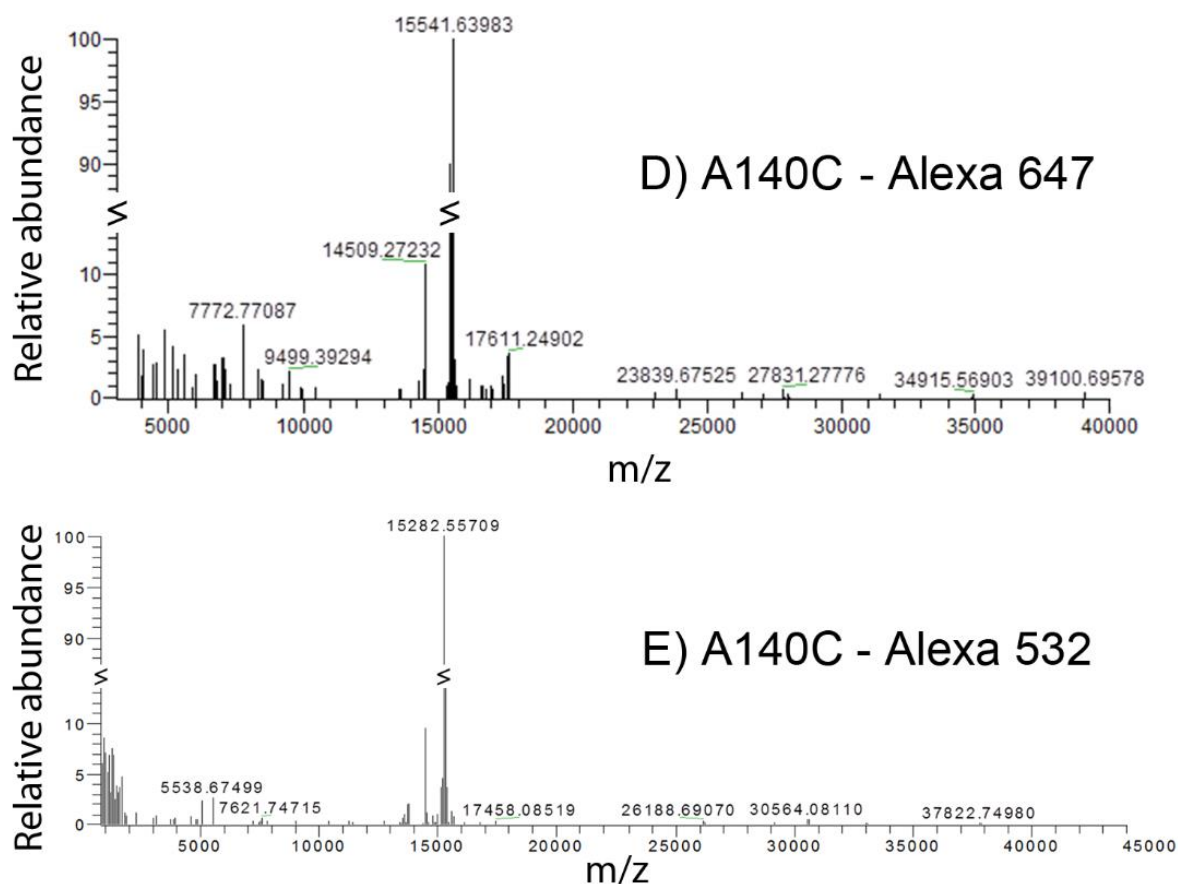


Figure S.2.3: Mass spectra of A140C  $\alpha$ -syn mutant (A), where dominant peak at 14 509.3 Dalton indicates that starting material is purely monomeric; A140C-Alexa 488 maleimide  $\alpha$ -syn (B); A140C-ATTO 655 maleimide  $\alpha$ -syn (C); A140C-Alexa 647 maleimide  $\alpha$ -syn (D); A140C-Alexa 532 maleimide  $\alpha$ -syn (E), show mass spectra of  $\alpha$ -syn after fluorescent labeling and dominant presence of labeled monomeric species. Electrospray mass spectroscopy (ESI-MS) on LTQ-Orbitrap hybrid mass spectrometer (Thermo Fisher) was used for analyzing the samples by direct injection of 200  $\mu$ l sample in 50  $\mu$ l acetonitrile/miliQ/formic acid (50:50:0.1 v/v/v). Spectra were analyzed using Xcalibur software. No significant mass components were observed beyond the mass range in the figures.

# Early events in $\alpha$ -synuclein aggregation<sup>1</sup>

### Abstract

Aggregation of  $\alpha$ -synuclein ( $\alpha$ -syn) followed by amyloid fibril formation and progressive neurodegeneration is one of the neuropathological hallmarks of Parkinson's disease (PD). Oligomeric forms of  $\alpha$ -syn appear to be the key factor in pathogenesis of PD. A detailed mechanism of  $\alpha$ -syn aggregation and the nature of the oligomeric species, however, remain unknown. In this study we followed the early events in  $\alpha$ -syn aggregation by gel electrophoresis and by fluorescence correlation spectroscopy (FCS). We observed formation of the dimer and tetramer of  $\alpha$ -syn by sensitive gel imaging based on fluorescence detection. The presence and the stoichiometry of these early species were confirmed by FCS and mass spectrometry (MS). Moreover, we tracked the accumulation of these early oligomeric species in time which suggests their conversion to or incorporation into larger aggregates.

---

<sup>1</sup> This chapter is based on a manuscript in preparation for publication: M. Mučibabić, D. Vliegthart, H. van den Elst, H. Overkleeft, G. W. Canters, and T. J. Aartsma.

### 3.1. Introduction

While describing the symptoms of shaking palsy in 1817, James Parkinson hoped for a prompt elucidation of the underlying mechanism of the disease [1]. Almost a century later a big step towards the better understanding of it was made by Fritz Jakob Heinrich Lewy, who identified in the postmortem brain tissue the insoluble cellular inclusions, the so-called Lewy bodies [2], that are a characteristic of Parkinson's disease (PD). In 1997 Polymeropoulos and coworkers found a rare mutation (Ala53Thr) in the  $\alpha$ -syn gene (SNCA) to be the cause of a familiar form of PD [3]. In the same year Spillantini and her colleagues found that both Lewy bodies and neurites were immunoreactive for  $\alpha$ -syn [4]. They subsequently discovered unbranched  $\alpha$ -syn fibrils [5] in Lewy bodies and neurites using electron microscopy (EM). Like other amyloids,  $\alpha$ -syn fibrils have a cross  $\beta$ -structure [6], a typical length of several microns [7] and a diameter of about 10 nm. Based on solid-state nuclear magnetic resonance a model of the  $\alpha$ -syn fibril core was proposed consisting of a sandwich-like structure made up of five  $\beta$ -strands [8].

The formation of  $\alpha$ -syn fibrils involves the nucleation-polymerization process [9] that starts with the formation of oligomers from monomeric protein. Although a significant research effort was invested in characterizing the monomeric form of  $\alpha$ -syn, as well as  $\alpha$ -syn fibrils, the nature and role of intermediary oligomers in the transition from monomers to fibrils remain largely a mystery. A number of *in vitro* studies were performed in order to stabilize such oligomers [10,11] and make them available for further characterization. Preparation protocols include the addition of dopamine [12,13], lipids [14], organic solvents [10] or metal ions [10,11]. These factors are known to promote the formation of  $\alpha$ -syn oligomers, the shape of which may vary, ranging from spherical [15] to annular [10] depending on the preparation protocol. Chains of spheres [16] have been observed as well under a particular set of conditions. Oligomers can be imaged by atomic force microscopy (AFM) and/or EM. Their height is typically between 2 and 10 nm [15,16], but can extend to 30 nm depending on the preparation protocol [17]. Some studies suggest that prolonged incubation promotes the formation of annular shaped oligomers [18]. It has been shown that stirring or shaking promotes heterogeneity among oligomers [19]. It is difficult, however, to determine whether or not these oligomers are on-pathway of fibril formation. On the other hand, growing evidence suggests that oligomers are cytotoxic [20,21] and play an important role in the development of amyloid diseases [22,23].

A detailed characterization of the mechanism of  $\alpha$ -syn aggregation and toxicity of the formed species is crucial for understanding the pathology of PD. The logical first step in oligomerization is the formation of a dimeric  $\alpha$ -syn encounter complex. It is now well-established that oxidizing conditions promote the formation of  $\alpha$ -syn covalent dimers [24]. In particular, it was found that the presence of  $\text{CO}_3^{\cdot-}$  and  $\text{NO}_2^{\cdot}$  radicals leads to the formation of a covalent dityrosine bond between  $\alpha$ -syn molecules [25], thereby enhancing aggregation. This is particularly interesting because of the increasing evidence [26] that oxidative stress, for example through formation of reactive oxygen species by mitochondrial dysfunction, is an important factor in the pathogenesis of PD. Oxidative conditions appear to accelerate the aggregation reaction [24,26] and it has been claimed that dimer formation is the rate-limiting step in the formation of  $\alpha$ -syn fibrils. Importantly, Roostae et al. [27] showed that the resulting  $\alpha$ -syn pre-fibrillar aggregates are indeed neurotoxic when injected into the hippocampus of wild-type mice.

Although the  $\alpha$ -syn protein contains 4 tyrosine residues (Y39, Y125, Y133 and Y136), Van Maarschalkerweerd et al. [28] recently showed that it is specifically residue Y39 that appears to be directly involved in linking  $\alpha$ -syn molecules. They demonstrated by mass spectrometry that dityrosine-linked dimers of  $\alpha$ -syn were formed during chromatography under ambient conditions. Apparently, oxidative or nitrating agents are not required for dimer formation, and it is suggested that  $\alpha$ -syn is more prone to chemical modification than previously assumed [26].

Attempts to directly observe  $\alpha$ -syn multimers, for example in a gel, have so far met with little success. Here, we report the spontaneous formation of stable dimers and tetramers in carefully prepared solutions of monomeric  $\alpha$ -syn. The process could be followed by gel electrophoresis. Rapid accumulation of multimeric species in time was observed, with the tetramer appearing later than the dimer. The decrease of dimers and tetramers at later times suggests that the early multimeric species are incorporated into larger aggregates, and possibly are precursors for fibril formation.

## **3.2. Materials and Methods**

### **3.2.1. Protein preparation and purification**

Protein preparation and purification of WT, A53T, A140C and A53T A140C  $\alpha$ -syn followed protocols that have been described elsewhere [29]. *E. coli* BL21 (DE3) was transformed with

the pT7-7 plasmid carrying the  $\alpha$ -syn gene and cultured in lysogeny broth medium with 100  $\mu$ g/ml ampicillin. After isopropylthio- $\beta$ -galactoside induction (1 mM, 4 h) bacterial cell pellets were harvested by centrifugation ( $6,000 \times g$ , 10 min), resuspended in 10 mM Tris-HCl, pH 8.0, 1 mM EDTA and 1mM PMSF (10% of the culture volume) and stirred for 1 h at 4°C. Cells were lysed by sonication for 2 min and then centrifuged ( $10,000 \times g$ , 20 min, 4°C).

DNA was precipitated from the cell extract by adding streptomycin sulfate (1%, 15 min, 4°C) and removed by centrifugation at  $13,500 \times g$  for 30 min. Then  $\alpha$ -syn was salted out from the solution by slow addition of 0.295 g/ml of ammonium sulfate and mild stirring for 1 h at 4°C. Precipitated protein was collected by centrifugation ( $13,500 \times g$ , 30 min, 4°C). The pellet was gently resuspended 10 mM Tris-HCl, pH 7.4 and filtered through 0.22  $\mu$ m filter. The solution was loaded onto a 6 ml ResourceQ anion exchange column (GE Healthcare) using an Äkta Purifier system (GE Healthcare) and a linear gradient of NaCl (0–500 mM) in 10 mM Tris-HCl, pH 7.4 at a flow-rate of 3 ml/min (for purification of  $\alpha$ -syn-A140C both buffers contained 1 mM dithiothreitol (DTT) to avoid the formation of disulfide bridges). Fractions containing  $\alpha$ -syn (eluted at  $\sim 300$  mM NaCl) were pooled, concentrated (Vivaspin-20, 10 kDa; GE Healthcare) and then desalted with a PD-10 column (GE Healthcare) using 10 mM Tris-HCl pH 7.4 (containing 1 mM DTT in the case of the cysteine mutants A140C and A53T A140C). Protein concentration was determined on the basis of the tyrosine absorption at 275 nm by using  $5600 \text{ M}^{-1}\text{cm}^{-1}$  for the extinction coefficient of WT and A53T and  $5745 \text{ M}^{-1}\text{cm}^{-1}$  of A140C and A53T A140C  $\alpha$ -syn [28].

### 3.2.2. Protein labeling

Prior to labeling, the  $\alpha$ -syn mutant A140C was incubated with a 5-fold molar excess of DTT for 30 min to reduce possible disulfide bonds. DTT was removed using Zeba Spin desalting columns (Pierce, Rockford, IL, USA). A volume of 0.5–1 ml of 140  $\mu$ M A140C  $\alpha$ -syn was incubated overnight at 4°C with 4-fold molar excess ATTO 655 maleimide. Afterwards, the excess of free dye was removed using two desalting steps on Zeba Spin desalting columns. The labeling efficiency was higher than 95% for all samples, confirmed by using mass spectrometry (MS), gel electrophoresis and as calculated from the absorbance of the labeled sample. The concentration of labeled protein was estimated using the absorbance of ATTO 655 maleimide ( $\epsilon_{663} = 125,000 \text{ cm}^{-1}\text{M}^{-1}$ ) in 6 mM phosphate buffer at pH 7.4. ATTO 655 maleimide was purchased from ATTO-TEC GmbH, Siegen, Germany.



### 3.2.3. Mass spectroscopy

Electrospray mass spectroscopy (ESI-MS) on an LTQ-Orbitrap hybrid mass spectrometer (Thermo Fisher) was used for analyzing samples. Direct injection of 200  $\mu$ l sample in 50  $\mu$ l acetonitrile/milliQ/formic acid (50:50:0.1 v/v/v) was applied. Spectra were analyzed using Xcalibur software.

### 3.2.4. The process of fibrillization

Aggregation experiments were performed in 6 mM sodium phosphate, pH 7.4 containing 9 mM sodium azide ( $\text{NaN}_3$ ) and 0.1 mM EDTA. The total protein concentration was 350  $\mu$ M. The WT  $\alpha$ -syn sample was mixed with 5% A140C-ATTO 655  $\alpha$ -syn, while in the case of the A53T mutant the sample contained 1.5% A53T A140C-ATTO 655  $\alpha$ -syn. All reactions were performed in 1.5 ml Protein Low Binding Tubes (Sigma-Aldrich). All reactions were performed in 200  $\mu$ l solutions contained in 1.5 ml Protein Low Binding Tubes (Sigma-Aldrich) in dark, without shaking at 37°C. Aliquots were taken at several time points between 0 and 432 h, immediately flash frozen, and kept at -80°C for further experiments.

### 3.2.5. Thioflavin T (ThT) assay

The fluorescence increase of ThT upon binding to the  $\beta$ -sheet secondary structure was used as an indicator of the protein aggregation state. A stock solution of 1 mM ThT was prepared in 6 mM sodium phosphate buffer pH 7.4 and filtered using a 0.22  $\mu$ m syringe filter. A total of 4  $\mu$ l aliquots of aggregated mixture were added to 996  $\mu$ l of a 10  $\mu$ M ThT solution in 6 mM phosphate buffer pH 7.4.

The probe was excited at 446 nm in a fluorescence spectrophotometer (Cary Eclipse, Varian Inc., Palo Alto, CA, USA), and emission spectra were recorded from 400 to 600 nm using an optical band width of 10 nm. The fluorescence spectrum of ThT in pure buffer was subtracted from each spectrum. ThT fluorescence detected aggregation curves were made by plotting the emission signals at 485 nm on y-axis vs the aggregation time on x-axis. All measurements were performed in triplicate.

### 3.2.6. Glass cover slip cleaning procedure

Cover slips (25 mm, 0.16-0.19 mm thick, Gerhard Menzel GmbH, Germany) were cleaned using 30 min sonication first in acetone and then in 4 M sodium hydroxide. In between these

steps cover slips were thoroughly rinsed and sonicated in milliQ for 30 minutes. Cover slips were ozone cleaned for 30 min prior to use.

### 3.2.7. Polyacrylamide gel electrophoresis

Polyacrylamide gel electrophoresis was used to analyze the species formed during the fibrillization process. Before loading on the gel the WT + 5% A140C-ATTO 655  $\alpha$ -syn samples were diluted to 125  $\mu$ g/ml in 50 mM TRIS pH 6.8, 25% glycerol. In the case of A53T + 1.5% A53T-A140C  $\alpha$ -syn samples were diluted to 37.5  $\mu$ g/ml. It should be noted that we did not use SDS and  $\beta$ -mercaptoethanol in the buffer, nor did we preheat the samples. The 400 mA constant current was applied while running 12% Mini Protean TGX gels for 50 min (BioRad, Hercules, California, United States). Electrophoresed gels were visualized with a gel imager (Typhoon 9400, GE Healthcare, Waukesha, WI, USA) using 633 nm excitation.

### 3.2.8. Fluorescence Correlation Spectroscopy in gel

For FCS measurements *in situ*, the band corresponding to specific  $\alpha$ -syn aggregates was excised from the gel, put on a cleaned glass coverslip and placed on the microscope stage of a home-built confocal microscope. In all cases the  $\alpha$ -syn sample concentration was adjusted to have less than one molecule in the confocal volume in order to optimize the conditions for FCS. The microscope was equipped with a 635 nm diode laser (Power Technology, Little Rock, AR, USA) and a 488 nm diode laser (Power Technology, Little Rock, AR, USA) for excitation of the sample. Each of the two laser beams was passed through a narrow band pass filter centered at the laser wavelength, after which the two beams were adjusted for spatial overlap using a dichroic mirror and focused into a single-mode optical fiber for obtaining a clean gaussian beam profile. The gaussian beam was focussed on the sample by a 60 $\times$  water-immersion objective (NA = 1.2, Olympus, Zoeterwoude, The Netherlands). The epifluorescent light, collected by the objective, was focussed on a 50  $\mu$ m pinhole for spatial filtering, recollimated and then passed through a dichroic mirror for separating the 488 nm and 635 nm fluorescent light. The two fluorescence beams were then separately focussed on single-photon avalanche photodiodes (SPCM AQRH-15, Perkin Elmer Inc., USA). The signal from the photodiodes was processed by a TimeHarp200 counting board (PicoQuant GmbH, Berlin, Germany). In a typical experiment, FCS time traces were recorded during 5 min at ambient temperature. The FCS traces were analyzed using the SymphoTime software

package (PicoQuant, GmbH, Berlin, Germany). The data obtained was fitted to the following equation:

$$G(t) = G(0) * G_{diff}(t) * G_1(t) \quad (3.1)$$

$$G_1(t) = \frac{1 - F_1 + F_1 e^{-t/t_1}}{1 - F_1} \quad (3.2a)$$

$$G_{diff}(t) = \frac{1}{\langle N \rangle} \left( 1 + \frac{4Dt}{w_0^2} \right)^{-1} \left( 1 + \frac{4Dt}{k^2 w_0^2} \right)^{-\frac{1}{2}} \quad (3.2b)$$

where,  $k = \frac{z_0}{w_0}$ , and

$$G(0) = \frac{1}{\langle N \rangle} = \frac{1}{c * V_{eff} * N_A} \quad (3.3)$$

$G(t)$  is the autocorrelation function,  $G_1(t)$  relates to zero-order reactions such as fluorophore blinking,  $G_{diff}(t)$  accounts for the diffusion component of the autocorrelation function,  $G(0)$  is a constant which depends on the average number of molecules in the confocal volume,  $F_1$  is the fraction of molecules associated with such process,  $t_1$  is the relaxation time required for the reaction,  $k$  is the eccentricity of the confocal volume,  $w_0$  and  $z_0$  are the lateral and axial  $1/e^2$  radius respectively,  $\langle N \rangle$  corresponds to the average number of molecules in the confocal volume, and  $D$  the diffusion coefficient of the fluorescent molecule,  $V_{eff}$  represents the effective volume,  $c$  sample concentration and  $N_A$  Avogadro's number. We obtained the values for  $k$ ,  $w_0$  and  $z_0$  experimentally using the well-known diffusion coefficient of the ATTO 655 fluorophore in aqueous solution, following the protocol described in reference [30].

### 3.3. Results

#### 3.3.1. A140C $\alpha$ -syn mutant testing and preparation for further use

To follow early events in  $\alpha$ -syn aggregation by fluorescence detection it is necessary to fluorescently label the protein. We chose to have one fluorescent dye-molecule per  $\alpha$ -syn monomer by specific labeling of an exposed cysteine residue using maleimide-thiol

chemistry. Since, WT  $\alpha$ -syn does not contain a cysteine we used the A140C  $\alpha$ -syn mutant for labeling of the protein at the end of the carboxyl terminus. Prior to labeling the A140C  $\alpha$ -syn sample was purified to remove any possible aggregates. The purity of the sample was checked by mass spectrometry (MS). In the mass spectrum after purification, shown Figure 3.1A, the peak at 14.509 kD, corresponding to  $\alpha$ -syn monomer, was dominant. Mass peaks from  $\alpha$ -syn multimers were absent. A small extra peak at 8.113 kD is probably due to a degradation product of the A140C  $\alpha$ -syn monomer. This small component was removed by separation using size-based filtration. Thus, the starting material did not contain multimeric species of A140C  $\alpha$ -syn.

To be able to follow the early events in aggregation of  $\alpha$ -syn samples using fluorescence detection the A140C  $\alpha$ -syn mutant protein was specifically labeled with the ATTO 655 maleimide fluorophore. Before the aggregation step, the fluorescently labeled A140C  $\alpha$ -syn sample was also purified and subsequently checked by MS (Figure 3.1B). The peak at 15.18 kD confirmed that monomeric A140C  $\alpha$ -syn, fluorescently labeled with ATTO 655, was dominant in the spectrum. No peaks of higher mass were observed. Also in this case traces of lower molecular weight peaks were present, probably from degradation products which were then removed by size filtration. The labeled sample of A140C-ATTO 655  $\alpha$ -syn was further checked for purity by gel electrophoresis. The gel showed a single band which corresponded to the molecular weight of the labeled  $\alpha$ -syn monomer (see Figure 3.2A).

To make a calibration curve of A140C-ATTO 655  $\alpha$ -syn monomer concentrations ranging from 50 to 0.25 nM were loaded onto the gel. The relative intensities of the monomer band from each lane were measured and are plotted in Figure 3.2C which shows a nonlinear correlation between the brightness and the sample concentration. We will use this result for later reference.

### **3.3.2. Early $\alpha$ -syn aggregated species separated by polyacrylamide gel electrophoresis**

In a series of aggregation experiments of fluorescently labeled  $\alpha$ -syn we analyzed the sample composition as a function of time by gel electrophoresis. By this method fluorescent staining of the gel after electrophoresis is avoided, and, more importantly, enhanced sensitivity of detection can be achieved. These experiments required well-defined starting material which was prepared and verified as described in the previous section. The corollary is that our starting material of labeled  $\alpha$ -syn was exclusively in the monomeric form.

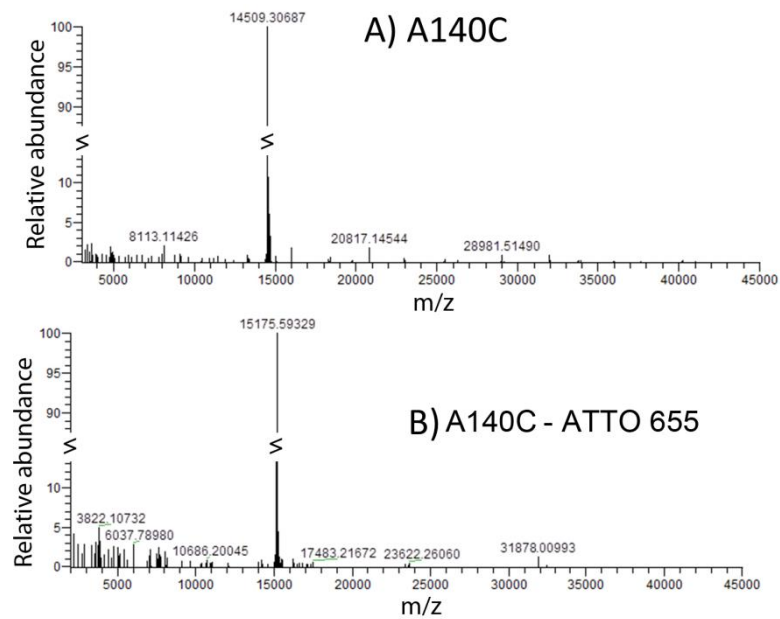


**Figure 3.1:** Mass spectrum of A140C  $\alpha$ -syn (A), where the dominant peak at 14.509 kD represents  $\alpha$ -syn monomer and of A140C-ATTO 655 (B), where the main peak at 15.175 kD corresponds to  $\alpha$ -syn monomers labeled with ATTO 655 fluorescent dye.

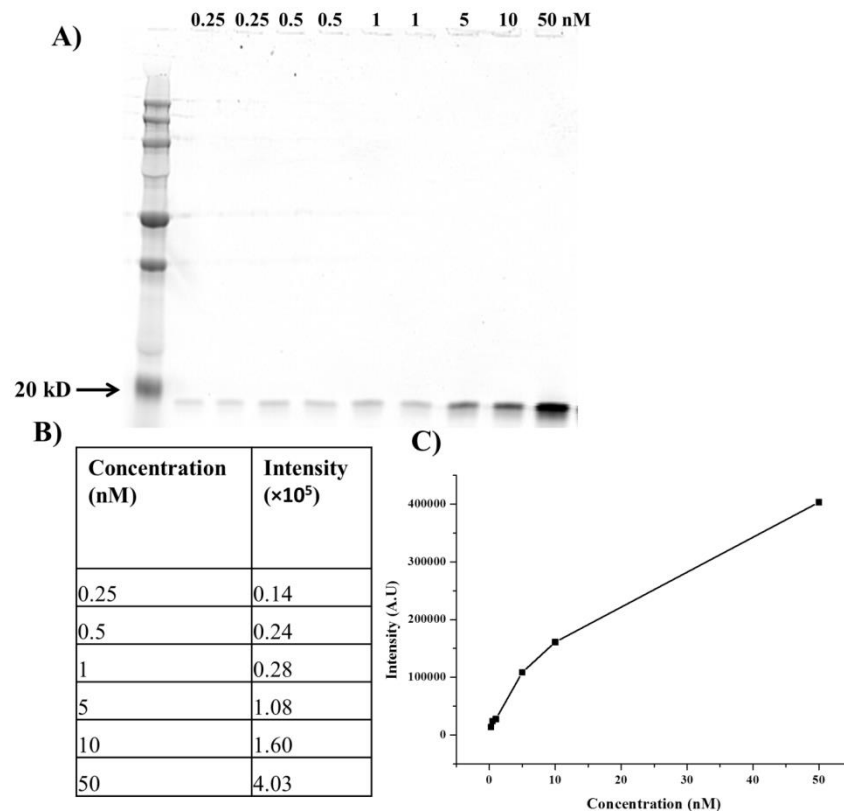


**Figure 3.2:** Quantification of the  $\alpha$ -syn monomer band at  $t = 0$  h in electrophoresed gel in the concentration range of 50 to 0.25 nM A140C-ATTO 655  $\alpha$ -syn (A). Intensities of the bands calculated by ImageJ (B) and presented in the table as a function of  $\alpha$ -syn concentration. Intensity data shown in the table (B) were plotted against the sample concentration (C), solid dots; the black line is a visual guide.

A drawback of using fluorescently labeled  $\alpha$ -syn is the potential effect of the label on the aggregation properties of the protein. Indeed, we showed in Chapter 2 that the morphology of  $\alpha$ -syn fibrils is affected in mixtures of fluorescently labeled and WT  $\alpha$ -syn [29]. The effect becomes more pronounced with increasing fractions of labeled  $\alpha$ -syn in the sample. For this reason the experiments described here were performed with a mixture of A140C-ATTO 655 and WT  $\alpha$ -syn in a ratio of 20:1 by which this effect is negligible.

Samples of this mixture were aged at 37°C in the dark without shaking, in parallel with a sample of WT  $\alpha$ -syn only. Aliquots were taken at regular intervals and flash frozen at -80°C for later analysis. Right after collecting every aliquot, a conventional ThT fluorescence assay was carried out on the WT-only  $\alpha$ -syn sample to assess its aggregation state. Once the ThT fluorescent signal reached the plateau phase, aggregation of the samples was terminated.

At this stage all aliquots of the aggregated, partially labeled, WT  $\alpha$ -syn samples were analyzed in parallel by gel electrophoresis. In parallel with the aggregated  $\alpha$ -syn samples a set of fluorescently marked proteins (Precision Plus Protein Dual Xtra standard, Bio Rad) was loaded in a separate lane of the gel as a reference for the molecular weight. The gel was imaged using 633 nm excitation on a scanning Typhoon 9400 imager which offers high spatial resolution with significantly enhanced sensitivity compared to conventional imagers where gels are stained with common fluorescent dyes and imaged by a standard camera. The bands in the gel were analyzed for brightness with ImageJ software (developed by National Institute of Health, USA).

The results for the WT  $\alpha$ -syn samples mixed with 5% A140C-ATTO 655 are shown in Figure 3.3A, where each lane is from an aliquot at a different time point in the aggregation process. The lane at 0 h shows a single band with a molecular weight below 20 kD compare to the marker (M) in the far left lane (see Figure 3.3). This band is attributed to the labeled  $\alpha$ -syn monomer (Figure 3.2A).

From 14 h onwards additional bands appeared in the gel at higher mass (red and blue arrows in Figure 3.3A). Although much weaker than the monomer band, they are very distinct as shown in the integrated intensity profile of the lane at 14 h (see Figure 3.3B). Compared to the marker M (far left lane, Figure 3.3A), the molecular weights of these species are around 40 and 80 kD, respectively. Although these numbers are not precise, the observed mass ratio

leads to the tentative conclusion that these additional bands correspond to the dimer and tetramer of  $\alpha$ -syn.

The intensity of the dimer band as a function of time (red line, Figure 3.3C) shows a steady increase in the first 24 h and then decreases gradually. The time profile suggests that one of the possibilities is that the dimer is incorporated into larger aggregates, likely the tetramer. Incorporation of dimer into larger aggregates must be rather efficient since it out-competes the rate of dimer formation. From the intensity calibration plot in Figure 3.2B we estimate that the dimer content after 24 h corresponds to an equivalent concentration of about 5 nM  $\alpha$ -syn monomers.

The time profile of the tetramer band is very different from that of the dimer; its appearance is delayed with respect to the dimer band and levels off at the time scale of the experiment (blue line, Figure 3.3C). The intensity of the tetramer band from 120 h onwards shows that it amounts to an equivalent concentration of about 75 nM  $\alpha$ -syn monomers, much higher than that of the dimer species at its maximum.

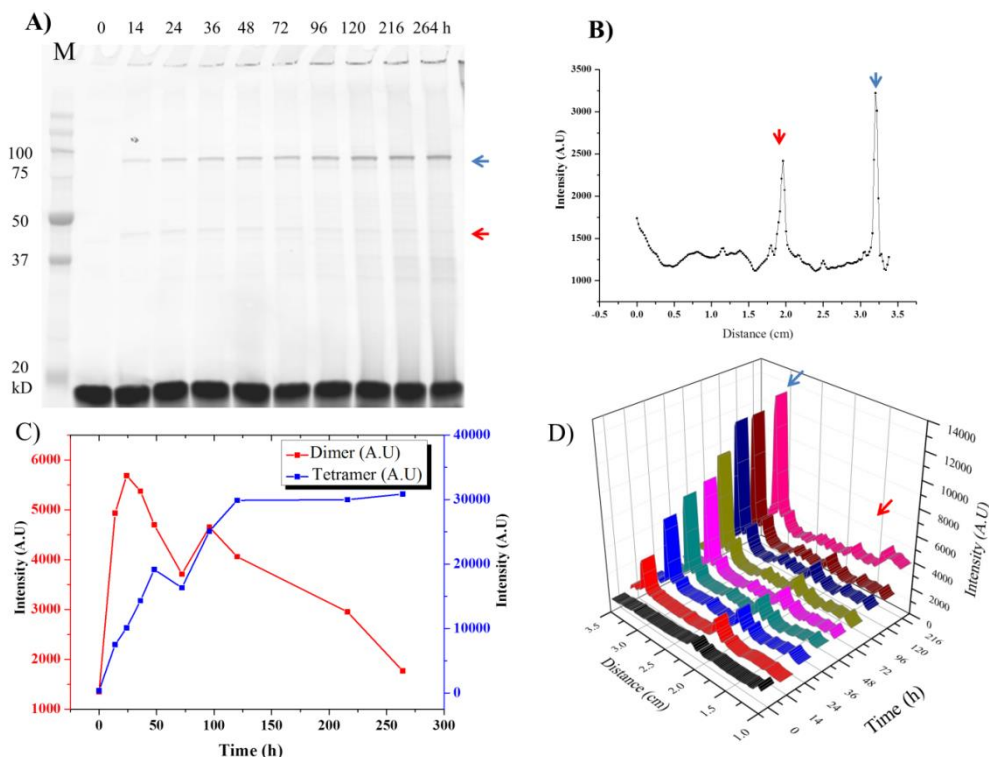


**Figure 3.3:** Electrophoresed polyacrylamide gel of aged WT+5% A140C-ATTO 655  $\alpha$ -syn (A) and intensity plot of dimer and tetramer after 14 h (B), followed by intensity plot of the whole time profile of dimer and tetramer of  $\alpha$ -syn (C) and the distance profile of dimer and tetramer intensity for each time point (D). The dimer band is framed in red (A) and the tetramer in blue (A). The intensity of dimer reaches maximum after 24 h and decreases in time, while the increase of the tetramer band intensity levels off after 120 h.

### The A53T $\alpha$ -syn mutant

It has been reported that the aggregation of the pathogenic A53T mutant  $\alpha$ -syn is accelerated *in vitro* [3] and that it contributes to an early onset of familiar PD [31]. To test if there is a difference in the dynamics of the formation of WT the early species of A53T  $\alpha$ -syn aggregates, we aggregate A53T samples mixed with 1.5% A53T A140C-ATTO 655 at 37°C for 432 h, in parallel with A53T  $\alpha$ -syn only. Samples were treated the same way as WT  $\alpha$ -syn.

Also, in the case of A53T  $\alpha$ -syn mutant we observe distinct bands in the gel, although the background shows a significant degree of smearing, especially at the later time points of aggregation. The observed smearing can be attributed to the presence of large  $\alpha$ -syn aggregates which form much quicker in the case of the A53T  $\alpha$ -syn mutant. These large aggregates stay on top of the gel but release presumably small-sized  $\alpha$ -syn species in the course of time.

At  $t = 0$  h time we observed a single band on the electrophoresis gel (see Figure 3.4A), that can be assigned to the monomer by comparison with the molecular weight marker in the far left lane of the gel. From 14 h on additional bands are observed which also in this case are attributed to the  $\alpha$ -syn dimer and tetramer based on their apparent molecular weight. The intensity of the dimer band increases within the first 24 h, followed by a rapid decrease (Figure 3.4C). The intensity of the tetramer band increases almost at the same rate as that of the dimer, and then gradually decreases within the time frame of the experiment. In this case we also note that the intensity of the monomer band gradually decreases because of monomer depletion in the aggregation process, concomitant with an increase of the top band that represents all the species bigger than 200 kD. Comparing the intensities of A53T dimer and tetramer bands to the intensities of the pure monomer band in Figure 3.1B we found that the maximum content of dimers and tetramers is around 50 nM and 25 nM equivalent monomer concentration, respectively.

The A53T  $\alpha$ -syn mutant is known to be more prone to aggregate formation than WT  $\alpha$ -syn [3], which may explain the almost complete disappearance of, both, the dimer and the tetramer band in the mutant sample. Presumably in this case the  $\alpha$ -syn dimer and tetramer were completely incorporated into larger aggregates after 432 h. Based on the intensities of the monomer band at 0 h and at 432 h we estimated that at least 90% of A53T monomer was



consumed in the process. Monomer depletion is significantly slower in the case of WT  $\alpha$ -syn. The increase in the amount of larger aggregates, accumulated in the top of the gel, is more pronounced for the A53T  $\alpha$ -syn mutant than for WT  $\alpha$ -syn.

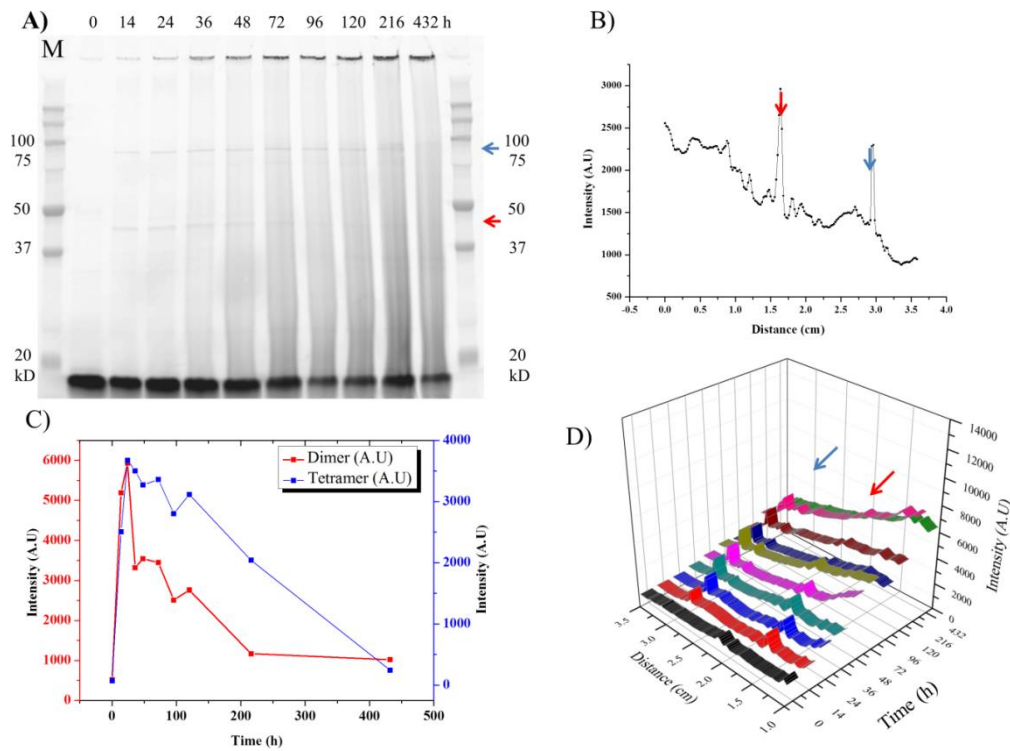


**Figure 3.4:** Electrophoresed polyacrylamide gel of aged A53T+1.5% A53T A140C-ATTO 655  $\alpha$ -syn (A) and intensity plot of dimer and tetramer after 14 h (B), followed by intensity plot of the whole time profile of dimer and tetramer of  $\alpha$ -syn (C) and the fluorescence intensity profile (raw data) of each lane in panel A. The dimer band is framed in red (A) and the tetramer in blue (A). The intensity of dimer and tetramer reaches the maximum after 36 h and then decreases in time.

### 3.3.3. Early $\alpha$ -syn aggregated species separated by mass spectrometry

The bands observed in the mass range of up to 100 kD in gel electrophoresis of labeled  $\alpha$ -syn at various stages of aggregation were tentatively attributed in the previous sections to monomer, dimer and tetramer species. The question is to what extent this observation is affected, or may be even caused by the fluorescent label, or whether it is intrinsic to  $\alpha$ -syn aggregation. To clarify this issue we aged unlabeled WT  $\alpha$ -syn for 14 h at 37°C for analysis by mass spectrometry, together with a sample taken at  $t = 0$  h. The results are shown in Figure 3.5. The mass spectrum of the 14 h sample (Figure 3.5A) shows two series of peaks which can be assigned to monomers and dimers, respectively, based on molecular weight  $M$  (in kD) and the number of elementary charges  $z$ . For example, the peak with  $M/z = 1207.3$  is

consistent with the molecular weight (14.477 kD) of an  $\alpha$ -syn monomer carrying 12 elementary charges. Similarly, the peak at of  $M/z = 1523.1$  corresponds to  $z = 19$  and  $M = 28.919$  kD, the molecular weight of an  $\alpha$ -syn dimer.

A dimer signal was also present in the reference sample at  $t = 0$  h, but with much lower amplitude compared to the aged sample. The dimer at 0 h possibly formed during the time needed for handling the sample: possibly some dimerization occurred also during the spraying of the sample. The MS data were limited to the early time points because the samples obtained at later time points coagulated and blocked the spraying nozzle, possibly because of the presence of larger aggregates.

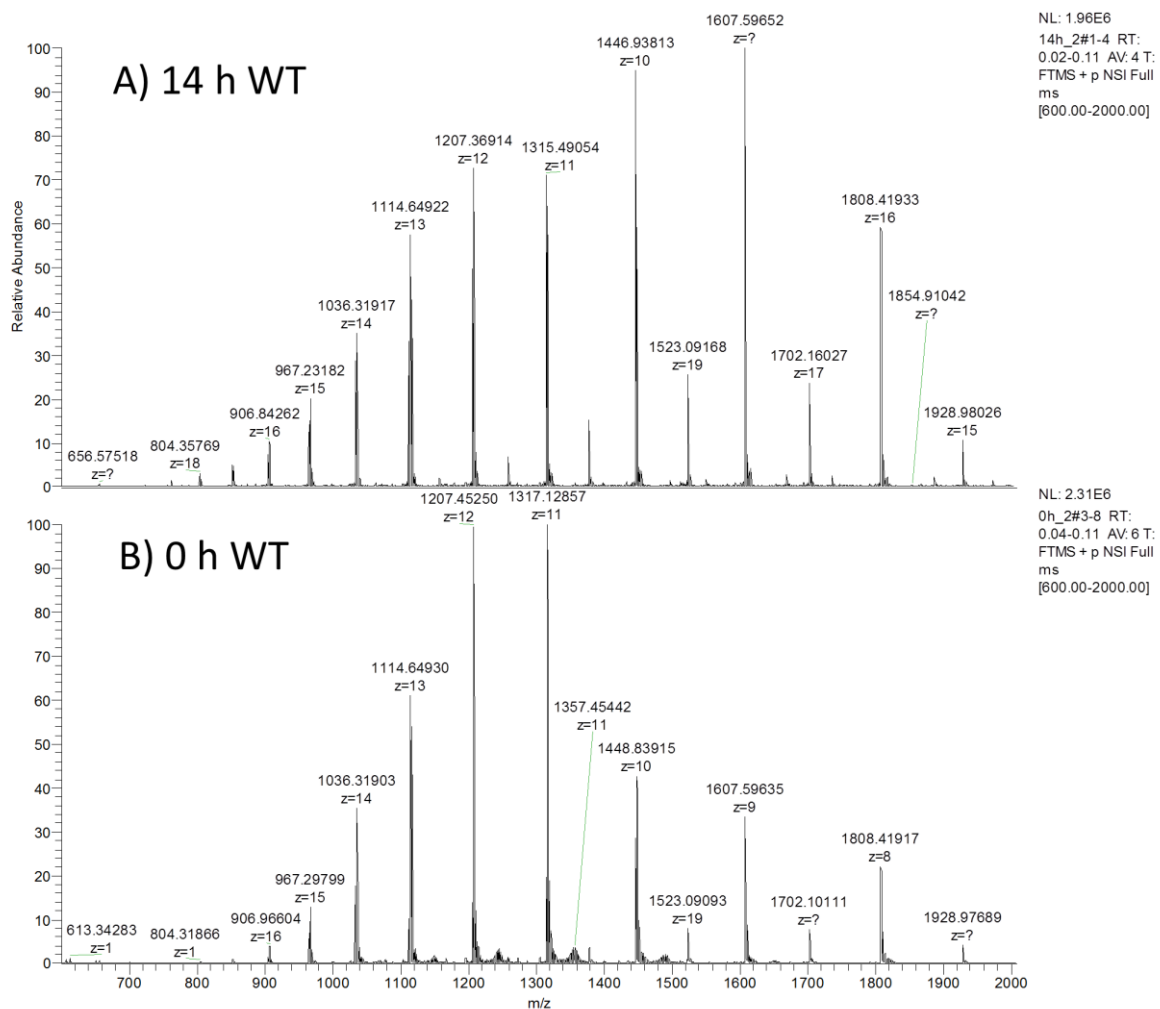


**Figure 3.5: Mass spectra of 0 (B) and 14 h WT  $\alpha$ -syn (A) where the center of  $\alpha$ -syn monomer peak has charge  $z = 12$  and dimer  $z = 19$ . Relative absorbance of dimer peak is higher at 14 h than at 0 h, indicating dimer formation in time and no influence of fluorescent probe on dimerization.**

We thus conclude that the MS data confirm the formation of dimers under the present experimental conditions, and support the assignment of the bands in the electrophoresis.

### 3.3.4. Early $\alpha$ -syn aggregated species separated by FCS

Further support for the assignment of the bands in the electrophoresis data was sought by performing fluorescence correlation spectroscopy (FCS) of the  $\alpha$ -syn species *in situ*. FCS provides information about the diffusion properties of fluorescent molecules. For these experiments the bands on the electrophoresed gels were excised and transferred to a glass cover slip, which was then mounted on the sample stage of a confocal fluorescence microscope. The concentration of fluorescently labeled  $\alpha$ -syn species was sufficiently low to meet the requirement of FCS to have on average less than one molecule in the confocal volume. The autocorrelation curves that were obtained by FCS of the three bands in the gels are shown in Figure 3.6. Each of the curves was fitted to equation 3.2, from which the diffusion coefficients of the different species could be determined. The data are summarized in Table 3.1, and represent averages over 10–20 different time traces in each case.

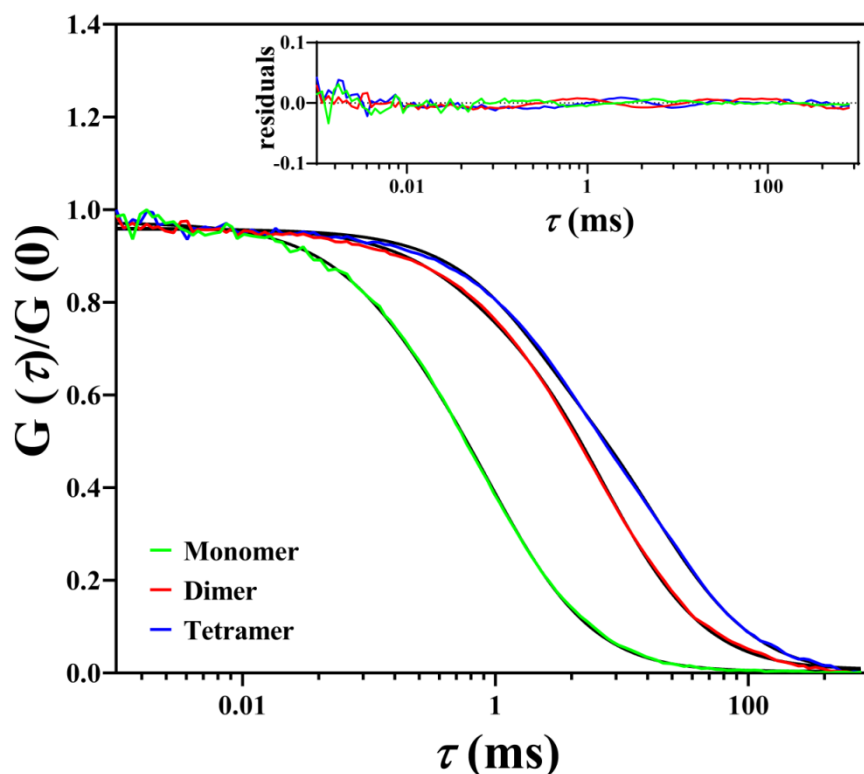


Figure 3.6: Normalized fitted autocorrelation curves of  $\alpha$ -syn monomer (green), dimer (red) and tetramer (blue). The shift in curves to higher diffusion times ( $\tau$ ) point to slower diffusion of the molecules in the confocal volume, which is consistent with an increase in the molecular weight of the measured species.

On average, the measured diffusion coefficient of  $\alpha$ -syn monomer, dimer and tetramer were 11.4, 2.8 and 1.3  $\mu\text{m}^2/\text{s}$  respectively (Table 3.1). The resistance of the gel is higher for the

bigger molecules, resulting in a lower diffusion coefficient, as shown in Table 3.1, where  $\alpha$ -syn monomer has the highest diffusion coefficient and  $\alpha$ -syn tetramer the lowest one.

A lot of effort has been made in the field to relate the diffusion coefficients of polymers to their molecular weight [32]. A well-established model is based on the reptation theory which was developed to describe self-diffusion in a polymer melt, but it has also been applied to the diffusion of linear polymers in a gel [33,34]. In this model the polymers are thought to move through a fictitious tube that is static at the time scale of motion. The polymer is modeled as a chain of  $N$  segments with flexible links, which are laterally confined to the tube, *i.e.*, the only allowed motion is along the tube axis. The motion of the polymer chain is driven by random thermal fluctuations. The outcome of this model is that the diffusion constant  $D$  of linear polymers in a gel is proportional to  $N^{-2}$  for sufficiently large  $N$ . Of course, the length of the polymer and the molecular weight must be proportional to  $N$ .

When applied to the diffusion of  $\alpha$ -syn species in the gel one might expect that the diffusion constant scales according to this prediction of the reptation theory. The diffusion constants derived from FCS measurements *vs* molecular weight of the presumed monomer, dimer and tetramer bands in the gel are plotted in Figure 3.7. The obtained slope of  $-1.96$  is close to the predicted value from the reptation theory, and at first sight appears to support the assignment of these bands. However, the data in Figure 3.7 must be interpreted with great caution.

First of all, as we will point out in the discussion (see 3.4), it is unlikely that the dimer and tetramer can be modeled as a linear polymer. This violates an essential assumption in the reptation model, and the  $N^{-2}$  dependence probably does not hold in our case [35]. Secondly, the pore size of the gel is poorly defined and may be too large compared to the length of an  $\alpha$ -syn molecule to allow the application of the reptation model. The alternative is to model the diffusion of  $\alpha$ -syn in the gel as that of a more globular polymer, but some parameters for the application of such models are lacking. For example, the phenomenological scaling law of Phillies et al. [36–39] requires the diffusion coefficients of  $\alpha$ -syn dimers and tetramers in aqueous solution, which are not available.

### 3.4. Discussion

It has been debated in the recent literature whether the formation of covalently bound  $\alpha$ -syn dimers plays a role in the early stages of  $\alpha$ -syn oligomerization.  $\alpha$ -Syn dimerization is implied in accelerated aggregation and in the concurrent formation of neurotoxic species

[25,26]. Supporting data, however, has been largely inferred from experiments that were performed under special circumstances, including, for example, the presence of oxidative and nitrating agents or by using recombinant oligomers [24–27].

Here, we showed by gel electrophoresis that dimers and tetramers of  $\alpha$ -syn are formed *in vitro* under ambient conditions without the addition of oxidative or nitrating agents. Of particular interest is the fact that, starting with a 350  $\mu$ M solution of monomeric  $\alpha$ -syn, we can determine the time profile of the sample composition in terms of dimers and tetramers.

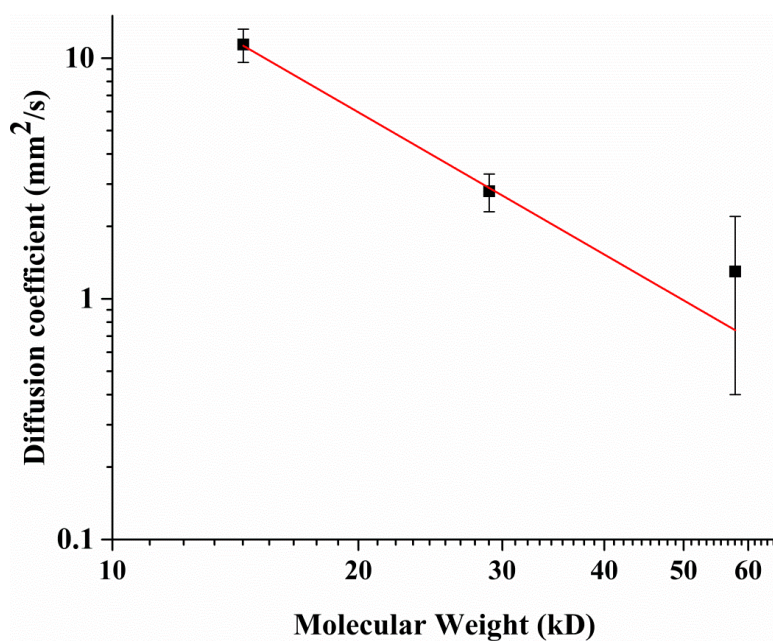


Figure 3.7: Fitted dependence of the diffusion coefficient on molecular weight, where the obtained slope was -1.96, while the predicted one was -2.

Table 3.1: The diffusion coefficient and diffusion time of  $\alpha$ -syn monomer, dimer and tetramer measured in the band of the electrophoresed gel by FCS. The numbers are the average values of 10-20 different time traces in each case. The diffusion coefficient decreases with the molecular weight of the  $\alpha$ -syn sample.

	Diffusion coefficient ( $\mu\text{m}^2/\text{s}$ )		Diffusion time (ms)	
	Average	SD	Average	SD
Monomer	11.4	1.8	2.3	0.4
Dimer	2.8	0.5	9.2	1.5
Tetramer	1.3	0.9	26.5	13.2

The fact that these small oligomers are stable under electrophoresis conditions is a strong indication that the constituent  $\alpha$ -syn molecules are covalently linked. Support for this conjecture is provided by Van Maarschalkerweerd et al. [28] who report the spontaneous formation of covalently linked dityrosine  $\alpha$ -syn dimers at high monomer concentration during gel-filtration, followed by mass spectrometry analysis. Moreover, their results show that the covalent linkage is site-specific and involves a Y39-Y39 dimer. It is reasonable to assume that the same dimer is formed in our case, although we do not have direct evidence. It also implies that the  $\alpha$ -syn dimers and tetramers are branched polymers which are not congruent with the conditions for application of the reptation theory to the FCS diffusion data (Figure 3.7).

Except for the work by Van Maarschalkerweerd et al. [28], this facile formation of dimers has not been reported before, and we are the first to report the formation of tetramers under standard *in vitro* conditions. These species remain at a low concentration and, therefore, their detection by electrophoresis is not straightforward since standard staining and gel-imaging is not sufficiently sensitive. For this reason we used fluorescently labeled  $\alpha$ -syn samples and fluorescent imaging of the electrophoresis gels. However, we showed in Chapter 2 of this thesis that fluorescent labeling changes the morphology of  $\alpha$ -syn aggregates depending on the fraction of labeled  $\alpha$ -syn in a mixture with the WT species [29]. Apparently, fluorescent labeling may affect to some extent the intermolecular interaction between  $\alpha$ -syn molecules and  $\alpha$ -syn aggregation properties. This was avoided by using samples in which only 5% of  $\alpha$ -syn molecules were fluorescently labeled. The low fraction of fluorescently labeled  $\alpha$ -syn, however, requires a sensitive technique to image the electrophoresed gels. The fact that we also observe dimer formation of WT  $\alpha$ -syn by mass spectrometry indicates that dimerization is not induced by fluorescent labeling.

In the case of WT  $\alpha$ -syn we find that dimers form on a timescale of hours, reaching a maximum after about 24 h after which we observe a decline of the dimer content. The formation of tetramers is clearly delayed with respect to the dimer formation, and reaches a stable plateau on the timescale of the experiment. The rate of formation is significantly faster in case of the A53T  $\alpha$ -syn mutant. Here, the dimer and tetramer appear almost concurrently, although the depletion of dimers is much faster than that of tetramers.

The concentration of  $\alpha$ -syn dimers and tetramers was estimated by comparing the intensity of the fluorescent bands in the gel with those of a known concentration of monomeric,

fluorescently labeled  $\alpha$ -syn solution. We estimate that the maximal concentration of dimers and tetramers is about 0.5% of the monomers in the sample. The transient character of the time profiles strongly suggests that the dimers and tetramers are incorporated into larger oligomers and fibrils. Indeed, the typical timescales of  $\alpha$ -syn fibrillization, monitored by the thioflavin T assay, are consistent with the decrease of the dimer bands. It is interesting that the timescales of the latter for the WT and the A53T  $\alpha$ -syn mutant are significantly different; it correlates well with the fact that the aggregation rate of the A53T mutant is much faster than that of WT  $\alpha$ -syn.

The underlying chemistry of covalent  $\alpha$ -syn dimerization in the absence of oxidizing or nitrating agents is unclear, although it is reasonable to assume, based on the existing literature, that some oxidation process is involved to couple the two tyrosines. From our data this appears to be a relatively slow step. An important question is whether or not this reaction is unique for  $\alpha$ -syn, especially in view of the ubiquity of tyrosine residues in the protein world. A relevant piece of information is provided in a recent publication by Zhengjian Lv et al. [40], who report the lifetimes of transiently formed dimeric encounter complexes of  $\alpha$ -syn in the range of hundreds of milliseconds up to seconds. It is likely that the kinetic stability of these encounter complexes distinguishes  $\alpha$ -syn from many other proteins. Their long lifetime will certainly enhance the probability of auxiliary reactions that form a covalent link, and contribute to the efficacy of such a reaction.

The time profile of the  $\alpha$ -syn dimer and tetramer species suggests a sequential process, certainly in case of WT, *i.e.* the dimer is a precursor for the formation of the tetramer. In that case, the transition from the dimer to the tetramer must be faster by a few orders of magnitude than that of the monomer to the dimer, because of the low concentration of dimers. Krishnan et al. [26] already concluded that oxidative dimer formation is the key to  $\alpha$ -syn fibrillogenesis. We conclude that the dimers and tetramers we observe are incorporated in, or even initiate, the formation of larger oligomers and fibrils. If it is the dominant pathway, then dimer formation is certainly the critical rate-limiting step for fibril formation.

It is interesting that we do not see traces of a stable  $\alpha$ -syn trimer. We surmise that it is formed transiently in a metastable state, possibly as an intermediate for the formation of the tetramer.

### 3.5. Conclusion

This study presents results in the investigation of early  $\alpha$ -syn aggregates formation by combining polyacrylamide gel electrophoresis, fluorescence correlation spectroscopy and mass spectrometry. We succeeded in observing dimers and tetramers of  $\alpha$ -syn spontaneously being formed during the fibrillization process using polyacrylamide gel electrophoresis. Dimers and tetramers were present in WT  $\alpha$ -syn aggregates, as well as A53T  $\alpha$ -syn mutant. Next to it, we presented the time profile of  $\alpha$ -syn aggregate for both WT and A53T. We estimated that the formation of dimers and tetramers together contributed not more than 0.5% in total sample composition, but their intensity profile changed in time. Therefore, it was less likely that dimers and tetramers represented off-pathway species. In case they represent on-pathway species further examination of their cytotoxicity would be even more important, as the evidence of their toxicity of oligomers already exist [21]. By the help of two additional techniques, fluorescence correlation spectroscopy and mass spectrometry, we confirmed the differences between isolated species. The physiological relevance of isolated species is of great importance for understanding the mechanism of PD.

### Acknowledgements

We thank Ms. N. Schilderink from University of Twente for  $\alpha$ -synuclein expression and purification. This work was performed in the framework of the research program “A Single Molecule View on Protein Aggregation”, supported by the Foundation for Fundamental Research on Matter (FOM), which is part of the Netherlands Organization for Scientific Research (NWO).



### 3.6. References

- [1] J. Parkinson, An essay on the shaking palsy. 1817., *J. Neuropsychiatry Clin. Neurosci.* 14 (2002) 223–236; discussion 222. doi:10.1176/appi.neuropsych.14.2.223.
- [2] M. Goedert, M.G. Spillantini, K. Del Tredici, H. Braak, 100 years of Lewy pathology, *Nat. Rev. Neurol.* 9 (2012) 13–24. doi:10.1038/nrneurol.2012.242.
- [3] M.H. Polymeropoulos, C. Lavedan, E. Leroy, S.E. Ide, A. Dehejia, A. Dutra, B. Pike, H. Root, J. Rubenstein, R. Boyer, E.S. Stenroos, S. Chandrasekharappa, A. Athanassiadou, T. Papapetropoulos, W.G. Johnson, A.M. Lazzarini, R.C. Duvoisin, G. Di Iorio, L.I. Golbe, R.L. Nussbaum, Mutation in the  $\alpha$ -Synuclein Gene Identified in Families with Parkinson's Disease, *Science* (80-. ). 276 (1997) 2045–2047. doi:10.1126/science.276.5321.2045.
- [4] M.G. Spillantini, M.L. Schmidt, V.M. Lee, J.Q. Trojanowski, R. Jakes, M. Goedert, Alpha-synuclein in Lewy bodies., *Nature.* 388 (1997) 839–840. doi:10.1038/42166.
- [5] M.G. Spillantini, R.A. Crowther, R. Jakes, M. Hasegawa, M. Goedert,  $\alpha$ -Synuclein in filamentous inclusions of Lewy bodies from Parkinson's disease and dementia with Lewy bodies, *Proc. Natl. Acad. Sci.* 95 (1998) 6469–6473. doi:10.1073/pnas.95.11.6469.
- [6] L.C. Serpell, J. Berriman, R. Jakes, M. Goedert, R.A. Crowther, Fiber diffraction of synthetic alpha-synuclein filaments shows amyloid-like cross-beta conformation., *Proc. Natl. Acad. Sci. U. S. A.* 97 (2000) 4897–4902. doi:10.1073/pnas.97.9.4897.
- [7] J.D. Schmit, K. Ghosh, K. Dill, What drives amyloid molecules to assemble into oligomers and fibrils?, *Biophys. J.* 100 (2011) 450–458. doi:10.1016/j.bpj.2010.11.041.
- [8] M. Vilar, H.-T. Chou, T. Lührs, S.K. Maji, D. Riek-Loher, R. Verel, G. Manning, H. Stahlberg, R. Riek, The fold of alpha-synuclein fibrils., *Proc. Natl. Acad. Sci. U. S. A.* 105 (2008) 8637–8642. doi:10.1073/pnas.0712179105.
- [9] S.J. Wood, J. Wypych, S. Steavenson, J. Louis, M. Citron, A.L. Biere,  $\alpha$ -Synuclein Fibrillogenesis is Nucleation-dependent, *Biochemistry.* (1999) 19509–19512.
- [10] R. Lowe, D.L. Pountney, P.H. Jensen, W.P. Gai, N.H. Voelcker, Calcium(II) selectively induces alpha-synuclein annular oligomers via interaction with the C-terminal domain., *Protein Sci.* 13 (2004) 3245–3252. doi:10.1110/ps.04879704.
- [11] L. Giehm, D.I. Svergun, D.E. Otzen, B. Vestergaard, Low-resolution structure of a vesicle disrupting  $\alpha$ -synuclein oligomer that accumulates during fibrillation, *Proc. Natl. Acad. Sci.* 108 (2011) 3246–3251. doi:10.1073/pnas.1013225108.
- [12] A. Rekas, R.B. Knott, A. Sokolova, K.J. Barnham, K.A. Perez, C.L. Masters, S.C. Drew, R. Cappai, C.C. Curtain, C.L.L. Pham, The structure of dopamine induced  $\alpha$ -synuclein oligomers, *Eur. Biophys. J.* 39 (2010) 1407–1419. doi:10.1007/s00249-010-0595-x.
- [13] R. Cappai, S.-L. Leck, D.J. Tew, N.A. Williamson, D.P. Smith, D. Galatis, R.A. Sharples, C.C. Curtain, F.E. Ali, R.A. Cherny, J.G. Culvenor, S.P. Bottomley, C.L. Masters, K.J. Barnham, A.F. Hill, Dopamine promotes alpha-synuclein aggregation into SDS-resistant soluble oligomers via a distinct folding pathway., *FASEB J.* 19 (2005) 1377–1379. doi:10.1096/fj.04-3437fje.

- [14] E.R. Georgieva, T.F. Ramlall, P.P. Borbat, J.H. Freed, D. Eliezer, Membrane-bound alpha-synuclein forms an extended helix: Long-distance pulsed ESR measurements using vesicles, bicelles, and rodlike micelles, *J. Am. Chem. Soc.* 130 (2008) 12856–12857. doi:10.1021/ja804517m.
- [15] K.M. Danzer, D. Haasen, A.R. Karow, S. Moussaud, M. Habeck, A. Giese, H. Kretschmar, B. Hengerer, M. Kostka, Different species of alpha-synuclein oligomers induce calcium influx and seeding., *J. Neurosci.* 27 (2007) 9220–9232. doi:10.1523/JNEUROSCI.2617-07.2007.
- [16] K.A. Conway, S.J. Lee, J.C. Rochet, T.T. Ding, R.E. Williamson, P.T. Lansbury, Acceleration of oligomerization, not fibrillization, is a shared property of both alpha-synuclein mutations linked to early-onset Parkinson's disease: implications for pathogenesis and therapy., *Proc. Natl. Acad. Sci. U. S. A.* 97 (2000) 571–576. doi:10.1073/pnas.97.2.571.
- [17] H.-Y. Kim, M.-K. Cho, A. Kumar, E. Maier, C. Siebenhaar, S. Becker, C.O. Fernandez, H.A Lashuel, R. Benz, A. Lange, Structural Properties of Pore-Forming Oligomers of alpha -Synuclein., *J.- Amer. Chem. Soc.* 131 (2009) 17482–17489.
- [18] H.A. Lashuel, B.M. Petre, J. Wall, M. Simon, R.J. Nowak, T. Walz, P.T. Lansbury, A-Synuclein, Especially the Parkinson's Disease-Associated Mutants, Forms Pore-Like Annular and Tubular Protofibrils, *J. Mol. Biol.* 322 (2002) 1089–1102. doi:10.1016/S0022-2836(02)00735-0.
- [19] M.M. Apetri, N.C. Maiti, M.G. Zagorski, P.R. Carey, V.E. Anderson, Secondary structure of  $\alpha$ -synuclein oligomers: Characterization by Raman and atomic force microscopy, *J. Mol. Biol.* 355 (2006) 63–71. doi:10.1016/j.jmb.2005.10.071.
- [20] S.W. Chen, S. Drakulic, E. Deas, M. Ouberai, F.A. Aprile, R. Arranz, S. Ness, C. Roodveldt, T. Guilleims, E.J. De-Genst, D. Klenerman, N.W. Wood, T.P.J. Knowles, C. Alfonso, G. Rivas, A.Y. Abramov, J.M. Valpuesta, C.M. Dobson, N. Cremades, Structural characterization of toxic oligomers that are kinetically trapped during  $\alpha$ -synuclein fibril formation, *Proc. Natl. Acad. Sci.* 112 (2015) E1994–E2003. doi:10.1073/pnas.1421204112.
- [21] M.J. Volles, P.T. Lansbury, Zeroing in on the pathogenic form of  $\alpha$ -synuclein and its mechanism of neurotoxicity in Parkinson's disease, *Biochemistry.* 42 (2003) 7871–7878. doi:10.1021/bi030086j.
- [22] R. Kaye, E. Head, J.L. Thompson, T.M. Mcintire, S.C. Milton, C.W. Cotman, C.G. Glabe, Amyloid Oligomers Implies Common, 300 (2003) 486–490.
- [23] V.N. Uversky, NIH Public Access, 277 (2011) 2940–2953. doi:10.1111/j.1742-4658.2010.07721.x.Mysterious.
- [24] J.M. Souza, B.I. Giasson, Q. Chen, V.M.Y. Lee, H. Ischiropoulos, Dityrosine cross-linking promotes formation of stable  $\alpha$ -synuclein polymers: Implication of nitrative and oxidative stress in the pathogenesis of neurodegenerative synucleinopathies, *J. Biol. Chem.* 275 (2000) 18344–18349. doi:10.1074/jbc.M000206200.
- [25] C. Andrekopoulos, H. Zhang, J. Joseph, S. Kalivendi, B. Kalyanaraman, Bicarbonate enhances alpha-synuclein oligomerization and nitration: intermediacy of carbonate radical anion and nitrogen dioxide radical, *Biochem. J.* 378 (2004) 435–447. doi:10.1042/bj20031466.

- [26] S. Krishnan, E.Y. Chi, S.J. Wood, B.S. Kendrick, C. Li, W. Garzon-Rodriguez, J. Wypych, T.W. Randolph, L.O. Narhi, A.L. Biere, M. Citron, J.F. Carpenter, Oxidative dimer formation is the critical rate-limiting step for Parkinson's disease  $\alpha$ -synuclein fibrillogenesis., *Biochemistry*. 42 (2003) 829–837. doi:10.1021/bi026528t.
- [27] A. Roostae, S. Beaudoin, A. Staskevicius, X. Roucou, Aggregation and neurotoxicity of recombinant  $\alpha$ -synuclein aggregates initiated by dimerization., *Mol. Neurodegener.* 8 (2013) 5. doi:10.1186/1750-1326-8-5.
- [28] A. Van Maarschalkerweerd, M.N. Pedersen, H. Peterson, M. Nilsson, T.T.T. Nguyen, T. Skamris, K. Rand, V. Vetri, A.E. Langkilde, B. Vestergaard, Formation of covalent di-tyrosine dimers in recombinant  $\alpha$ -synuclein, *Intrinsically Disord. Proteins*. 3 (2015) 1–12. doi:10.1080/21690707.2015.1071302.
- [29] M. Mučibabić, M.M. Apetri, G.W. Canters, T.J. Aartsma, The effect of fluorescent labeling on  $\alpha$ -synuclein fibril morphology, *Biochim. Biophys. Acta - Proteins Proteomics*. (2016). doi:10.1016/j.bbapap.2016.07.007.
- [30] V. Buschmann, B. Krämer, F. Koberling, R. Macdonald, S. Rüttinge, Quantitative FCS: Determination of the Confocal Volume by FCS and Bead Scanning with the MicroTime 200, *AppNote Quant. FCS*. (2007) 1–8.
- [31] O.A. Ross, A.T. Braithwaite, L.M. Skipper, J. Kachergus, M.M. Hulihan, F.A. Middleton, K. Nishioka, J. Fuchs, T. Gasser, D.M. Maraganore, C.H. Adler, L. Larvor, M.C. Chartier-Harlin, C. Nilsson, J.W. Langston, K. Gwinn, N. Hattori, M.J. Farrer, Genomic investigation of  $\alpha$ -synuclein multiplication and parkinsonism, *Ann. Neurol.* 63 (2008) 743–750. doi:10.1002/ana.21380.
- [32] L. Masaro, X.X. Zhu, Physical models of diffusion for polymer solutions, gels and solids, 1999. doi:10.1016/S0079-6700(99)00016-7.
- [33] G.W. Slater, DNA gel electrophoresis: The reptation model(s), *Electrophoresis*. 30 (2009). doi:10.1002/elps.200900154.
- [34] S.J. Hubert, M. Krzywinski, G.W. Slater, Reptation Dynamics with Random Local Interactions, *Macromolecules*. 31 (1998) 181–192. doi:10.1021/ma970763f.
- [35] P.G. De Gennes, P.G.D.G. Reptation, *J. De Physique*, Reptation of stars To cite this version :, 36 (1975) 1199–1203.
- [36] G.D.J. Phillies, Dynamics of polymers in concentrated solutions: the universal scaling equation derived, *Macromolecules*. 20 (1987) 558–564. doi:10.1021/ma00169a015.
- [37] G.D.J. Phillies, The hydrodynamic scaling model for polymer dynamics, *Nucl. Phys. B (Proceedings Suppl.)* 5 (1988) 214–219. doi:10.1016/0920-5632(88)90043-6.
- [38] G.D.J. Phillies, C. Richardson, C.A. Quinlan, S.Z. Ren, Transport in intermediate and high molecular weight hydroxypropylcellulose/water solutions, *Macromolecules*. 26 (1993) 6849–6858. doi:10.1021/ma00077a022.
- [39] G.D.J. Phillies, P. Peczak, The Ubiquity of Stretched-Exponential Forms in Polymer Dynamics, *Macromolecules*. 21 (1988) 214–220. doi:10.1021/ma00179a041.
- [40] Z. Lv, A.V. Krasnoslobodtsev, Y. Zhang, D. Ysselstein, J.C. Rochet, S.C. Blanchard, Y.L. Lyubchenko, Direct detection of  $\alpha$ -synuclein dimerization dynamics: Single-molecule fluorescence analysis, *Biophys. J.* 108 (2015) 2038–2047. doi:10.1016/j.bpj.2015.03.010.

### 3.7. Supporting information

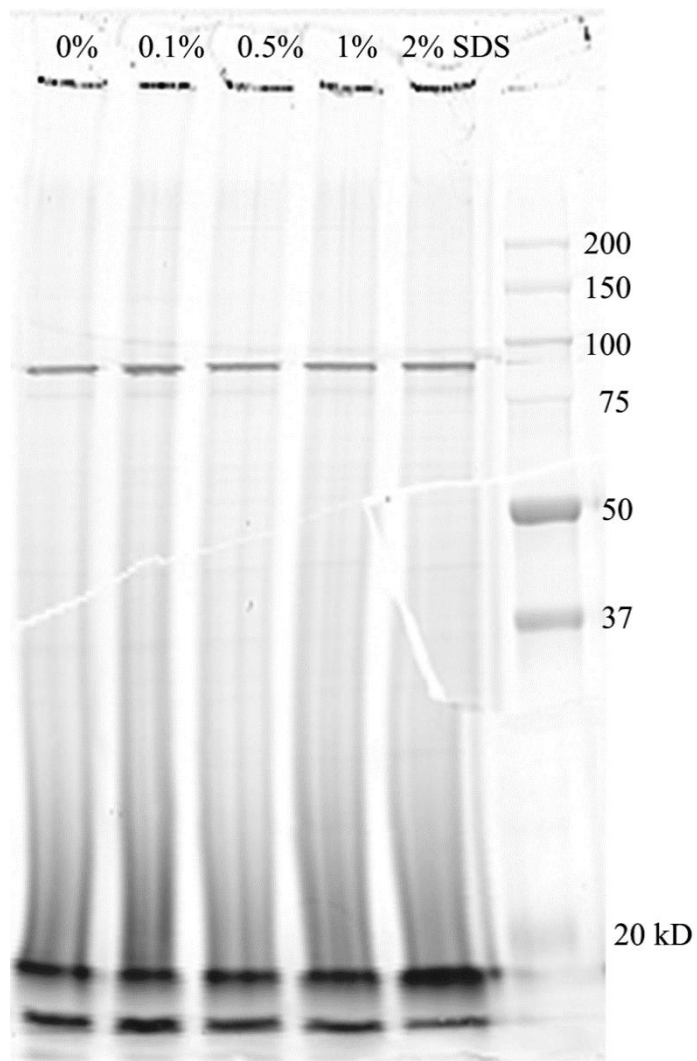


**Figure S.3.1: SDS effect on  $\alpha$ -syn sample stability and separation. The same aged  $\alpha$ -syn sample was electrophoresed without and in the presence of up to 2% SDS.**

# Influence of solution conditions on $\alpha$ -synuclein aggregation kinetics

### **Abstract**

Parkinson's disease (PD) is a neurodegenerative disorder characterized by the presence of abnormal deposits of aggregated proteins known as Lewy bodies in brain tissue. The major components of Lewy bodies are aggregates of a small presynaptic protein known as  $\alpha$ -synuclein ( $\alpha$ -syn). Despite a significant research effort the mechanism of oligomer and fibril formation and the conditions which trigger the aggregation process are not well understood. The aim of this study was to determine the effect of solution conditions on seeded  $\alpha$ -syn aggregation and fibril growth by the use of a Thioflavin T fluorescence assay. The relationship between  $\alpha$ -syn elongation kinetics of ionic strength and pH was measured, and a detailed analysis is presented in terms of a kinetic model. The effect of pH and of salt concentration on elongation kinetics of preformed  $\alpha$ -syn fibrils deviates significantly from their effect on the lag phase, suggesting that the mechanism for  $\alpha$ -syn nucleation and fibril elongation are different.

## 4.1. Introduction

Amyloid fibrils are in the spotlight of the scientific community not only for their relevance in diseases such as Parkinson's and Alzheimer's disease [1], but also for their application in nanotechnology and biotechnology [2]. Discovering the steps in the conversion of functional proteins into amyloid fibrils [3] is crucial for understanding their origin and proliferation and for understanding how amyloid fibrils are associated with a range of health disorders [4]. The past decade has seen numerous theoretical and experimental studies attempting to determine and characterize the kinetic process involved in the self-assembly of amyloid proteins into fibrils [5–7]. However, the outcomes of the experiments often differ [8], which is usually connected to the heterogeneity in the early events of the fibrillization process. Interestingly, despite their very different primary peptide sequences, amyloid fibrils share common structural features, such as their micrometer length, twisted appearance [9,10] and rich  $\beta$ -sheet structure [11]. It has been reported that many amyloid fibrils, including  $\alpha$ -syn, elongate by binding of monomers to fibril ends [12,13]. Mechanisms of the *de novo* fibril formation include oligomerization [14], fibril breaking [15–17] and fibril-catalyzed secondary nucleation [18].

Protein aggregation is often monitored using an assay based on the fluorescence enhancement of Thioflavin T (ThT) dye, which specifically binds to  $\beta$ -sheets structures [19]. It has been previously reported that a typical aggregation curve, as followed by ThT fluorescence, has a sigmoidal shape and is described by first order kinetics [20] (see Chapter 1, Figure 1.3). The aggregation curve is determined by nucleation (lag phase), growth (exponential phase) and saturation (plateau phase). During the lag phase initiation of aggregation occurs by forming the nuclei for the start of the reaction, described in the literature as primary nucleation [21]. At this stage there is no ThT fluorescence increase. The growth phase is characterized by exponential growth of the ThT fluorescence. Several processes are underlying it, such as elongation of existing aggregates by monomer addition to fibril end(s) [22] and formation of new growing centers by breaking of existing fibrils [15] – so called secondary nucleation. In the saturation phase ThT fluorescence reaches a plateau, where most of the monomer pool has been depleted by incorporation into aggregates [3] and the rate of the monomer addition to the fibril ends is equal to the dissociation rate. The time scale for primary nucleation of  $\alpha$ -syn aggregation is highly variable, and though the nucleation phase is most important in the aggregation process it is still not very well understood. Concerning the overall mechanism of

$\alpha$ -syn aggregation, the rate-limiting steps, the role and nature of intermediates still remain not well elucidated [5,6,8]. The lag phase that represents the primary nucleation [6] can be largely eliminated by using preformed fibrils (seeds) and, provides a convenient way to focus especially on the elongation reaction of  $\alpha$ -syn fibrils.

Effects of solution conditions on  $\alpha$ -syn aggregation were studied by bulk experiments [23,24] and atomic force microscopy [25]. In the study by Hoyer and coworkers [23] the effect of solution conditions on the overall rate of  $\alpha$ -syn aggregation was reported, together with the change in aggregate morphology, especially at low pH. Their finding indicates that adding 200 mM NaCl can accelerate the formation of aggregation nuclei [21]. Buell et al. [13] showed that primary and secondary nucleation govern the proliferation of aggregates at pH 7, with secondary nucleation being particularly prominent at pH below 6. They also reported that the fibril elongation rate is strongly influenced by the salt concentration. As  $\alpha$ -syn aggregation kinetics and morphology depend significantly on pH, ionic strength, temperature etc., it is important to determine which phase of the process is affected the most and to gain new information about it.

Here we report to what extent the fibrillar growth phase of  $\alpha$ -syn aggregation is affected by solution conditions, in particular ionic strength and pH, based on a recording of the  $\alpha$ -syn fibril elongation kinetics in bulk. The bulk fibrillar growth was monitored by the ThT assay, and the average initial elongation rate of the fibrils was measured. To skip largely the nucleation phase and focus on fibril elongation only, we monitored WT  $\alpha$ -syn in the presence of preformed fibrils (seeds). Under those conditions the lag phase is effectively suppressed in the growth kinetics. The present study resulted in direct experimental evidence that the initial elongation rate of the  $\alpha$ -syn fibrils increases at relatively low concentrations of sodium chloride (up to 30 mM NaCl) and decreases at higher NaCl concentrations. No particular trend is observed in the pH dependence of the initial growth rate, consistent with earlier reports [13].

## **4.2. Materials and Methods**

### **4.2.1. Expression and purification of $\alpha$ -syn**

Preparation and purification of  $\alpha$ -syn was performed as described elsewhere [26]. WT  $\alpha$ -syn was expressed in *E.coli* BL21 (DE3) transformed with the pT7-7 plasmid carrying the  $\alpha$ -syn gene. Culturing was done in lysogeny broth medium with 100  $\mu$ g/ml ampicillin. After

induction by addition of isopropylthio- $\beta$ -galactoside (1 mM, 4 h) bacterial cell pellets were harvested by centrifugation ( $6,000 \times g$ , 10 min), resuspended in 10 mM Tris-HCl, pH 8.0, 1 mM ethylenediaminetetraacetic acid (EDTA) and 1mM phenylmethylsulfonyl fluoride (10% of the culture volume) and stirred for 1 h at 4°C. Cells were lysed by sonication for 2 min and centrifuged ( $10,000 \times g$ , 20 min, 4°C).

By adding streptomycin sulfate (1%, 15 min, 4°C) DNA was precipitated and removed by centrifugation at  $13,500 \times g$  for 30 min. Next,  $\alpha$ -syn was salted out from the solution by slowly adding ammonium sulfate up to a concentration of 0.295 g/ml and mild stirring (1 h, 4°C). Precipitated  $\alpha$ -syn was collected by centrifugation ( $13,500 \times g$ , 30 min, 4°C). The pellet was gently resuspended in 10 mM Tris-HCl, pH 7.4 and the solution was eluted over a 6 ml ResourceQ anion exchange column (GE Healthcare) using the Äkta Purifier system (GE Healthcare) and a linear gradient of NaCl (0–500 mM) in 10 mM Tris-HCl, pH 7.4 at a flowrate of 3 ml/min. Fractions containing  $\alpha$ -syn (eluted at  $\sim 300$  mM NaCl) were pooled, concentrated (Vivaspin-20, 10 kDa; GE Healthcare) and desalted using a PD-10 column (GE Healthcare) in 10 mM Tris-HCl pH 7.4 (containing 1 mM DTT in the case of cysteine mutant). Protein concentration was determined on the basis of the tyrosine absorption at 275 nm by using  $5600 \text{ M}^{-1} \text{ cm}^{-1}$  for the extinction coefficient of WT [24].

#### 4.2.2. Kinetic model of aggregation

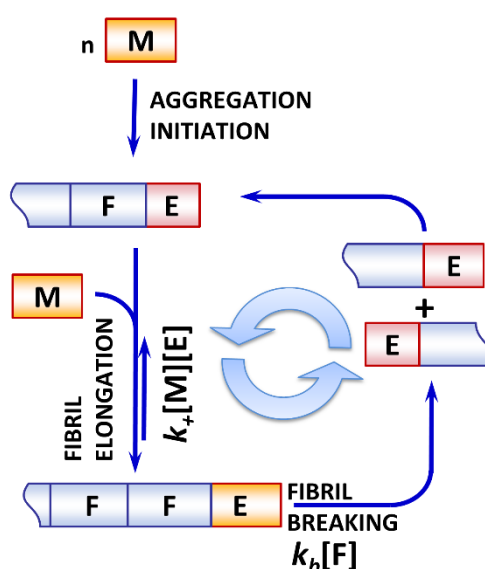


Figure 4.1: Kinetic model of  $\alpha$ -syn aggregation, which includes three steps: initiation, growth and formation of new fibril ends, where  $[M]$  is the monomer concentration,  $[E]$  the concentration of active growing ends,  $[F]$  the amount of fibrillar  $\alpha$ -syn,  $k_+$  the elongation rate and  $k_b$  the breaking rate (Figure reprinted with permission from 15 given by ACS Publications).



The data were analyzed with a kinetic model which is described in detail elsewhere [15]. In this proposed model [15]  $\alpha$ -syn aggregation includes three steps (see Figure 4.1). It starts with an initial phase, where new aggregates are formed spontaneously and it continues with a growth phase, where mostly monomers bind to existing fibril ends and fibrils get elongated. The fluorescence intensity growth is nonlinear, and upon monomer depletion slows down. During the aggregation process, especially under agitation, fibrils can break which produces new fibril ends. In the presence of seeds and at the time scale of the experiments reported here, the initial increase in ThT fluorescence is governed by seed elongation. Ignoring the primary nucleation, seed elongation can be described by following equation:

$$\frac{\Delta F(t)}{\Delta t} = \frac{F_t - F_0}{(t - t_0)} = k_+[M][E]$$

Here  $\Delta F(t)$  is the change in concentration of fibrillized protein during the time interval of  $\Delta t$ ,  $F_0$  is the concentration of the fibrillized protein at  $t_0$  while  $F_t$  is the concentration of the fibrillized protein at a later time  $t$ . The change in fluorescence intensity is converted to equivalent monomer concentration by scaling to the intensity in the plateau phase where we assume that all  $\alpha$ -syn is in aggregated form.  $[M]$  is the monomer concentration,  $[E]$  the seed concentration and  $k_+$  the fibril elongation rate. The initial elongation rate was measured by following the increase of the ThT signal during the first 30000 s of the measurement, where the increase in the ThT fluorescence was linear in time. It was assumed that during the first 30000 s fibril breaking did not occur which means that  $[E]$  is essentially constant. Longer fibrils are more prone to breaking, but during the first 30000 s of seed elongation long fibrils are not common. Control experiments under identical conditions, but in the absence of seeds, showed that at this time scale primary nucleation did not make a significant contribution to the ThT signal. Thus we have for  $k_+$ :

$$k_+ = \frac{F_t - F_0}{(t - t_0) [M][E]}$$

The units of  $k_+$  are  $\text{mM}^{-1} \text{s}^{-1}$ .

### 4.2.3. Kinetic measurements and the aggregation model

The aggregation experiments were performed in a Tecan Infinite M200pro plate reader and seed elongation was monitored by recording the ThT fluorescence. All experiments were performed at 37°C, under shaking conditions (300 s of linear shaking with 6 mm amplitude)

in 384 well plates (Nunc, Thermo Fisher Scientific) sealed with a transparent, polyolefin film (Viewseal, Greiner Bio One) to avoid evaporation, using a volume of 50  $\mu$ L per well. The final solution used for aggregation contained 6 mM sodium phosphate buffer at pH 4-10, 0-200 mM NaCl, 9 mM  $\text{NaN}_3$ , 0.1 mM EDTA (to remove divalent ions), and 5  $\mu$ M ThT ( $\geq 5\%$  of  $\alpha$ -syn concentration). The  $\alpha$ -syn monomer concentration was 100  $\mu$ M unless otherwise indicated. Samples were measured in at least 8 replicates. Fluorescence of ThT was always recorded from the bottom of the plate. Excitation was at 446 nm, emission at 485 nm, excitation and emission spectral bandwidths were set at 9 and 20 nm, respectively.

A solution of mature  $\alpha$ -syn fibrils was obtained by combining four separately aggregated 100  $\mu$ M  $\alpha$ -syn samples that had reached the plateau phase of ThT fluorescence, all grown under the same experimental conditions, in 6 mM phosphate buffer pH 7.2 with 150 mM NaCl, at 37°C, using constant agitation.. A stock solution of seeds was obtained by sonicating approximately 200  $\mu$ l of this solution of mature fibrils for 300 s in a water bath sonicator (VWR 75D ultrasonic cleaner, power 90 W, bath volume 2.5 L). All experiments were performed with the same stock solution of seeds.

### 4.3. Results

#### 4.3.1. Initial aggregation rate at different salt concentrations

To determine to what extent the ionic strength of the solution has an influence on  $\alpha$ -syn elongation the NaCl concentration was varied in the range of 0 to 200 mM. For this purpose WT  $\alpha$ -syn seeds were added to a solution of 100  $\mu$ M WT  $\alpha$ -syn monomers, with a final concentration of 0.16 nM. The initial elongation rate was determined based on the increase of the ThT fluorescence signal in time during the first 30000 s as described in Materials and Methods, applying the kinetic model established by Shvadchak and coworkers [15].

shows the dependence of the average initial elongation rate on NaCl concentration. The error bars denote standard deviations of the initial elongation rate. The data show that the average initial elongation rate increases with increasing NaCl concentrations up to 30 mM NaCl and decreases after that.

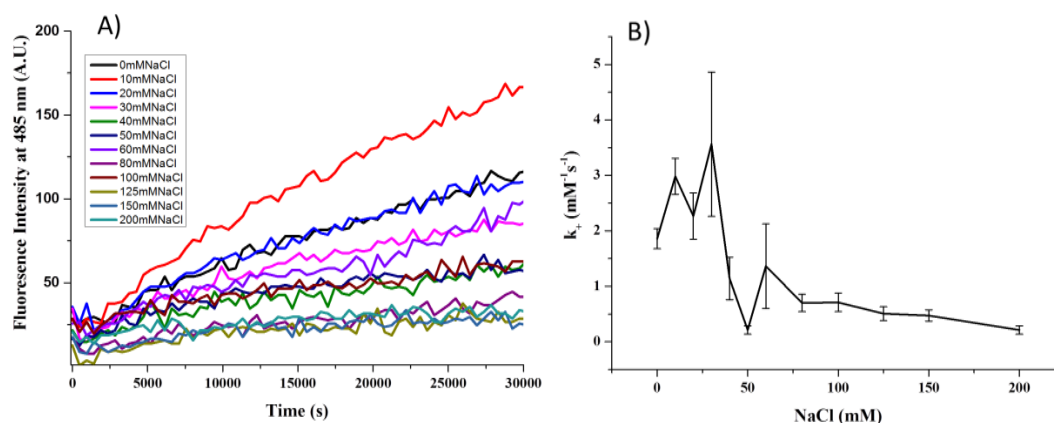


Figure 4.2: (A) Initial elongation kinetics of WT  $\alpha$ -syn seeds before secondary nucleation sets in, measured by ThT fluorescence. Each curve is an average of 8 samples. (B) The initial elongation rate as a function of NaCl concentration. The initial elongation rate decreased with NaCl concentrations above 30 mM. All measurements were performed under the same conditions: samples contained 0.16 nM  $\alpha$ -syn preformed seeds in the presence of 100  $\mu$ M  $\alpha$ -syn, 6 mM sodium phosphate buffer at pH 7.2, 0-200 mM NaCl, and 0.1 mM EDTA, at 37°C, under shaking. The error bars represent the standard deviation.

#### 4.3.2. Initial aggregation rate as a function of pH

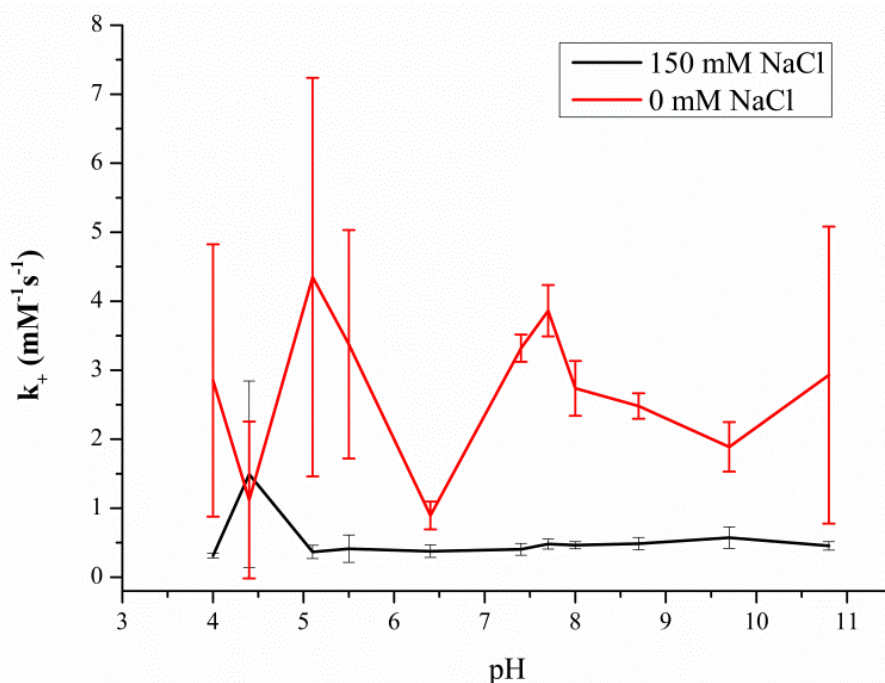
Previous studies reported structural changes of  $\alpha$ -syn when the pH was varied [27], differences in aggregate morphology between pH 4 and 7 [21] and variation of fibril growth kinetics in going from neutral to lower pH [13]. However, detailed information about the kinetics of fibrillar growth from seeds as a function of pH is still incomplete and we aimed to test the effect of a wider range of pH values on  $\alpha$ -syn elongation. Our experiments were performed in 6 mM sodium phosphate buffer from pH 4 to 10 in the presence of 0 and of 150 mM NaCl, respectively, while keeping constant the other experimental conditions such as protein and seeds concentration, temperature and shaking.

Figure 4.3 shows the initial elongation rates of  $\alpha$ -syn seeds as a function of pH, where the red and black symbols apply to 0 and 150 mM NaCl respectively. In general, the average initial elongation rates are higher in case of the former.

#### 4.4. Discussion

Using the ThT aggregation assay in the presence of preformed fibrils (seeds) we observed that the average initial elongation rate of  $\alpha$ -syn showed a pronounced dependence on salt concentration. The highest average initial elongation rate was measured at 30 mM NaCl. It is concluded that electrostatic interactions play an important role during the elongation process. In general, proteins can be stabilized or destabilized by the presence of salts in solution. This

may also apply to the range of conformational structures that  $\alpha$ -syn can adopt. The high negative charge of the C-terminal domain will be effectively screened at high salt concentrations which will affect Coulombic intra- and intermolecular interactions.



**Figure 4.3:** Dependence of the initial elongation rate on pH of 0.16 nM WT  $\alpha$ -syn seeds in the presence of 100  $\mu$ M WT  $\alpha$ -syn monomers at two different NaCl concentrations, obtained from plate reader measurements. Black: 150 mM NaCl, red: 0 mM NaCl. The error bars show the standard deviation of the initial elongation rate of 8 replicates.

This point has been used to explain the effect of salt on the aggregation rate of (monomeric)  $\alpha$ -syn [28] and to account for the different conformations reported for  $\alpha$ -syn at 0 and 150 mM, respectively [29]. At high salt concentrations  $\alpha$ -syn aggregates assemble within hours, whereas the lag phase extends to several days under low-salt conditions [25,29]. Moreover, these two salt conditions result in different fibril morphologies. In a recent study employing 19F-NMR Bai et al. [28] showed that  $\alpha$ -syn adopts a more compact structure in the absence of NaCl, consistent with a reduced hydrodynamic radius [29]. Long-range interaction of the C-terminal with the N-terminal domain appears to play a key role.

The data on the pH dependence of the initial elongation rate of  $\alpha$ -syn seeds (Figure 4.3) do not show a clear trend in the data other than that the measured rates are higher in the case of 0 mM NaCl. In the mild acidic range we observe a relatively large standard deviation in the results from 8 replicate measurements. We attribute this spread in the rates to the fact that secondary nucleation can probably not be neglected under the shaking conditions in the present experiments. Buell et al. [13], for example, have shown that the rate of secondary

nucleation increases dramatically in going from neutral to pH 5.2. In line with their results we conclude that the initial elongation rate of  $\alpha$ -syn seeds does not show a strong variation in the range of pH 4 to 8 at 150 mM NaCl, although at 0 mM NaCl the initial elongation rates do vary somewhat with pH.

This is in contrast to an earlier report by Uversky et al. [30], where it was shown that the rate of fibrillization of  $\alpha$ -syn was strongly pH dependent. In their case, however, the experiment involved the aggregation kinetics of monomers in solution and the data show that the pH dependence is dominated by the variation in lag time. They concluded that a decrease in pH leads to the formation of a precursor, possibly a partially folded intermediate, with a strongly enhanced propensity for the formation of  $\alpha$ -syn fibrils [30]. Indeed, it is generally assumed that conformational intermediates play a key role in the nucleation dependent pathway of  $\alpha$ -syn aggregation. The large change in net charge of  $\alpha$ -syn and in its internal charge distribution as a function of pH is believed to be involved in concomitant changes of the molecular conformation associated a collapse of the normally highly acidic and extended C-terminal tail at low pH [27]. Most likely as a result of long-range interactions  $\alpha$ -syn at low pH appears to adopt a more compact conformation, which presumably exhibits a larger rate of aggregation [30].

However, this precursor or intermediate does not lead to enhancement of the elongation rate of existing fibrils according to our conclusion above. Thus, we surmise that the affinity of this intermediate to bind to the fibril end is not significantly affected by the pH. This suggests that the mechanism of nucleation is possibly different from that of fibril elongation. An explanation may be that the  $\alpha$ -syn fibrils are stabilized by a change of conformation of the constituent initial aggregate, i.e., the fibrillar template is formed in a secondary step after nucleation. Such a conformational change may lead to a different reactivity for binding of  $\alpha$ -syn monomers to the fibril end compared to primary nucleation.

These previous reports [25,29,30] build a strong case for the effect of solution conditions on the  $\alpha$ -syn monomeric structure. Thus, solution conditions may affect the kinetics of fibril formation and fibril morphology. We note, however, that they specifically apply to measurements of aggregation in monomeric  $\alpha$ -syn solutions and that they show that in particular the duration of the lag phase is affected by the presence of salt [6,25,29].

The results in Figure 4.2 apply to seeded aggregation where the lag phase is largely absent, and where the initial rate is dominated by fibril elongation. Here the difference in rates is significant between low salt (0 mM NaCl) and high salt (~150 mM NaCl) conditions, but the highest at 30 mM NaCl. Presumably the  $\alpha$ -syn monomer addition to the fibril end involves a different molecular conformation than the one which promotes nucleation, being stabilized at the lower salt concentration of around 30 mM and that might point to the different nucleation and elongation mechanism.

#### **4.5. Conclusion**

Our results address the effect of solution conditions on the seeded aggregation of  $\alpha$ -syn by using the ThT fluorescence assay. The effect of pH on the initial elongation rate is not significant, in contrast to its effect on the lag phase. Also the influence of salt on the elongation rate deviates from that on the lag phase. Both observations suggest that the nucleation and elongation proceed by different mechanisms.

#### **Acknowledgements**

We thank Ms. N. Schilderink from University of Twente for  $\alpha$ -synuclein expression and purification and Dr. Volodymyr Shvadchak for his help with data analysis. This work was performed in the research program entitled “A Single Molecule View on Protein Aggregation”, supported by the Foundation for Fundamental Research on Matter (FOM), which is part of the Netherlands Organization for Scientific Research (NWO).

#### 4.6. References

- [1] C.M. Dobson, Alzheimer's disease: addressing a twenty-first century plague, *Rend. Lincei*. 26 (2015) 251–262. doi:10.1007/s12210-015-0453-y.
- [2] S. Mankar, A. Anoop, S. Sen, S.K. Maji, Nanomaterials: amyloids reflect their brighter side, *Nano Rev.* 2 (2011) 1–12. doi:10.3402/nano.v2i0.6032.
- [3] S.I.A. Cohen, M. Vendruscolo, C.M. Dobson, T.P.J. Knowles, From macroscopic measurements to microscopic mechanisms of protein aggregation, *J. Mol. Biol.* 421 (2012) 160–171. doi:10.1016/j.jmb.2012.02.031.
- [4] F. Chiti, C.M. Dobson, Protein misfolding, functional amyloid, and human disease., *Annu. Rev. Biochem.* 75 (2006) 333–366. doi:10.1146/annurev.biochem.75.101304.123901.
- [5] T.P.J. Knowles, C.A. Waudby, G.L. Devlin, S.I.A. Cohen, A. Aguzzi, M. Vendruscolo, et al., An analytical solution to the kinetics of breakable filament assembly., *Science*. 326 (2009) 1533–1537. doi:10.1126/science.1178250.
- [6] P. Arosio, T.P.J. Knowles, S. Linse, On the lag phase in amyloid fibril formation, *Phys. Chem. Chem. Phys.* 17 (2015) 7606–7618. doi:10.1039/C4CP05563B.
- [7] S. Prigent, A. Ballesta, F. Charles, N. Lenuzza, P. Gabriel, L.M. Tine, et al., An Efficient Kinetic Model for Assemblies of Amyloid Fibrils and Its Application to Polyglutamine Aggregation, *PLoS One*. 7 (2012) 1–9. doi:10.1371/journal.pone.0043273.
- [8] L. Giehm, D.E. Otzen, Strategies to increase the reproducibility of protein fibrillization in plate reader assays, *Anal. Biochem.* 400 (2010) 270–281. doi:10.1016/j.ab.2010.02.001.
- [9] M.E. van Raaij, J. van Gestel, I.M.J. Segers-Nolten, S.W. de Leeuw, V. Subramaniam, Concentration dependence of alpha-synuclein fibril length assessed by quantitative atomic force microscopy and statistical-mechanical theory., *Biophys. J.* 95 (2008) 4871–4878. doi:10.1529/biophysj.107.127464.
- [10] A. Sidhu, I. Segers-Nolten, V. Subramaniam, Solution conditions define morphological homogeneity of  $\alpha$ -synuclein fibrils., *Biochim. Biophys. Acta*. 1844 (2014) 2127–2134. doi:10.1016/j.bbapap.2014.09.007.
- [11] D. Eisenberg, M. Jucker, The Amyloid State of Proteins in Human Diseases, *Cell*. 148 (2012) 1188–1203. doi:10.1016/j.cell.2012.02.022.
- [12] D. Pinotsi, A.K. Buell, C. Galvagnion, C.M. Dobson, G.S. Kaminski Schierle, C.F. Kaminski, Direct observation of heterogeneous amyloid fibril growth kinetics via two-color super-resolution microscopy, *Nano Lett.* 14 (2014) 339–345. doi:10.1021/nl4041093.
- [13] A.K. Buell, C. Galvagnion, R. Gaspar, E. Sparr, M. Vendruscolo, T.P.J. Knowles, et al., Solution conditions determine the relative importance of nucleation and growth processes in  $\alpha$ -synuclein aggregation., *Proc. Natl. Acad. Sci. U. S. A.* 111 (2014) 7671–7676. doi:10.1073/pnas.1315346111.
- [14] A.T. Sabareesan, J.B. Udgaonkar, Amyloid fibril formation by the chain B subunit of monellin occurs by a nucleation-dependent polymerization mechanism., *Biochemistry*.

- 53 (2014) 1206–17. doi:10.1021/bi401467p.
- [15] V.V. Shvadchak, M.M.A.E. Claessens, V. Subramaniam, Fibril Breaking Accelerates  $\alpha$ -Synuclein Fibrillization, *J. Phys. Chem. B.* 119 (2015) 1912–1918. doi:10.1021/jp5111604.
- [16] S.R. Collins, A. Douglass, R.D. Vale, J.S. Weissman, Mechanism of prion propagation: Amyloid growth occurs by monomer addition, *PLoS Biol.* 2 (2004). doi:10.1371/journal.pbio.0020321.
- [17] V. Meyer, P.D. Dinkel, E. Rickman Hager, M. Margittai, Amplification of Tau fibrils from minute quantities of seeds., *Biochemistry.* 53 (2014) 5804–9. doi:10.1021/bi501050g.
- [18] S.I.A. Cohen, S. Linse, L.M. Luheshi, E. Hellstrand, D. A. White, L. Rajah, et al., Proliferation of amyloid-42 aggregates occurs through a secondary nucleation mechanism, *Proc. Natl. Acad. Sci.* 110 (2013) 9758–9763. doi:10.1073/pnas.1218402110.
- [19] H. LeVine, Thioflavine T interaction with synthetic Alzheimer's disease beta-amyloid peptides: detection of amyloid aggregation in solution., *Protein Sci.* 2 (1993) 404–410. doi:10.1002/pro.5560020312.
- [20] S.J. Wood, J. Wypych, S. Steavenson, J. Louis, M. Citron, A.L. Biere,  $\alpha$ -Synuclein Fibrillogenesis is Nucleation-dependent, *Biochemistry.* (1999) 19509–19512.
- [21] C. Galvagnion, A.K. Buell, G. Meisl, T.C.T. Michaels, M. Vendruscolo, T.P.J. Knowles, et al., Lipid vesicles trigger  $\alpha$ -synuclein aggregation by stimulating primary nucleation, *Nat. Chem. Biol.* 11 (2015) 229–234. doi:10.1038/nchembio.1750.
- [22] R. Khurana, C. Ionescu-Zanetti, M. Pope, et al., A general model for amyloid fibril assembly based on morphological studies using atomic force microscopy., *Biophys. J.* 85 (2003) 1135–44. doi:10.1016/S0006-3495(03)74550-0.
- [23] L.A. Munishkina, J. Henriques, V.N. Uversky, A.L. Fink, Role of Protein - Water Interactions and Electrostatics in  $\alpha$ -Synuclein Fibril, (2004) 3289–3300.
- [24] V.N. Uversky, J. Li, A.L. Fink, Metal-triggered structural transformations, aggregation, and fibrillation of human  $\alpha$ -synuclein: A possible molecular link between parkinson's disease and heavy metal exposure, *J. Biol. Chem.* 276 (2001) 44284–44296. doi:10.1074/jbc.M105343200.
- [25] W. Hoyer, T. Antony, D. Cherny, G. Heim, T.M. Jovin, V. Subramaniam, Dependence of  $\alpha$ -synuclein aggregate morphology on solution conditions, *J. Mol. Biol.* 322 (2002) 383–393. doi:10.1016/S0022-2836(02)00775-1.
- [26] M. Mučibabić, M.M. Apetri, G.W. Canters, T.J. Aartsma, The effect of fluorescent labeling on  $\alpha$ -synuclein fibril morphology, *Biochim. Biophys. Acta - Proteins Proteomics.* (2016). doi:10.1016/j.bbapap.2016.07.007.
- [27] S. McClendon, C.C. Rospigliosi, D. Eliezer, Charge neutralization and collapse of the C-terminal tail of alpha-synuclein at low pH, *Protein Sci.* 18 (2009) 1531–1540. doi:10.1002/pro.149.
- [28] J. Bai, K. Cheng, M. Liu, C. Li, Impact of the  $\alpha$ -Synuclein Initial Ensemble Structure on Fibrillation Pathways and Kinetics, *J. Phys. Chem. B.* 120 (2016) 3140–3147. doi:10.1021/acs.jpcc.6b01225.



- [29] L. Bousset, L. Pieri, G. Ruiz-Arlandis, J. Gath, P.H. Jensen, B. Habenstein, et al., Structural and functional characterization of two alpha-synuclein strains., *Nat. Commun.* 4 (2013) 2575. doi:10.1038/ncomms3575.
- [30] V.N. Uversky, Evidence for a Partially Folded Intermediate in alpha-Synuclein Fibril Formation, *J. Biol. Chem.* 276 (2001) 10737–10744. doi:10.1074/jbc.M010907200.



# Intermittent growth of $\alpha$ -synuclein fibrils

### **Abstract**

A large variety of diseases appears to be associated with the occurrence of amyloid fibrils. This has urged studies aimed at the understanding of their underlying structure and the mechanism of their formation. The aggregation of  $\alpha$ -synuclein ( $\alpha$ -syn) from monomers via intermediate oligomers to amyloid fibrils is implied in the pathology of Parkinson's disease. Here, we studied the kinetics of  $\alpha$ -syn elongation, using short preformed  $\alpha$ -syn fibrils with active growing ends. The elongation of  $\alpha$ -syn was followed by monitoring their length increase with total internal reflection microscopy. From the length distribution of fibrils and the average fibrillar length increase in time we concluded that the elongation of  $\alpha$ -syn fibrils proceeds in a highly discontinuous pattern. This observation was corroborated by single fibril measurements that showed intermittent periods of halted elongation.

## 5.1. Introduction

The growing interest in the properties of amyloid fibrils and protein misfolding comes mostly from their association with around 50 health disorders [1]. Among the disorders connected to protein misfolding and the formation of depositions of insoluble amyloid fibrils are the two most common neurodegenerative diseases, namely Parkinson's disease (PD) and Alzheimer's disease. Considerable efforts are being made in the development of potential therapeutics for diseases derived from depositions of amyloids [2]. Amyloid fibrils are formed from intrinsically disordered proteins or unfolded protein domains adopting a parallel  $\beta$ -sheet conformation [3]. They typically consist of thousands of the monomer constituents [4], where all monomers adopt the same conformation that is stabilized by intermolecular hydrogen bonds and hydrophobic interactions [5,6]. Fibrils show extraordinary thermodynamic stability [7], but their formation is relatively slow since elongation proceeds by monomer addition to the fibril ends [8].

The formation of new fibrillization nuclei occurs not only by primary [9], but also by secondary nucleation [10] processes too. Fibril breaking, which involves existing fibrils, is one of the possible secondary nucleation processes [11]. In fact, the presence of amyloid fibrils may accelerate the formation of new fibrils [10] by secondary nucleation by which the process becomes autocatalytic and the fraction of fibrillized protein increases exponentially, slowing down only when monomeric protein is depleted [9]. The propensity of the protein to aggregate into fibrils is determined by 1) the rate of initial fibril formation from monomers and oligomers, 2) the rate of monomer binding to fibril ends, and 3) the efficiency of the secondary nucleation. Initial fibril formation and secondary nucleation rates strongly depend on experimental conditions [12]. Fibril elongation rate constants of different amyloidogenic proteins vary significantly, ranging from  $3 \times 10^6 \text{ M}^{-1}\text{s}^{-1}$  for amyloid beta (1-42) [10] to  $1.3 \times 10^3 \text{ M}^{-1}\text{s}^{-1}$  for  $\alpha$ -syn [9]. It has been shown that amyloid fibril growth is a heterogeneous process *i.e.* it has fibril-to-fibril variation [7,13].

To study the growth kinetics of  $\alpha$ -syn at the single fibril level,  $\alpha$ -syn elongation was followed in real time by fluorescence imaging. The rate of monomer binding to fibril ends was determined by measuring the length of individual fibrils at successive time intervals using total internal reflection microscopy (TIRF). The experiment involved the monitoring of surface-adsorbed  $\alpha$ -syn seeds in the presence of monomeric  $\alpha$ -syn. The use of seeds to initiate

the process bypasses the primary nucleation step which is inherently stochastic, and establishes a specific focus on fibril elongation. The evolution of the fibril length in time clearly indicated that the elongation rate of  $\alpha$ -syn fibrils is very heterogeneous. This finding was corroborated by additional two-color TIRF experiments. The intermittent fibrillar growth shown in this study provides a new view into the  $\alpha$ -syn aggregation process and emphasizes the heterogeneity of the growth kinetics.

## 5.2. Materials and Methods

### 5.2.1. Protein preparation and purification

Protein preparation and purification was performed as described elsewhere [14]. Briefly, protein was expressed in *E.coli* BL21 (DE3) transformed with the pT7-7 plasmid carrying the  $\alpha$ -syn gene. Culturing was done in LB medium containing 100  $\mu$ g/ml ampicillin. After IPTG induction (1 mM, 4 h) bacterial cell pellets were harvested by centrifugation ( $6,000 \times g$ , 10 min) and resuspended in 10 mM Tris-HCl, pH 8.0, 1 mM EDTA and 1 mM PMSF (10% of the culture volume) and stirred for 1 h at 4°C. Cells were lysed by sonication for 2 min and centrifuged ( $10,000 \times g$ , 20 min, 4°C).

DNA was precipitated by adding streptomycin sulfate (1%, 15 min, 4°C) and removed by centrifugation at  $13,500 \times g$  for 30 min. Then  $\alpha$ -syn was salted-out from the solution by slow addition of 0.295 g/ml of ammonium sulfate and mild stirring for 1 h at 4°C. Precipitated protein was collected by centrifugation ( $13,500 \times g$ , 30 min, 4°C). The pellet was gently resuspended in and purified on a 6 ml ResourceQ column using an Äkta Purifier system (GE Healthcare) and a linear gradient of NaCl (0–500 mM) in 10 mM Tris-HCl, pH 7.4 at a flow-rate of 3 ml/min (for purification of  $\alpha$ -syn-A140C both buffers contained 1 mM dithiothreitol (DTT)). Fractions containing  $\alpha$ -syn (eluted at  $\sim 300$  mM NaCl) were pooled, concentrated (Vivaspin-20, 10 kDa; GE Healthcare) and then desalted with a PD-10 column (GE Healthcare) using 10 mM Tris-HCl pH 7.4 (containing 1 mM DTT in the case of the cysteine mutant). Protein concentration was determined by the Tyrosine absorption at 275 nm using  $\epsilon=5600 \text{ M}^{-1} \text{ cm}^{-1}$  for WT  $\alpha$ -syn and  $5475 \text{ M}^{-1} \text{ cm}^{-1}$  for A140C  $\alpha$ -syn mutant.

### 5.2.2. Protein labeling

Prior to labeling  $\alpha$ -syn mutant A140C was incubated in 6 mM sodium phosphate buffer at pH 7.2, 150 mM NaCl with a 5-fold molar excess of DTT for 30 min to reduce possible disulfide bonds. DTT was removed using Zeba Spin desalting columns (Pierce, Rockford, IL, USA). A volume of 0.5–1 ml of 140  $\mu$ M A140C  $\alpha$ -syn was incubated overnight at 4°C with a 2-fold molar excess Alexa 488 maleimide or Alexa 647 maleimide, or with a 4-fold molar excess ATTO 655 maleimide. Afterwards, the excess of free dye was removed using two desalting steps on Zeba Spin desalting columns. The labeling efficiency was usually approximately 95% for all samples, confirmed by using mass spectrometry, gel electrophoresis and then calculated from the absorbance of the labeled sample. The concentration of labeled protein was estimated by using the absorbance of Alexa 488 maleimide ( $\epsilon_{490} = 73,000 \text{ cm}^{-1}\text{M}^{-1}$ ), Alexa 647 maleimide ( $\epsilon_{650} = 273,000 \text{ cm}^{-1}\text{M}^{-1}$ ), ATTO 655 maleimide ( $\epsilon_{663} = 125,000 \text{ cm}^{-1}\text{M}^{-1}$ ) in pH 7.4 phosphate buffer. Alexa 488 maleimide and Alexa 647 maleimide were purchased from Life Technologies Europe BV, Bleiswijk, The Netherlands and ATTO 655 maleimide from ATTO-TEC GmbH, Siegen, Germany.

### 5.2.3. Kinetic measurements

Aggregation experiments were performed using a Tecan Infinite M200 Pro plate reader and monitored by Thioflavin T (ThT) fluorescence. All experiments were performed at 37°C, under quiescent conditions in 96 plates (Nunc, Thermo Fisher Scientific) sealed with film (Viewseal, Greiner Bio One) to avoid evaporation, using a volume of 150  $\mu$ L per well. The final solution used for aggregation contained 6 mM sodium phosphate buffer at pH 7.2, 150 mM NaCl, 9 mM  $\text{NaN}_3$ , 0.1 mM EDTA (to remove divalent ions bound to  $\alpha$ -syn), and 5  $\mu$ M ThT. Protein concentration was 50  $\mu$ M unless otherwise indicated. Seeds were prepared using 10 min sonication in the water bath sonicator. Seeds were prepared from 1  $\mu$ M and 0.1  $\mu$ M solution of WT  $\alpha$ -syn monomer and their actual concentration was 1.6 and 0.16 nM respectively in our experiments. Fluorescence of ThT was recorded from the bottom of the plate. Excitation was at 446 nm, emission at 485 nm, excitation and emission spectral slit widths were 9 and 20 nm, respectively.

#### 5.2.4. TIRF Microscopy

Microscopy slides (26 × 76 mm, 1.5 mm thick, Menzel-Glazer) were cleaned in a 2% Hellmanex solution at 70°C, rinsed with milliQ water, and dried in an oven for 5 min at 80°C. As a final step, they were placed in a 3:1 solution mixture of sulfuric acid and hydrogen peroxide for 8 min. While performing this step extra precautions should be taken during chemical handling. After rinsing and sonicating for 5 min in milliQ water they were stored in milliQ water for a maximum 5 days. Before use microscopy slides were taken from storage, rinsed in ethanol and milliQ water and dried with a gentle nitrogen flow, and then mounted to a microfluidic cell (Ibidi Sticky-Slide VI 0.4). To 50  $\mu$ M monomeric solution of WT  $\alpha$ -syn we added 0.02 nM WT  $\alpha$ -syn seeds and aged the sample in 6 mM sodium phosphate buffer at pH 7.2, 150 mM NaCl, 9 mM NaN<sub>3</sub>, 0.1 mM EDTA, 6  $\mu$ M ThT at 37°C for 140 h in a microfluidic cell (180  $\mu$ L).

Imaging of seeded fibrils was performed using a homemade TIRF microscopy setup equipped with an argon ion laser (Innova 70C-5 Coherent) for excitation at 457 nm. The beam splitter (T425lpxr-UF1) and emission filter (zt458rdc-UF2) were purchased from Chroma. The 100 $\times$  objective (alpha Plan-Apochromat, 100 $\times$ /1.46 oil DIC) provides a 45  $\mu$ m field of view. The images (512 $\times$ 512 pixels, 88 nm/px) were recorded using the iXon 897 camera (Andor). For measuring the average fibril length at each time point at least 25 images were taken at random locations in the sample. The sample was stored in the dark at 37°C between measurements.

#### 5.2.5. Two-color TIRF microscopy

Seeds were prepared by sonication of mature fibrils of WT  $\alpha$ -syn containing 5% A140C-Alexa 488  $\alpha$ -syn. Prior to experiment seeds were imaged by atomic force microscopy (AFM) and their length distribution was in the range 100-500 nm. A total of 200  $\mu$ L sample for the direct observation of fibril growth was prepared in the test tube as follows: 0.02 nM A140C-Alexa 488  $\alpha$ -syn seeds, 67.5  $\mu$ M WT  $\alpha$ -syn monomers, 3.5  $\mu$ M A140C-ATTO 655  $\alpha$ -syn monomers in 6 mM sodium phosphate buffer at pH 7.2, 150 mM NaCl, 9 mM NaN<sub>3</sub>, 0.1 mM EDTA. The sample was loaded into a microfluidic cell (Ibidi Sticky-Slide VI 0.4, Ibidi GmbH, Germany) which was then mounted onto the microscope stage. The first image was taken 10–15 min after the sample preparation. We chose a suitable position and imaged the

sample every 10 min for 18 h. We verified the morphology of the aged sample by imaging different, randomly chosen positions at the end of the experiment.

Images were acquired on a Nikon Eclipse Ti microscope equipped with a 100 $\times$  TIRF Apo objective (Nikon, Japan). Excitation at 405 nm and 488 nm was achieved by using two separate 100 mW solid state diode lasers, both from Coherent Inc. (Santa Clara, U.S.A), and 647 nm excitation was achieved with a 300 mW CW fiber laser (MPBC, Quebec, Canada). All laser lines were combined by a LU4A laser unit (Nikon, Japan) with a Nikon STORM TIRF quad band cube filter set in the light path. All images were captured by an Andor iXon Plus 897 High Speed EM-CCD camera (Andor Technology, Belfast, Northern Ireland). Acquisition was automated using NisElements software (LIM, Czech Republic). The measurements were performed with the sample at ambient temperature.

TIRF images were analyzed by measuring the length of fibrils by determining the start and the end point of each fibril from the intensity profile using Simple Neurite Tracer plugin in ImageJ software. Typically 100-300 fibrils were characterized for the comparison of fibril lengths.

#### **5.2.6. AFM measurements**

The length of fibrillar seeds formed after sonication was determined by using AFM microscopy. Sample preparation for AFM was as follows: 10  $\mu$ l of sonicated 100  $\mu$ M WT  $\alpha$ -syn fibrils was diluted by a factor of 5-10 in 6 mM sodium phosphate buffer pH 7.2 and placed on unmodified freshly cleaved mica, and let to adsorb for 2 min. Unbound protein was gently washed off with 5  $\times$  50  $\mu$ l of HPLC grade water and dried using a gentle stream of nitrogen gas. The sample was then mounted on the AFM stage. AFM images were acquired using a Nanoscope IIIa controller (Digital Instruments, Santa Barbara, CA, USA) with a Multimode scanning probe microscope equipped with an E-scanner. All measurements were carried out in tapping mode under ambient conditions using single-beam silicon cantilever probes with the force constant of 22 to 41 N/m. All AFM images were captured with a resolution of 512 samples/line, a scan rate of 1 Hz and a scan size of 4  $\mu$ m  $\times$  4  $\mu$ m. For each sample the lengths of 30 fibrils were analyzed using Nanoscope analysis software.



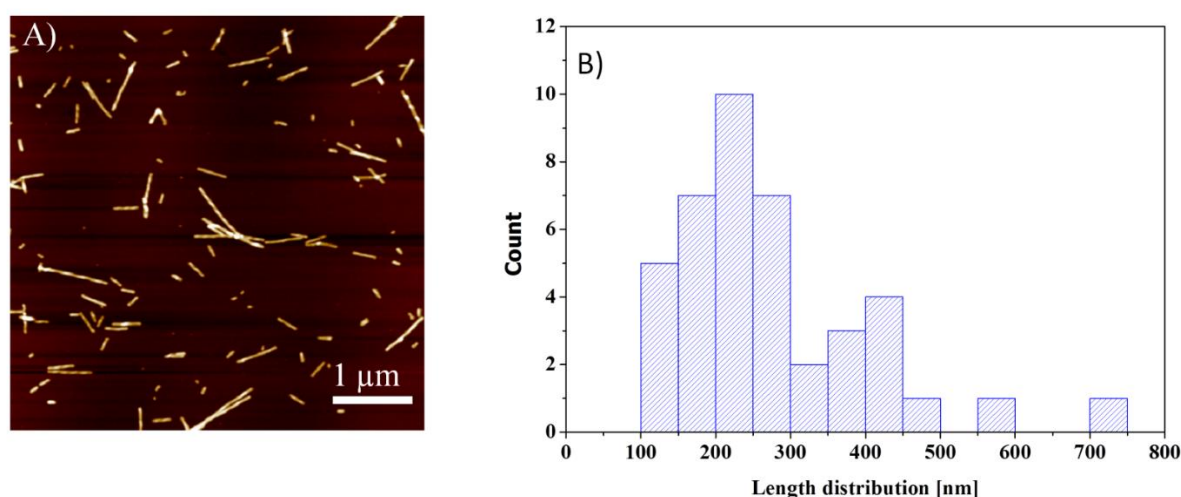


Figure 5.1: A) Representative atomic force microscopy (AFM) image of sonicated seed fibrils acquired with tapping mode in air. The fibrils were prepared in 6 mM sodium phosphate buffer pH 7.2, 150 mM NaCl, 9 mM  $\text{NaN}_3$ , 0.1 mM EDTA, and deposited on mica. AFM image size:  $4 \mu\text{m} \times 4 \mu\text{m}$ . B) Histogram of the seed length distribution. Average seed size is  $270 \pm 130$  nm.

### 5.3. Results and Discussion

#### 5.3.1. Fibrillar length propagation by TIRF microscopy

In order to determine the growth of  $\alpha$ -syn fibrils we monitored the elongation of seeds as a function of time using TIRF microscopy.  $\alpha$ -Syn seeds were prepared from samples containing "mature" fibrils, *i.e.*, from samples that were at the stage where the aggregation process reached the plateau phase as monitored by a ThT fluorescence assay. These samples were sonicated in a water bath sonicator by which the mature WT  $\alpha$ -syn fibrils break into smaller fragments which were then used as seeds. The average length of the seeds was 270 nm as determined by AFM (see Figure 5.1). Samples of 50  $\mu\text{M}$  monomeric solution of WT  $\alpha$ -syn and 0.02 nM WT  $\alpha$ -syn seeds were aged in the presence of 6  $\mu\text{M}$  ThT in quiescent conditions in a microfluidic cell. Seeds and growing fibrils that were adsorbed to the glass surface of the microfluidic cell were imaged by ThT fluorescence at intervals of 10-20 h over a total time span of 140 h, using a TIRF microscope. At this time scale the growth of seed fibrils by elongation dominates (Figure S.5.1) over spontaneous primary nucleation which occurs at a much slower rate than seed elongation [15]. At each time point we measured the length of at least 50 fibrils using ImageJ, and the experiment was repeated three times. Figure 5.2 shows the average fibrillar length as a function of time, where the time dependence of the average length increase is assumed to be linear within the first 10 h, at least to a good approximation. The increase of the average fibrillar length continued for about 20 h after which it levels off

and eventually remains constant. This observation cannot simply be explained by monomer depletion for the following reasons. Incorporation of one monomer increases the fibril length by 0.47 nm [16]. Taking into account the absorbance of the seed solution (equivalent to that of 12.5 nM solution of monomeric  $\alpha$ -syn) and the average length of the seeds (270 nm, *i.e.*, 570  $\alpha$ -syn monomers), the seed concentration is estimated to be 0.02 nM. The excess of monomer in solution is  $2.5 \times 10^6$  higher than the concentration of seeds and theoretically, if they all contributed to seed elongation, the fibrils would be over 100  $\mu\text{m}$  long. According to the results in Figure 5.2, the average length of the mature fibril is 2.3  $\mu\text{m}$  which means that only about 2% of the monomeric  $\alpha$ -syn pool was incorporated in the fibrils.

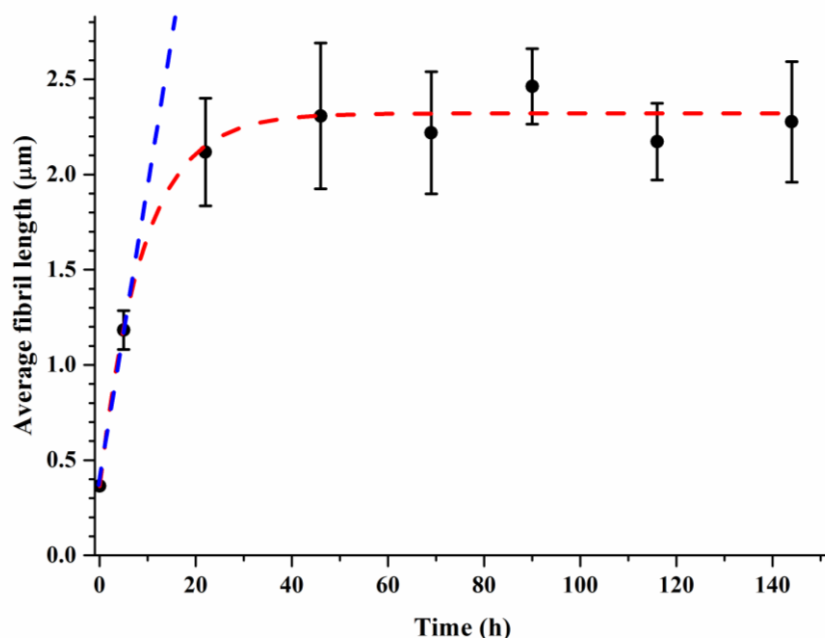


**Figure 5.2:** The increase in the average length of  $\alpha$ -syn fibrils with time. Samples were imaged at regular time intervals using a TIRF microscope and the length of observed fibrils was measured using ImageJ (Simple Neurite Tracer plugin). The average fibrillar length with the error bars of three independent experiments was fitted to  $\Delta L = a \exp(-k_q t)$ . At least 50 fibrils per sample were analyzed for each time point. The blue dashed line is the expected behavior not taking into account interruption of fibril growth.

Control experiments confirmed that the monomer concentration at the end stage of the experiment was still in large excess compared to the number of seeds. This was verified by measuring, using absorption spectrometry, and the residual monomer concentration in the supernatant after centrifuging the sample at the end of the plateau phase in Figure 5.2. The residual concentration of  $\alpha$ -syn monomers in solution was found to be  $10 \pm 3 \mu\text{M}$ . This is significantly higher than the  $K_d$  of  $\geq 3 \mu\text{M}$  of  $\alpha$ -syn monomers, and implies that elongation

still occurs. The possibility that the reduced monomer concentration was slowing down the fibril growth can be excluded since ThT signal did not increase further when  $\alpha$ -syn monomers were added to replenish the monomer concentration to 40  $\mu$ M, indicating that there was no additional growth. We also note that depletion of ThT molecules was not a limiting factor since the ThT signal did not increase upon addition of fresh 10  $\mu$ M of ThT.

We thus conclude that the fibrils actually stopped growing after approximately 20 h, reaching an average length of 2.3  $\mu$ m. To understand why such an impeded fibrillar growth occurred, the distribution of the fibrillar lengths after the first 19 h was analyzed (Figure 5.3A). In Figure 5.3A the red arrow indicates the average fibrillar length which clearly does not correspond to the most frequent length value. The most frequently observed fibrils are less than 1  $\mu$ m. It implies that most of the seeds indeed do elongate since their average length at the start of the experiment was 270 nm. The number of fibrils longer than 1  $\mu$ m up to 8  $\mu$ m is distinctly lower. In fact, the number distribution of fibrillar lengths decreases exponentially with increasing length, as shown in the insert of Figure 5.3A.

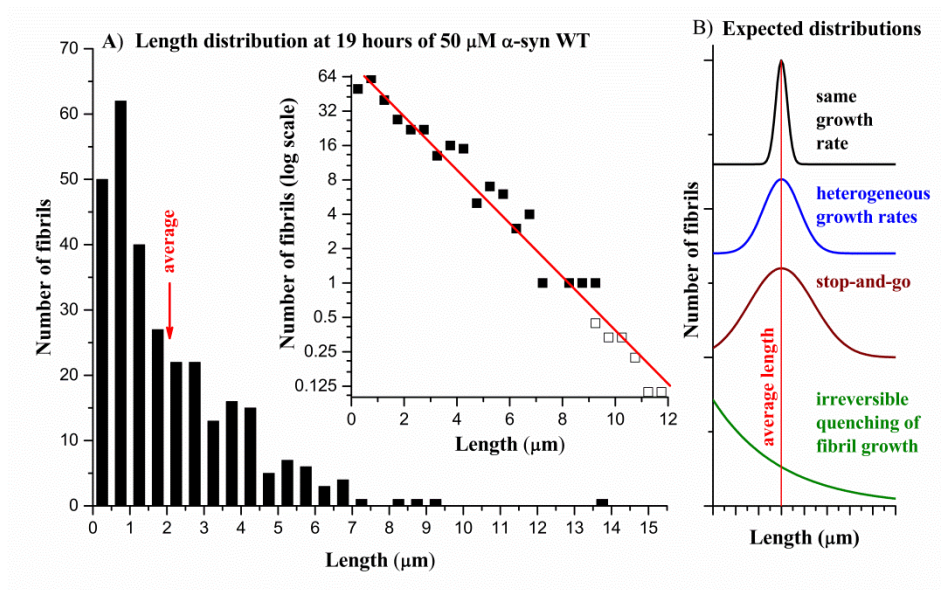


**Figure 5.3:** Measured fibrillar length distribution after 19 h aging. The elongation of 0.02 nM WT  $\alpha$ -syn seeds added to 50  $\mu$ M monomeric WT  $\alpha$ -syn and aged in 6 mM sodium phosphate buffer at pH 7.2, 150 mM NaCl, 9 mM  $\text{NaN}_3$ , 0.1 mM EDTA, 6  $\mu$ M ThT at 37°C was followed for 19 h. The bin size is 0.5  $\mu$ m. Open squares are recalculated from the data using a bin size of 3.5  $\mu$ m.

It is helpful to consider what one would expect in particular cases. For example, if we assume that the fibrils all elongate at a similar average elongation rate the distribution of fibril lengths would be a relatively narrow peak centered at the average fibril length which increases with time (Figure 5.3B). If fibrillar growth would follow a stop-and-go mechanism [13,17], it would result in a broader distribution with a maximum on the average length. Heterogeneity of fibril growth rates [8], *e.g.*, in case of two fibril populations, would result in two peaks with each centered at the average length of the corresponding population (Figure 5.3B).

The asymmetric length distribution is distinctly different from these assumed conditions, and is consistent with the conclusion that the fibrils stop growing after some time. The exponential shape of the distribution can be explained if we assume that the event that stops the growth of individual fibrils is randomly distributed in time. The distribution of time intervals (the number of occurrences of each interval *versus* duration) at which these events occur is then exponential. This translates into an exponential decrease of the length distribution if we assume that the average growth rate of each fibril is the same. It indicates that with time the fibril ends lose their ability to recruit additional protein molecules.

### 5.3.2. Relation of impeded fibrillar growth on monomer concentration

To determine if impeded fibrillar growth is a monomer-dependent process, the growth of fibrils out of seeds was evaluated at different concentrations of monomeric protein in solution. Here the rate  $k_q$  is introduced that represents the rate of occurrence of stopping events in fibril elongation. The dependence of the length distribution on the monomer concentration can be analyzed as follows.

The parameter  $z$  will be introduced as the probability of growth deactivation during the time necessary for the fibril to elongate by one monomer,  $z = k_q/k_+[M]$ . Here,  $k_+$  is the elongation rate and  $[M]$  the monomer concentration, and we have assumed that  $k_q \ll k_+[M]$ . Then the number of fibrils of length  $N + 1$  should be a factor of  $(1 - z)$  less than the number of fibrils with  $N$  monomers:  $C(N+1) = C(N) \times (1 - z)$ . By rewriting

$$\ln(1 - z) = \ln \frac{C(N+1)}{C(N)} = \frac{\ln C(N+1) - \ln C(N)}{(N+1) - N} = \frac{d \ln(C(N))}{dN}$$

Thus, we obtain for the number of fibrils containing  $N$  monomers

$$C(N) = \text{const} \times e^{N \ln(1-z)}$$

Since  $z \ll 1$  we can use the approximation  $\ln(1-z) \approx -z$  and we obtain

$$C(N) = \text{const} \times e^{-Nz}.$$

Thus a plot of  $\ln C(N)$  versus  $N$  is expected to result in a straight line with a slope of  $-k_q/k_+[M]$ :

$$\ln C(N) \propto -\frac{k_q}{k_+[M]} N$$

This expression corresponds to the experimentally observed fibril length distribution shown in Figure 5.3. Note that one monomer unit contributes approximately 0.47 nm to the fibril length [16].

To verify the expected dependence of the length distribution on the monomer concentration in case of impeded fibrillar growth, the growth of fibrils out of seeds was evaluated at different concentrations of monomeric protein in solution. The length of fibrils was measured after aggregating 5, 25 and 150  $\mu\text{M}$  monomeric  $\alpha$ -syn in the presence of 0.02 nM seeds for 19 h.

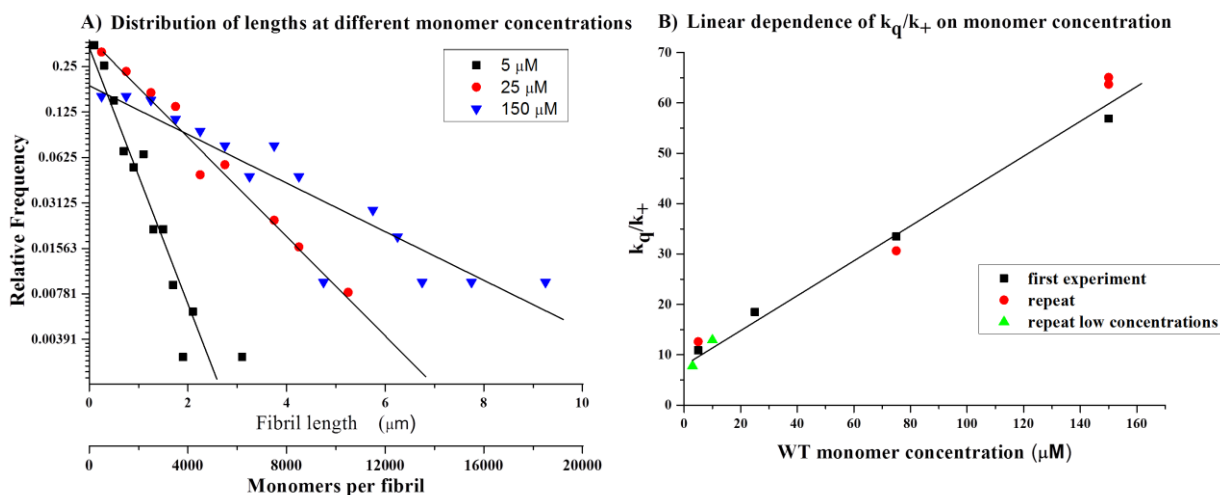


**Figure 5.4:** A) Length distribution of fibrils formed at different monomer concentrations after 19 h. B) Dependence of the  $k_q/k_+$  on monomer concentration.

In all cases the length distributions are exponential, but their slopes differ. By linear fitting the distribution in logarithmic coordinates (Figure 5.4A) the values of  $k_q/(k_+[M])$  could be calculated for each experiment and, since  $[M]$  is known, the dependence of  $k_q/k_+$  on monomer concentration is plotted in Figure 5.4B. The relation between  $k_q/k_+$  and  $[M]$  is clearly linear,

and implies that  $z$  is linearly increasing with monomer concentration. We surmise that stopping events of fibrillar growth are caused by the incorporation of monomers in a wrong conformation which then blocks further monomer addition.

### 5.3.3. Real-time observation of $\alpha$ -syn fibrillization by two color TIRF microscopy

To obtain more details of the dynamics of seed elongation we turned to the imaging of individual seeds and their development in real-time for 18 h using two-color TIRF. In this case, seeds were prepared by sonication of mature fibrils containing 5% of A140C-Alexa 488 labeled  $\alpha$ -syn. Monomeric  $\alpha$ -syn in a buffer solution consisted of a mixture of 67.5  $\mu$ M unlabeled WT and 3.5  $\mu$ M of A140C-ATTO 655 labeled  $\alpha$ -syn. At the start of the measurements seeds were localized on the surface, and the sample was imaged every 10-15 minutes thereafter for 18 h. The growth of filaments in time was observed in the red detection channel and distinguished from the seeds in green (Figure 5.6B).

The lengths of approximately 300 individual fibrils were measured after 18 h incubation. Approximately 85% of the observed fibrils grew bidirectionally. Our result is in agreement with the result of Pinotsi and coworkers [8]. For each fibril we measured the ratio of either fibril end to the length of the whole fibril. The distribution of this ratio is shown in Figure 5.5. The fit to a Gaussian function indicates that there is no correlation between the  $\alpha$ -syn elongation of two fibril ends, *i.e.*, the two ends grow independently of each other.

Figure 5.6A shows the lengths of individual fibrils as a function of time in the time window of 18 h. The observed increase of fibrillar length was not homogeneous, as active and inactive phases were observed in each case (Figure 5.6B). Some fibrils were not actively growing for several hours already in the starting phases of aggregation (Figure 5.6A), meaning that the intermittent fibrillar growth can occur regardless of the availability of the monomer in solution. The average elongation rate of  $\alpha$ -syn fibril in 18 h experiment was  $1.7 \pm 0.7 \text{ mM}^{-1}\text{s}^{-1}$ , which is in line with a previous report on the kinetics of  $\alpha$ -syn growth [11].

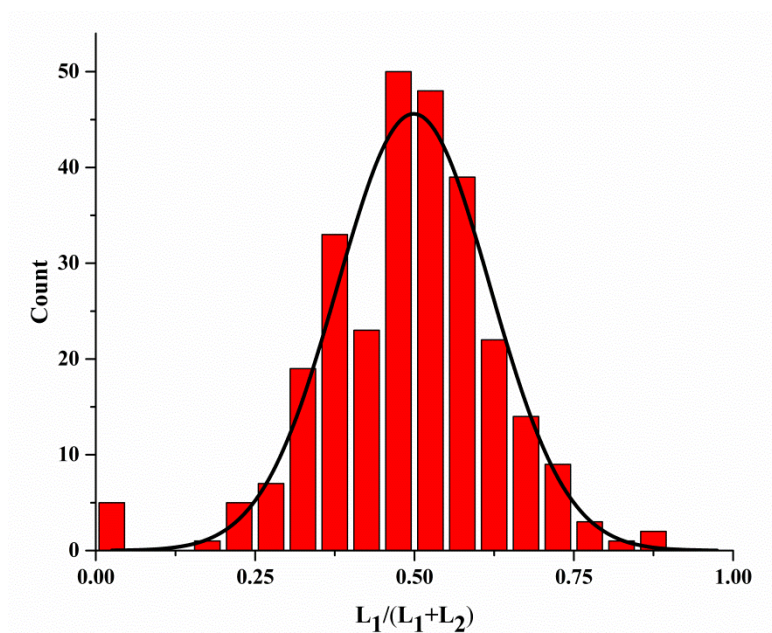


**Figure 5.5: Comparison of fibril elongation lengths in two directions. Distribution of elongation lengths of two fragments grown from the same seed (total 300 fibrils). The black line fits to the Gaussian provided peak at  $0.49 \pm 0.01$ . The spike at 0 corresponds to 5 fibrils that show growth only in one direction.**

Figure 5.6A shows the lengths of individual fibrils as a function of time in the time window of 18 h. The observed increase of fibrillar length was not homogeneous, as active and inactive phases were observed in each case (Figure 5.6B). Some fibrils were not actively growing for several hours already in the starting phases of aggregation (Figure 5.6A), meaning that the intermittent fibrillar growth can occur regardless of the availability of the monomer in solution. The average elongation rate of  $\alpha$ -syn fibril in 18 h experiment was  $1.7 \pm 0.7 \text{ mM}^{-1}\text{s}^{-1}$ , which is in line with a previous report on the kinetics of  $\alpha$ -syn growth [11].

Figure 5.6A shows the lengths of individual fibrils as a function of time in the time window of 18 h. The observed increase of fibrillar length was not homogeneous, as active and inactive phases were observed in each case (Figure 5.6B). Some fibrils were not actively growing for several hours already in the starting phases of aggregation (Figure 5.6A), meaning that the intermittent fibrillar growth can occur regardless of the availability of the monomer in solution. The average elongation rate of  $\alpha$ -syn fibril in 18 h experiment was  $1.7 \pm 0.7 \text{ mM}^{-1}\text{s}^{-1}$ , which is in line with a previous report on the kinetics of  $\alpha$ -syn growth [11].

Such intermittent fibril growth could be explained by  $\alpha$ -syn monomer binding to a fibril end in a misfolded conformation. In amyloid fibrils all monomer units adopt the same conformation and each amino acid in the parallel  $\beta$  strand forms hydrogen bonds with amino



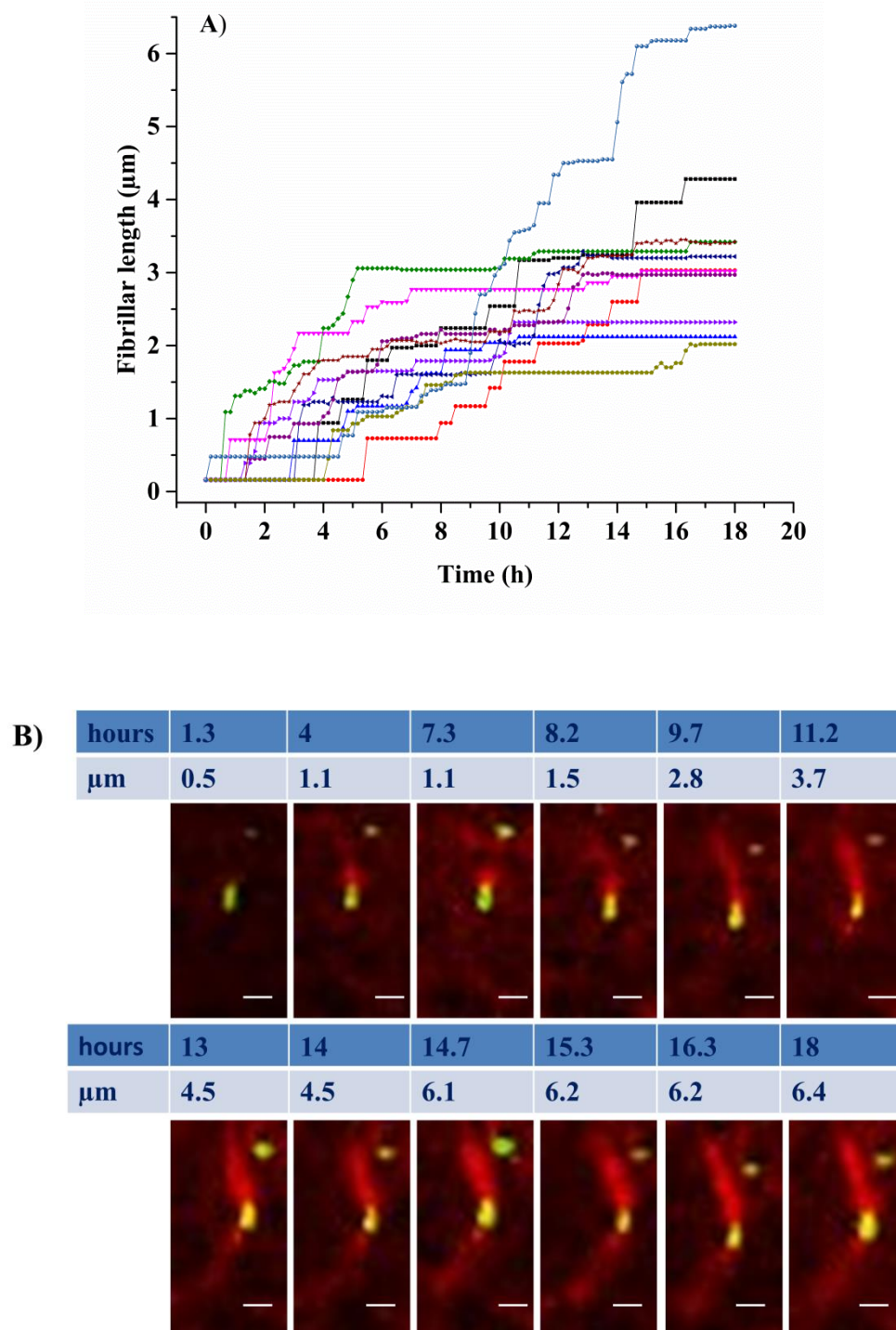


Figure 5.6: A) Elongation dynamics of 10 individual  $\alpha$ -syn fibrils. Fibrillar growth was followed using two-color TIRF imaging in the time interval of 18 h, imaged at every 10 min. Long plateaus correspond to stop states in the fibrillar growth. B) The elongation of the individual fibril.

acids at well-defined positions of the two surrounding monomer units [18,19]. Presumably, upon binding of an  $\alpha$ -syn monomer to the fibril end, some conformational optimization has to occur in order to facilitate further elongation. For the proper fibril elongation a new monomer



bound to the fibril end should adopt the same conformation as other proteins in the fibril as well as a proper hydrogen bonding configuration. Mismatched binding events may cause temporary or even permanent blockage of fibrillar growth. Addition of monomers to such seeds leads to their elongation, but also creates a probability of mismatched binding and subsequent deactivation that leads to discontinuities in the growth rate of individual fibrils with time (Figure 5.7).

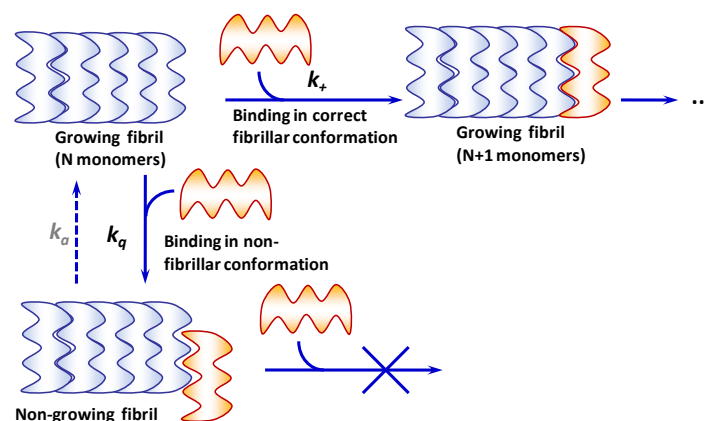


Figure 5.7: Proposed scheme of reversible interruption of fibril growth. Where new monomer (in orange) can bind the existing fibril in the proper conformation and lead to fibril elongation (N+1 monomer) or it might bind the existing fibril in wrong conformation and fibril cannot continue to elongate.

#### 5.4. Conclusion

The length increase of  $\alpha$ -syn fibrils in seeded aggregation proceeds in time in a discontinuous fashion with intermittent periods of halted elongation. Assuming that fibril elongation requires the addition of  $\alpha$ -syn in a more or less specific conformation to achieve continuous growth, it is concluded that the discontinuous elongation pattern probably results from monomer binding to fibril ends in a mismatched conformation for proper fibril elongation, blocking temporarily or even permanently further growth of the fibril. Fibrillar growth can continue if the mismatched  $\alpha$ -syn dissociates from the fibril or if it adopts the proper conformation for further elongation. This effect may account for the relatively low rate of aggregation compared to other amyloid proteins.

#### Acknowledgements

We thank Ms. N. Schilderink from University of Twente for  $\alpha$ -synuclein expression and purification, MSc Leffert Lanssink for collaborating in the single-color TIRF measurements,

and Dr. Volodymyr Shvadchak for help with kinetic model and data analysis. This work was performed in the framework of the research program “A Single Molecule View on Protein Aggregation”, supported by the Foundation for Fundamental Research on Matter (FOM), which is part of the Netherlands Organization for Scientific Research (NWO).

## 5.5. References

- [1] F. Chiti, C.M. Dobson, Protein misfolding, functional amyloid, and human disease., *Annu. Rev. Biochem.* 75 (2006) 333–366. doi:10.1146/annurev.biochem.75.101304.123901.
- [2] D.J. Selkoe, Folding proteins in fatal ways., *Nature.* 426 (2003) 900–904. doi:10.1038/nature02477.
- [3] R. Nelson, M.R. Sawaya, M. Balbirnie, A.Ø. Madsen, C. Riek, R. Grothe, D. Eisenberg, Structure of the cross-beta spine of amyloid-like fibrils., *Nature.* 435 (2005) 773–778. doi:10.1038/nature03680.
- [4] J.D. Schmit, K. Ghosh, K. Dill, What drives amyloid molecules to assemble into oligomers and fibrils?, *Biophys. J.* 100 (2011) 450–458. doi:10.1016/j.bpj.2010.11.041.
- [5] A.W.P. Fitzpatrick, G.M. Vanacore, A.H. Zewail, Nanomechanics and intermolecular forces of amyloid revealed by four-dimensional electron microscopy, *Proc. Natl. Acad. Sci.* 112 (2015) 3380–3385. doi:10.1073/pnas.1502214112.
- [6] J. Greenwald, R. Riek, Biology of amyloid: Structure, function, and regulation, *Structure.* 18 (2010) 1244–1260. doi:10.1016/j.str.2010.08.009.
- [7] F. Meersman, C.M. Dobson, Probing the pressure-temperature stability of amyloid fibrils provides new insights into their molecular properties., *Biochim. Biophys. Acta.* 1764 (2006) 452–60. doi:10.1016/j.bbapap.2005.10.021.
- [8] D. Pinotsi, A.K. Buell, C. Galvagnion, C.M. Dobson, G.S. Kaminski Schierle, C.F. Kaminski, Direct observation of heterogeneous amyloid fibril growth kinetics via two-color super-resolution microscopy, *Nano Lett.* 14 (2014) 339–345. doi:10.1021/nl4041093.
- [9] T.P.J. Knowles, C.A. Waudby, G.L. Devlin, S.I.A. Cohen, A. Aguzzi, M. Vendruscolo, E.M. Terentjev, M.E. Welland, C.M. Dobson, An analytical solution to the kinetics of breakable filament assembly., *Science.* 326 (2009) 1533–1537. doi:10.1126/science.1178250.
- [10] G. Meisl, X. Yang, E. Hellstrand, B. Frohm, J.B. Kirkegaard, S.I.A. Cohen, C.M. Dobson, S. Linse, T.P.J. Knowles, Differences in nucleation behavior underlie the contrasting aggregation kinetics of the A $\beta$ 40 and A $\beta$ 42 peptides., *Proc. Natl. Acad. Sci. U. S. A.* 111 (2014) 9384–9. doi:10.1073/pnas.1401564111.
- [11] V.V. Shvadchak, M.M.A.E. Claessens, V. Subramaniam, Fibril Breaking Accelerates  $\alpha$ -Synuclein Fibrillization, *J. Phys. Chem. B.* 119 (2015) 1912–1918. doi:10.1021/jp5111604.
- [12] C. Galvagnion, A.K. Buell, G. Meisl, T.C.T. Michaels, M. Vendruscolo, T.P.J. Knowles, C.M. Dobson, Lipid vesicles trigger  $\alpha$ -synuclein aggregation by stimulating primary nucleation, *Nat. Chem. Biol.* 11 (2015) 229–234. doi:10.1038/nchembio.1750.
- [13] M.M. Wördehoff, O. Bannach, H. Shaykhalishahi, A. Kulawik, S. Schiefer, D. Willbold, W. Hoyer, E. Birkmann, Single Fibril Growth Kinetics of  $\alpha$ -Synuclein, *J. Mol. Biol.* 427 (2015) 1428–1435. doi:10.1016/j.jmb.2015.01.020.
- [14] M. Mučibabić, M.M. Apetri, G.W. Canters, T.J. Aartsma, The effect of fluorescent labeling on  $\alpha$ -synuclein fibril morphology, *Biochim. Biophys. Acta - Proteins Proteomics.* (2016). doi:10.1016/j.bbapap.2016.07.007.
- [15] D. Pinotsi, C.H. Michel, A.K. Buell, R.F. Laine, P. Mahou, C.M. Dobson, C.F. Kaminski, G.S.K. Schierle, Nanoscopic insights into seeding mechanisms and toxicity of  $\alpha$ -synuclein species in neurons, *Proc Natl Acad Sci U S A.* I (2016) 1–5. doi:10.1073/pnas.1516546113.
- [16] L.C. Serpell, J. Berriman, R. Jakes, M. Goedert, R.A. Crowther, Fiber diffraction of synthetic alpha-synuclein filaments shows amyloid-like cross-beta conformation., *Proc. Natl. Acad. Sci. U. S. A.* 97 (2000) 4897–4902. doi:10.1073/pnas.97.9.4897.

- [17] W. Hoyer, D. Cherny, V. Subramaniam, T.M. Jovin, Rapid self-assembly of  $\alpha$ -synuclein observed by in situ atomic force microscopy, *J. Mol. Biol.* 340 (2004) 127–139. doi:10.1016/j.jmb.2004.04.051.
- [18] A.W.P. Fitzpatrick, G.T. Debelouchina, M.J. Bayro, D.K. Clare, M.A. Caporini, V.S. Bajaj, C.P. Jaroniec, L. Wang, V. Ladizhansky, S.A. Müller, C.E. MacPhee, C.A. Waudby, H.R. Mott, A. De Simone, T.P.J. Knowles, H.R. Saibil, M. Vendruscolo, E. V Orlova, R.G. Griffin, C.M. Dobson, Atomic structure and hierarchical assembly of a cross- $\beta$  amyloid fibril., 2013. doi:10.1073/pnas.1219476110.
- [19] M. Vilar, H.-T. Chou, T. Lührs, S.K. Maji, D. Riek-Loher, R. Verel, G. Manning, H. Stahlberg, R. Riek, The fold of  $\alpha$ -synuclein fibrils, *105* (2008) 8637–8642. doi:10.1073/pnas.0712179105.

## 5.6. Supporting Information

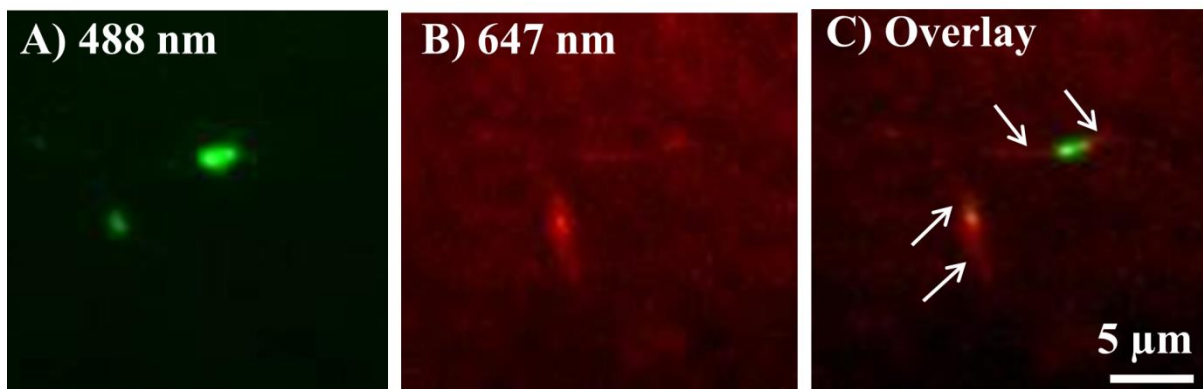


Figure S.5.1: Two-color TIRF images of elongated fibrils showing the  $\alpha$ -syn seeds (A) (in green) and their elongation (B) (in red), as well as the overlay (C) of images (A) and (B).

# Substrate surface affects $\alpha$ -synuclein aggregate morphology<sup>1</sup>

### Abstract

$\alpha$ -Synuclein ( $\alpha$ -syn), a small presynaptic protein, is one of the major components of the Lewy bodies found in the neurons of patients with Parkinson's disease. The interaction between  $\alpha$ -syn and cell membranes is believed to be a key factor mediating the normal function of the protein, but under particular circumstances, it may facilitate amyloid fibril formation. In the present study, the growth of  $\alpha$ -syn aggregates was observed and analyzed on a supported lipid bilayer (SLB), an untreated glass coverslip, and in solution, using real-time total internal reflection microscopy. Our results show that the morphology of aggregates depends on the conditions applied during the experiment. In addition to the formation of isolated linear fibrils, we observed the formation of extended three-dimensional aggregated structures composed of micrometer-long  $\alpha$ -syn fibrils on glass surfaces in real time. On SLBs and in solution, however, we found only linear amyloid fibrils. The occurrence of these distinct aggregate types strongly suggests that substrate surface properties may have a significant effect on the growth and morphology of  $\alpha$ -syn aggregates.

---

<sup>1</sup> This chapter is based on a manuscript in preparation for publication: M. Mučibabić, D. Donato, D. Heinrich, G. W. Canters, and T. J. Aartsma

## 6.1. Introduction

Parkinson's disease (PD) follows Alzheimer's disease on the list of the most common neurodegenerative disorders [1], affecting 1-2% of the population above the age of 65 [2]. PD is characterized by the loss of dopaminergic neurons in the *substantia nigra* of the patient's brain and by the occurrence of characteristic intracellular inclusions known as Lewy bodies [3]. Over the years, point mutations [4] and multiplications of the SNCA gene, coding for  $\alpha$ -syn, have been linked to PD. Confirmation that the fibrils of  $\alpha$ -syn are a major component of Lewy bodies [5] has brought this small presynaptic protein into the spotlight of the scientific community.

$\alpha$ -Syn is known to regulate the synaptic vesicle-pool size [6] and the release of dopamine [7]. Intrinsically disordered in solution, the 140 residue  $\alpha$ -syn binds to phospholipid membranes *via* the N-terminal region and then adopts a partially helical structure [8,9]. At sufficiently high concentrations,  $\alpha$ -syn forms several microns long fibrils in solution [10]. Amyloid-fibril formation has been studied extensively, taking into account, for example, the role of nucleation-dependent polymerization [11], fibril breaking [12,13], primary nucleation [14], and secondary nucleation processes [15].

Because many processes in live cells take place at interfaces, it is of great interest to study the effects of protein-surface interactions on the formation, the structure and the stability of protein aggregates, particularly when these aggregates are implicated in the pathology of neurodegenerative diseases. Interaction of monomeric or oligomeric  $\alpha$ -syn with lipid membranes affects the conformation of the protein itself as well as the ordering of the lipid bilayer [16]. Experimental evidence has shown that  $\alpha$ -syn aggregation occurs on the membrane surface [17] and that the interaction with lipid bilayers promotes and accelerates the formation of oligomeric species suspected to be cytotoxic [18]. These effects can occur in the nucleation phase of aggregation and/or at the elongation stage.

Current fluorescence-imaging techniques allow the direct observation in real time of single molecules and particles, especially when they are in close proximity to the surface. Here, we used high resolution fluorescence imaging to characterize the growth and morphology of  $\alpha$ -syn species on different surfaces, *i.e.*, supported lipid bilayers (SLB) and bare glass coverslips, where we focus specifically on the elongation stage. Thus, we were able to directly compare the growth rate on substrates with the growth rate in solution by

determining the length of surface-adsorbed fibrils as a function of time. We focused specifically on the elongation of individual fibrils and monitored the growth kinetics starting with preformed seeds. The seeds were obtained by sonication of mature  $\alpha$ -syn fibrils to break them into small fragments. These fragments are active templates for aggregation. Identifying individual seeds and the incorporation of  $\alpha$ -syn from solution was achieved by labeling the seeds and the monomers with spectrally distinct fluorophores.

Imaging of surface-adsorbed aggregates was performed by using two-color, real-time total internal reflection fluorescence (TIRF) microscopy, taking advantage of its high resolution and optimal signal to noise ratio [19–23]. Recently, it was shown that this form of microscopy is useful to study aggregation of various intrinsically disordered proteins [24–27], as it provides quantitative information about the growth of the aggregates.

On a glass surface we observed not only the growth of micrometer long fibrils, but also the growth of large, extended three-dimensional aggregated structures. These structures were composed of fibrillar networks of  $\alpha$ -syn, which was not reported previously. The extended three-dimensional aggregate structures of variable diameter and height were observed at the end stage of the experiment. It is remarkable that these structures are formed in a relatively short time, already after 3 h, which may have implications for understanding the formation of Lewy bodies. Our finding of the facile formation of two different aggregate morphologies suggests a significant impact of the surface on the growth of  $\alpha$ -syn aggregates and possibly on the underlying amyloid aggregation mechanism.

## **6.2. Materials and Methods**

### **6.2.1. Protein preparation and purification**

Protein preparation and purification were performed as previously described [28]. Briefly, protein expression was performed in *E. coli* BL21 (DE3) transformed with the pT7-7 plasmid carrying the  $\alpha$ -syn gene. Culturing in lysogeny broth medium was done with 100  $\mu$ g/ml ampicillin. After isopropylthio- $\beta$ -galactoside induction (1 mM, 4 h), bacterial cell pellets were harvested by centrifugation (6,000  $\times$  g, 10 min) and resuspended in a solution of 10 mM Tris-HCl, pH 8.0, 1 mM EDTA and 1 mM PMSF (10% of the culture volume) and stirred for 1 h at 4°C. Cells were lysed by sonication for 2 min and then centrifuged (10,000  $\times$  g, 20 min, 4°C).

DNA was precipitated from the cell extract by adding streptomycin sulfate (1%, 15 min, 4°C) and removed by centrifugation at  $13,500 \times g$  for 30 min. Then,  $\alpha$ -syn was salted out from the solution by slow addition of 0.295 g/ml of ammonium sulfate and mild stirring for 1 h at 4°C. Precipitated protein was collected by centrifugation ( $13,500 \times g$ , 30 min, 4°C). The pellet was gently resuspended in and purified on a 6 ml ResourceQ column using an Äkta Purifier system (GE Healthcare) and a linear gradient of NaCl (0–500 mM) in 10 mM Tris–HCl, pH 7.4 at a flow-rate of 3 ml/min (for purification of  $\alpha$ -syn-A140C both buffers contained 1 mM dithiothreitol (DTT)). Fractions containing  $\alpha$ -syn (eluted at ~300 mM NaCl) were pooled, concentrated (Vivaspin-20, 10 kDa; GE Healthcare) and then desalted with a PD-10 column (GE Healthcare) using 10 mM Tris–HCl pH 7.4 (containing 1 mM DTT in the case of the cysteine mutant). Protein concentration was determined by tyrosine absorption at 275 nm using  $5600 \text{ M}^{-1}\text{cm}^{-1}$  extinction coefficient for WT and  $5745 \text{ M}^{-1}\text{cm}^{-1}$  for A140C  $\alpha$ -syn [29,30].

### 6.2.2. Protein labeling

Prior to labeling,  $\alpha$ -syn mutant A140C was incubated with a 5-fold molar excess of DTT for 30 min to reduce possible disulfide bonds. Afterwards, DTT was removed using Zeba Spin desalting columns (Pierce, Rockford, IL, USA). A volume of 0.5–1 ml of 140  $\mu\text{M}$  A140C  $\alpha$ -syn was incubated overnight at 4°C with either 2-fold molar excess Alexa 488 maleimide, or Alexa 647 maleimide, or 4-fold molar excess ATTO 655 maleimide. Afterwards, the excess of free dye was removed using two desalting steps on Zeba Spin desalting columns. The labeling efficiency was approximately 95% for all samples, calculated from the absorbance of the labeled sample and confirmed by mass spectrometry and gel electrophoresis. The concentration of labeled protein was estimated using the absorbance of Alexa 488 maleimide ( $\epsilon_{490} = 73,000 \text{ cm}^{-1}\text{M}^{-1}$ ), Alexa 647 maleimide ( $\epsilon_{650} = 273,000 \text{ cm}^{-1}\text{M}^{-1}$ ) and ATTO 655 maleimide ( $\epsilon_{663} = 125,000 \text{ cm}^{-1}\text{M}^{-1}$ ) in 6 mM sodium phosphate buffer at pH 7.2. Alexa 488 maleimide and Alexa 647 maleimide were purchased from Life Technologies Europe BV, Bleiswijk, The Netherlands and ATTO 655 maleimide from ATTO-TEC GmbH, Siegen, Germany.

### 6.2.3. Glass cover slip cleaning procedure

Microscope slides (26 mm  $\times$  76 mm, 1.5 mm thick, Menzel-Glazer, Braunschweig, Germany) were cleaned using 30-min sonication steps in the following solutions: ethanol, methanol, 4



M sodium hydroxide. In between each step, the microscope slides were thoroughly rinsed and sonicated in milliQ for 30 min. Prior to imaging, the slides were ozone cleaned for 30 min and then attached to a complementary plate with fittings for in- and outlet tubing (Ibidi Sticky-Slide VI 0.4, Ibidi GmbH, Germany), thus forming a microchannel structure which was mounted on the microscope stage. Silanization of the glass slides was performed by 5-min sonication in methanol, followed by 30-min incubation with 1% acetic acid and 1% N-(2-aminoethyl)-3-aminopropyl-trimethoxysilan in methanol with 1-min sonication every 10 min [31]. Slides were subsequently rinsed in methanol and heated in an oven at 70°C for 2 h.

#### 6.2.4. Supported lipid bilayer (SLB) preparation

For SLB preparation, a zwitterionic 1-palmitoyl-2-oleoyl-sn-glycero-3-phosphocholine lipid (POPC) was used. Stock ampoules (25 mg) of POPC were purchased from Avanti polar and stored at -20°C. The lipid powders were dissolved in chloroform and dried with argon in glass vials 1 mg each and again stored at -20°C until required. Following the procedure reported in reference [32], we dissolved 1 mg POPC in 4 ml buffer at pH 7.2 containing 6 mM sodium phosphate and, in addition, 150 mM NaCl, resulting in a concentration of 0.25 mg/ml. After incubation at 4°C for 1 h, the vial was sonicated for 15 min in a water bath sonicator to make small unilamellar vesicles (SUV). The microfluidic cell was loaded with a total of 200  $\mu$ l of the SUV sample and kept for 2 h at room temperature to allow the formation of the supported lipid bilayer by vesicle fusion. The SUVs rupture and spread on the surface, forming a mostly uniform SLB as can be seen in the fluorescence image in Figure 6.1. After incubation, the excess of free vesicles and debris were removed from the microfluidic cell by rinsing with 6 mM sodium phosphate buffer at pH 7.2, 150 mM NaCl.

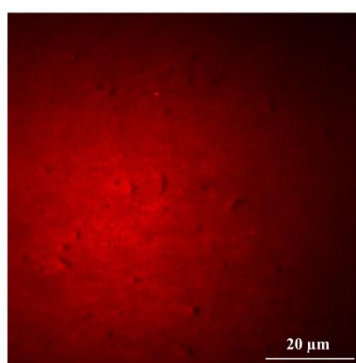


**Figure 6.1:** TIRF image of supported lipid bilayer (SLB) made of 100% POPC. 10 nM solution of ATTO 647N fluorescent dye was added to the surface of the SLB. Based on the intensity distribution of the fluorescent dye it can be estimated whether the SLB is homogeneous. Relatively equal intensity distribution of ATTO 647N dye used to characterize the surface of the SLB prior to aggregation experiment confirmed the homogeneity of the formed bilayer. TIRF image size: 82  $\times$  82  $\mu$ m.

### 6.2.5. Seeds preparation and characterization

$\alpha$ -Syn seeds were prepared in solution from aggregated  $\alpha$ -syn samples that had reached the end phase of aggregation as verified by ThT assays. The seeds were formed by breaking partially labeled mature  $\alpha$ -syn fibrils (95% WT + 5% A140C-Alexa 488) by sonication in a water bath. The length of the fragments or seeds after sonication was determined by atomic force microscopy (AFM).

Sample preparation for AFM was as follows: 10  $\mu$ l of sonicated fibrils containing 70  $\mu$ M  $\alpha$ -syn, was 5-10 times diluted in 6 mM sodium phosphate buffer pH 7.2 and then applied to unmodified freshly cleaved mica sheet. After letting it rest for 2 min, unbound protein was gently washed off with  $5 \times 50$   $\mu$ l of HPLC grade water and the mica surface with adsorbed fibrils was dried using a gentle stream of nitrogen gas. The sample was then mounted on the AFM stage.

AFM images were acquired using a Nanoscope IIIa controller (Digital Instruments, Santa Barbara, CA, USA) with a Multimode scanning probe microscope equipped with an E-scanner. All measurements were carried out in the tapping mode under ambient conditions using single-beam silicon cantilever probes with a force constant of 22 to 41 N/m. All AFM images were captured by scanning 512 lines with a resolution of 512 points/line, with a scan rate of 1 Hz and a scan size of 4  $\mu$ m  $\times$  4  $\mu$ m. About 30 fibrils of each image were analyzed for length determination, using the Nanoscope analysis software.

### 6.2.6. TIRF imaging

Images were acquired on a Nikon Ti Eclipse microscope equipped with a 100 $\times$  TIRF Apo objective (Nikon, Japan). Excitation at 405 nm and 488 nm was achieved using two separate 100 mW solid state diode lasers, both from Coherent Inc. (Santa Clara, U.S.A), and 647 nm excitation was achieved with a 300 mW CW fiber laser (MPBC, Quebec, Canada). All laser lines were combined by a LU4A 4-laser unit (Nikon, Japan) with a Nikon STORM TIRF quad band cube filter set in the light path. All images were captured by an Andor iXon Plus 897 High Speed EM-CCD camera (Andor Technology, Belfast, Northern Ireland). Acquisition was automated using NisElements software (LIM, Czech Republic). The measurements were performed with the sample at ambient temperature.

A total of 200  $\mu\text{l}$  sample for direct observation of fibril growth was prepared in the test tube by mixing 0.02 nM A140C-Alexa 488 labeled  $\alpha$ -syn seeds, 67.5  $\mu\text{M}$  WT  $\alpha$ -syn monomers, and 3.5  $\mu\text{M}$  A140C-ATTO 655 labeled  $\alpha$ -syn monomers in 6 mM sodium phosphate buffer at pH 7.2, which also contained 150 mM NaCl, 9 mM  $\text{NaN}_3$ , and 0.1 mM EDTA. The sample was loaded into a microfluidic cell (Ibidi Sticky-Slide VI 0.4, Ibidi GmbH, Germany) which was then mounted onto the microscope stage. The first image was taken 10–15 min after sample preparation. The sample was imaged every 10 min in TIRF mode for 18 h. At the end of each experiment additional images were taken of other areas of the sample to verify that the time-line data were representative. The system was switched to confocal mode for three-dimensional imaging at the end point of the time series.

### 6.2.7. TIRF image analysis

TIRF images were analyzed by measuring the length of fibrils by determining the start and the end point of each fibril from the intensity profile using ImageJ software (plugins-segmentation-simple neurite tracer function). The average elongation rate of individual fibrils was calculated from the length increase over a particular time interval  $\Delta t$ , expressed as follows:

$$\frac{\Delta N(t)}{\Delta t} = \frac{L_t - L_0}{0.47 \text{ nm} (t - t_0)} = k_+ [M]$$

Here,  $\Delta N(t)$  is the number of monomers that were added in the time interval of  $\Delta t$ ,  $[M]$  is the monomer concentration,  $L_0$  is the length of the fibril at  $t_0$  while  $L_t$  is the length of the fibril at a later time  $t$ .  $\Delta N(t)$  is calculated by using the experimentally determined length increase per monomer, which is 0.47 nm [33]. Thus we have for  $k_+$ :

$$k_+ = \frac{L_t - L_0}{0.47 \text{ nm}(t - t_0) [M]}$$

The units of  $k_+$  are  $\text{mM}^{-1} \text{s}^{-1}$ . For each elongation rate the lengths of at least 150 fibrils were analyzed.

## 6.3. Results

Aggregation of  $\alpha$ -syn, described as a three-step process, is initiated by the nucleation-dependent formation of small, soluble oligomers of different sizes and shapes [34].

Presumably, these initial aggregates are oligomeric species which undergo some structural reorganization [35] by which they develop an amyloidogenic, structural template that is required for the second step (*i.e.* the development and growth of fibrils). Elongation of fibrils proceeds by the addition of  $\alpha$ -syn monomers to the fibril ends [12,23,26]. Fibril breaking and secondary nucleation may enhance the growth rate. In the third, end phase, the  $\alpha$ -syn monomer is depleted and the fibrils stop growing [34].

The initial phase of the  $\alpha$ -syn aggregation process, governed by primary nucleation, exhibits a stochastic character and is kinetically poorly defined. To establish better defined conditions for real-time imaging, we bypassed the initiation phase of the aggregation process by focusing on  $\alpha$ -syn fibril elongation using seeds which consisted of short, preformed fibrils. The seeds were prepared from mature fibrils that were obtained by aging a solution of a 20:1 mixture of monomeric WT and A140C-Alexa 488 labeled  $\alpha$ -syn (green fluorescence). Due to this low labeling ratio, the effect of the attached label on the aggregation process was minimized. The seeds were then obtained by sonication of a solution of these mature fibrils, by which the fibrils broke into small fragments. Characterization by AFM showed that the seeds had an average length of 270 nm and the length distribution had a width of about 130 nm (Figure 5.1). The seeds were subsequently mixed with a solution of monomeric  $\alpha$ -syn consisting of a mixture of 95% WT and 5% A140C-ATTO 655  $\alpha$ -syn (red fluorescence). For all experiments described, the same batch of seeds was used to assure that the seeding conditions were the same in all cases.

TIRF microscopy allows imaging of fluorescent molecules close to glass surface. When a sample was deposited on a microscope slide, the seeds quickly adsorbed to the glass surface. Since the number of seeds adsorbed on the glass surface stayed constant in time, we concluded that no significant growth was occurring in solution. Surface-adsorbed seeds were visualized by monitoring the fluorescence in the green detection channel, whereas elongation was monitored in the red channel (Figure 6.2). Images were taken in TIRF mode every 10 minutes over a time span of up to 18 h or longer. Seeds (shown in green) and their characteristics, such as position and size, remained unchanged in time. On either end of the seeds, the binding of  $\alpha$ -syn was observed by the appearance of a red-fluorescent extension (Figure 6.2).

The results show that seeds elongate in both directions, consistent with an earlier report [23]. After 18 h, the end stage of aggregation, mature fibrils dominated the population with an

average length of 3.3  $\mu\text{m}$ . The average growth rate of the fibrils was  $k_+ = 1.54 \pm 0.39 \text{ mM}^{-1}\text{s}^{-1}$ . Here, we focused on a type of aggregate of  $\alpha$ -syn that has not been reported before under *in vitro* conditions.

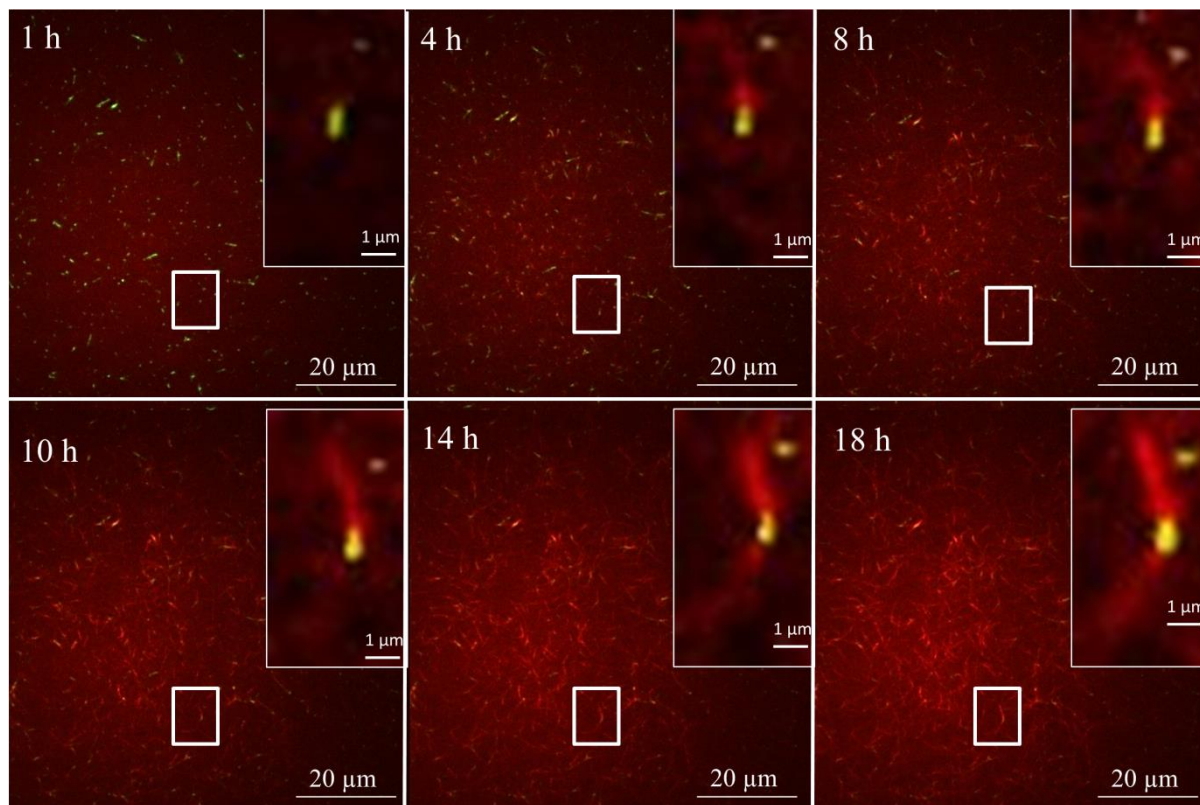


**Figure 6.2:**  $\alpha$ -syn aggregation on glass surface followed in real-time by TIRF microscopy. In the upper right corner of each image of a single fibril is shown. Sample was prepared in the presence of seeds in the microscopy chamber on a bare glass surface. 95% WT + 5% A140C-ATTO 655  $\alpha$ -syn was mixed with 0.02 nM A140C-Alexa 488  $\alpha$ -syn seeds in 6 mM sodium phosphate buffer at pH 7.2 with 150 mM NaCl, 0.1 mM EDTA, 1 mM DTT. Time points in hours are denoted in the upper left corner of each frame. TIRF image size: 82  $\mu\text{m}$  x 82  $\mu\text{m}$ .

In addition to these long fibrils, we observed much brighter and complex features at the later stages of aggregation on a glass surface (Figure 6.3). Although sparsely distributed, these larger aggregates were always present. Usually, after 18 h of aging they still continued to grow, and after 48 h they reached a diameter of up to 45  $\mu\text{m}$  and a height of almost 20  $\mu\text{m}$ . Upon closer inspection, these features correspond to extended three-dimensional (3D) aggregated structures of relatively densely packed  $\alpha$ -syn molecules.

These 3D aggregated structures had a well-defined fibrillar network of radially protruding fibrils that were aligned within the TIRF image plane (Figure 6.4A). This alignment suggests that this network of fibrils is adsorbed to the glass surface, and functions as an anchor for the extended aggregated structure. The 3D-structure, obtained by imaging in confocal mode at

the final stage of the experiment, is shown in Figure 6.4B, and seems to extend upward from the center of the fibrillar network on the glass surface. The part of the structure that extends into the solution is not very well resolved, unlike the fibrillar network that is adsorbed on the surface. This lack of resolution is in large part due to the limited resolution of confocal imaging in the longitudinal direction of the 3D-image. Moreover, the solution part of the structure is presumably somewhat flexible and may not be stationary during the image scan.

To further characterize the properties of the aggregates, we added the thioflavin T (ThT) reporter dye to the solution at the end of the aggregation experiment. ThT binds to cross- $\beta$  structures and then shows enhanced fluorescence [36]. It is a widely used assay to verify the presence of amyloids. We indeed found that the large structure, as well as the fibrillar networks on the surface are ThT positive, proving their amyloid character. These results suggest that the extended structure is also largely composed of fibrillar components. It is not clear what drives the formation of this large structure. We surmised that it was promoted by binding of the protein to the glass surface. Possibly, the affinity of  $\alpha$ -syn for a negatively charged surface, like that of the glass slide, plays a key role. For this reason we modified the glass surface in several ways and examined its effect on the growth of surface adsorbed aggregates.

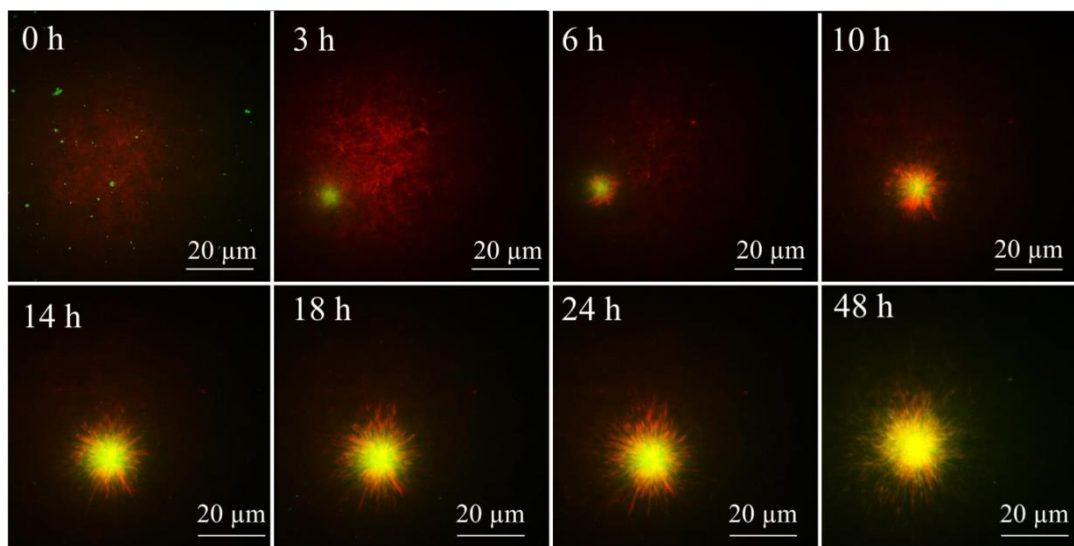


**Figure 6.3:**  $\alpha$ -syn aggregation followed in real-time by TIRF microscopy. The aggregate reaches a diameter of approximately 45  $\mu\text{m}$  after 48 h. Sample was prepared in the presence of seeds in the microscopy chamber on a bare glass surface. 95% WT + 5% A140C-ATTO 655  $\alpha$ -syn was mixed with 0.02 nM A140C-Alexa 488  $\alpha$ -syn seeds in 6 mM sodium phosphate buffer at pH 7.2 with 150 mM NaCl, 0.1 mM EDTA, 1 mM DTT, 48 h. Time points in hours are denoted in the upper left corner of each frame. TIRF image size: 82  $\mu\text{m}$  x 82  $\mu\text{m}$ .

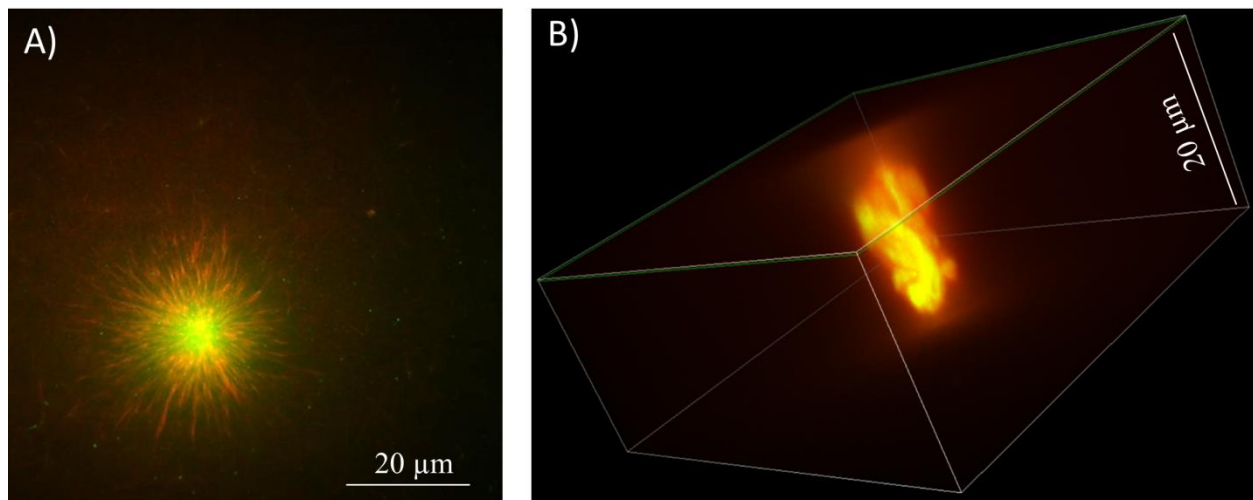


Figure 6.4: Aggregate after 24 h imaged by TIRF microscopy (A), where image size is 82  $\mu\text{m}$  x 82  $\mu\text{m}$ ; (B) 3D image of the aggregate, height: 89.2  $\mu\text{m}$ ; width: 89.2  $\mu\text{m}$ ; height: 20  $\mu\text{m}$ . Sample was prepared in the presence of seeds in the microscopy chamber on a bare glass surface. 95% WT + 5% A140C-ATTO 655  $\alpha$ -syn was mixed with 0.02 nM A140C-Alexa 488  $\alpha$ -syn seeds in 6 mM sodium phosphate buffer at pH 7.2 with 150 mM NaCl, 0.1 mM EDTA, 1 mM DTT. Please note that the  $\alpha$ -syn seeds (in green) are not only attached to the surface, but contribute in 3D growth with monomer (in red), as observed by the yellow color in the 2-color overlay.

### 6.3.1. Silanized glass surface

A monolayer of N-(2-aminoethyl)-3-aminopropyl-trimethoxysilan was used to "silanize" the glass surface [31]. The trimethoxysilane covalently binds to the glass by reaction with the hydroxyl groups at the surface, leaving the amine groups exposed to the solution. The surface is therefore more positively charged than that of bare glass, although it still remains hydrophilic with a significant hydrogen bonding capacity. We then performed the same experiment as above, by exposing the surface to a solution of Alexa 488-labeled  $\alpha$ -syn seeds and ATTO 655 (partially) labeled  $\alpha$ -syn monomers. After the seeds settled on the surface we observed essentially the same aggregation process as on bare glass. In the time frame of the experiment, 18 h, long fibrils as well as large structures up to 40  $\mu\text{m}$  in diameter were formed. The average length of the long fibrils was essentially the same as the ones that formed on bare glass. Apparently the morphology of the fibrils and of the larger aggregates was not affected by the amine-functionalized trimethoxysilane-monolayer.

### 6.3.2. Supported zwitterionic lipid bilayer surface

Another condition of the glass surface charge can be achieved by covering it with a supported zwitterionic lipid bilayer (SLB). For this purpose we used POPC. The glass surface is incubated with a solution of small unilamellar POPC vesicles which then rupture and spread as a bilayer on the surface. The zwitterionic character of POPC implies that the surface charge is approximately neutral. Small defects in the SLB may act as nucleation points [37],



so it was important to verify that the surface was defect-free. We checked the SLB by adding a free dye, ATTO 647 NHS, to the solution, which is then incorporated in the SLB. TIRF images of the SLB, after flushing with buffer solution, showed a rather homogeneous intensity distribution of ATTO 647 NHS fluorescence, but some defects appear to be present (Figure 6.1). After applying a sample of  $\alpha$ -syn seeds to the POPC-functionalized surface only growth of these seeds was observed, and only in the form of isolated fibrils. Fibrils were on average 3.2  $\mu\text{m}$  long and their calculated average elongation rate was  $1.34 \pm 0.54 \text{ mM}^{-1}\text{s}^{-1}$ , essentially the same as on bare and on silanized glass. The surface coverage with fibrils was, however, much lower on the zwitterionic SLB (Figure 6.5), which can be explained by the lower affinity of the  $\alpha$ -syn to a neutral surface. Most importantly, the larger 3D aggregated structures were notably absent. Apparently, the  $\alpha$ -syn seeds have a low affinity for this surface. In contrast, monomeric  $\alpha$ -syn molecules do adsorb to the SLB surface as shown in the image in Figure 6.5 by the red, diffuse fluorescence. These adsorbed  $\alpha$ -syn monomers appear to be less prone to aggregation when adsorbed to POPC.

### 6.3.3. Effect of salt concentration

Solution conditions may have a significant effect as well on  $\alpha$ -syn aggregation morphology as on the kinetics of aggregate formation [38]. For example, the morphology of  $\alpha$ -syn aggregates is more heterogeneous in buffer solutions at higher salt concentration [38]. It was investigated [38] if such an effect plays a role in the formation of the large 3D aggregated structures that we observed here. Therefore, we compared the aggregation properties of  $\alpha$ -syn on the glass surface at NaCl concentrations of 0, 25, 150 and 500 mM, to evaluate their effect on the morphology of aggregates. For all probed NaCl concentrations we observed the formation of  $\alpha$ -syn fibrils on the glass surface, as well as the large structures that extended upward from the surface. The average length of the fibrils and the dimensions of the larger 3D aggregates were comparable between the samples prepared in different NaCl concentrations. From our findings we conclude that these distinct aggregate morphologies were not directly influenced by the salt concentration.



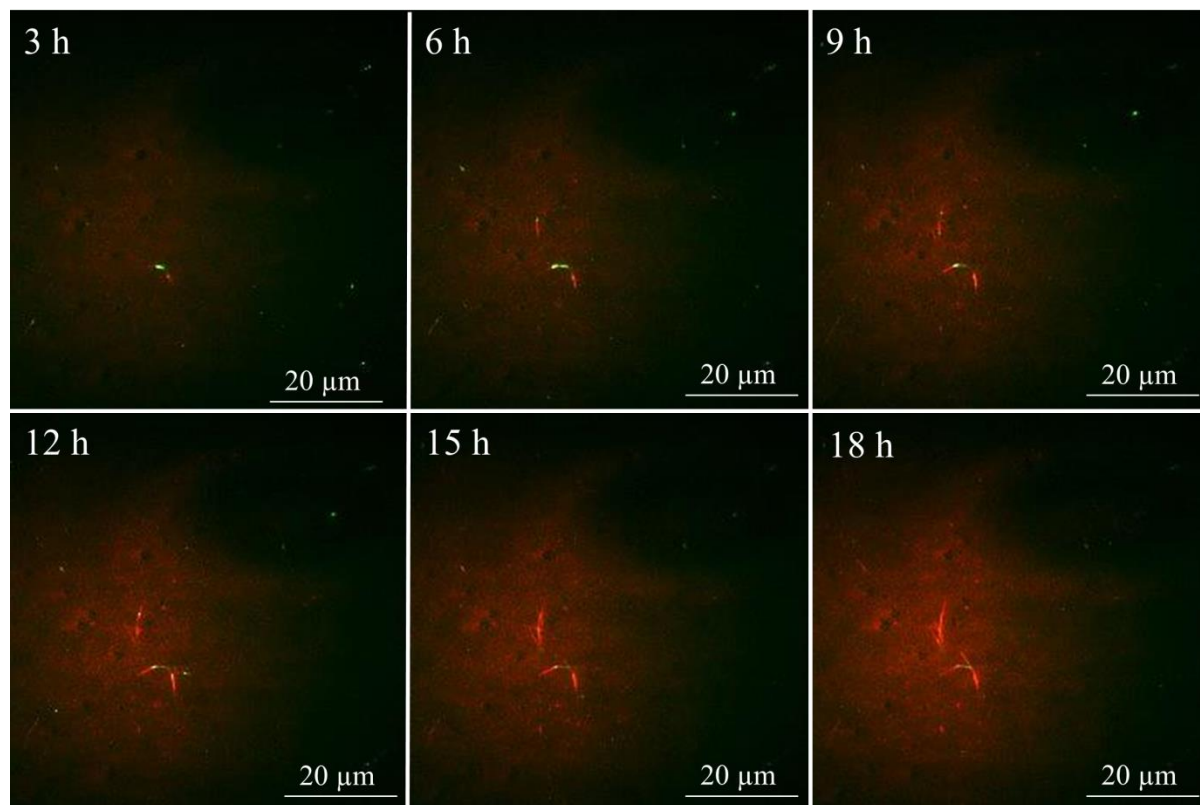


**Figure 6.5:**  $\alpha$ -syn aggregation on supported lipid bilayer (SLB) followed in real-time by TIRF microscopy. Sample was prepared in the presence of seeds in the microscopy chamber on the 100% POPC covered glass surface. 95% WT + 5% A140C-ATTO 655  $\alpha$ -syn was mixed with 0.02 nM A140C-Alexa 488 seeds in 6 mM sodium phosphate buffer at pH 7.2 with 150 mM NaCl, 0.1 mM EDTA, 1 mM DTT. Time points in hours are denoted in the upper left corner of each frame. TIRF image size: 82  $\mu\text{m}$  x 82  $\mu\text{m}$ .

#### 6.3.4. Aggregation in solution

A next consideration is the question of whether these large 3D aggregates are surface specific, or if they also are found in solution. This question was addressed by examining seeded aggregation in solution. A solution sample of  $\alpha$ -syn was prepared as previously described in section 6.2. Briefly, seeds of 5% Alexa 488 labeled  $\alpha$ -syn were mixed with a solution of monomeric  $\alpha$ -syn consisting of a mixture of 95% WT and 5% A140C-ATTO 655  $\alpha$ -syn. This sample was then incubated in a test tube under quiescent conditions. After 18 h of incubation, 180  $\mu\text{L}$  of the sample was deposited on a microscope cover slip, after which the aggregates that adsorbed on the surface were imaged by two-color TIRF. Micrometer long fibrils were observed and their average length was similar to the fibrils originating from seeded aggregation on the glass surface, 3.3  $\mu\text{m}$  on average, although no 3D aggregated structures were observed (Figure 6.6). The average elongation rate in solution was  $1.41 \pm 0.78 \text{ mM}^{-1}\text{s}^{-1}$ . Thus, our results show that the surface properties play a significant role in the

$\alpha$ -syn aggregate whereas average elongation rates among samples grown on different surfaces were similar.

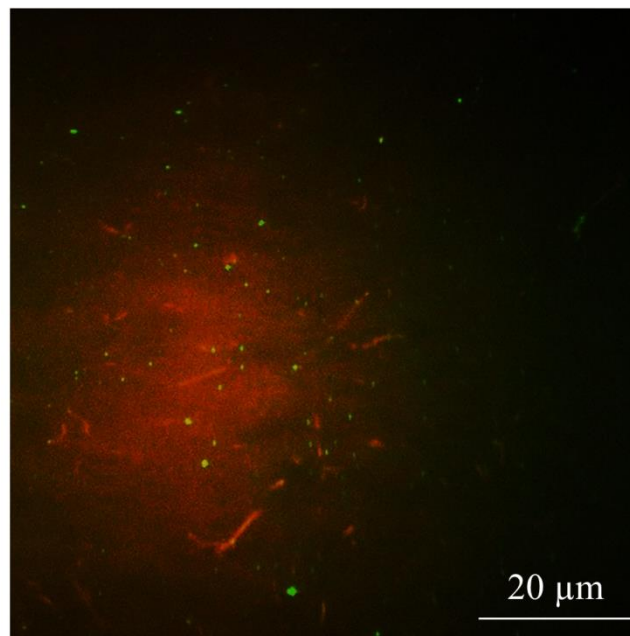


**Figure 6.6:** Results of the end stage of seeded  $\alpha$ -syn aggregation in a test tube. Representative TIRF image of  $\alpha$ -syn fibrils formed after 18 h in the presence of seeds in the test tube. 95% WT + 5% A140C-ATTO 655  $\alpha$ -syn was mixed with 0.02 nM A140C-Alexa 488  $\alpha$ -syn seeds in 6 mM sodium phosphate buffer at pH 7.2 with 150 mM NaCl, 0.1 mM EDTA, 1 mM DTT. TIRF image size: 82  $\mu$ m x 82  $\mu$ m.

#### 6.4. Discussion

In this study, we employed real-time TIRF microscopy to explore the morphology of  $\alpha$ -syn aggregates formed under various conditions. The aggregation of  $\alpha$ -syn primarily leads to the formation of long fibrils of variable length, and with a well-defined diameter, which suggests that the  $\alpha$ -syn molecules are packed in a specific conformation [39]. These fibrils are well characterized, and contain the typical amyloid cross- $\beta$  structure that stabilizes the rod-like conformation [40].

In particular, the elongation of  $\alpha$ -syn seeds on a glass surface in the presence of  $\alpha$ -syn monomers resulted in predominantly micrometer-long, fibrillar structures. Both, the seeds and the fibrils appeared to be immobile on the surface. In addition, we observed large aggregated structures, which protruded from the glass surface into solution (Figure 6.3). These aggregates appeared to be anchored on the surface by a network of fibrils (Figure 6.4A) absorbed on the surface, in direct contact with the glass. This network reached a diameter of tens of microns. The extended aggregated structure was protruding in the z-direction, away from the surface. 3D imaging of the structures revealed that they were up to

20  $\mu\text{m}$  in height (Figure 6.4B). The large structure kept the same position for the duration of the experiment, indicating a stable connection between the large aggregate and the fibrillar network. The formation of the large structure was observed already after 3 h. Occasionally more than one large structure was present on the glass surface in the frame of view.

These large aggregated structures appeared to be absent when the experiment was performed on a zwitterionic SLB and in solution. In those cases only fibril formation was observed. It has been shown that already formed  $\alpha$ -syn fibril added to solution have the ability to move on the 100% POPC SLB [41], that was not observed when fibrils were formed on 100% POPC SLB. A distinct difference between the glass surface and the zwitterionic SLB is the charge of the former [42] versus the neutral character of the latter. Presumably the charge contributes to the facile adsorption of  $\alpha$ -syn seeds on the glass surface, whereas it appears that the affinity for the neutral surface of the POPC SLB is significantly reduced. The elongation was uninhibited by the adsorption to the glass surface since the average lengths of the fibrils formed on glass surface, SLB and in solution were comparable, as well as their average elongation rate. We surmise that the formation of the large structures is specific for the interaction of  $\alpha$ -syn with a charged surface.

This conjecture is corroborated by a recent report by Rabe et al. [43] describing two different morphologies of  $\alpha$ -syn aggregates on glass surfaces and on cell membrane mimicking SLBs. These aggregates formed from monomers in solution at low ( $\sim 1$  nM) concentration and were imaged by three-dimensional supercritical angle fluorescence (3D-SAF) microscopy [44,45]. The first type of aggregate (type 1) was restricted to growth in the surface plane, while the second type (type 2) showed an extended structure that was tethered to the surface and protruded into the solution [43]. Apparently the two types of aggregate did not interconvert over time. Importantly, the aggregation events reported by Rabe et al. [43] specifically occurred on hydrophilic, negatively charged surfaces.

Although the present results are obtained by seeded aggregation, they concur with the results by Rabe et al. [43]. The growth of aggregates in the surface plane is presumably dominated by fibril formation. In particular, the growth of fibrils by elongation was not impeded by adsorption to a negatively charged surface. The larger aggregates observed in the present work are likely to be similar to the type 2 aggregates described by Rabe et al. [43]. Our results show in real time that fibrils elongate radially, at least in the surface plane, from the center of the observed structure. It suggests that the large aggregated structure increased in

size by monomer binding to the ends of existing fibrils that emanate from a central core. Indeed, the fact that the large structure is ThT positive confirms that they largely consist of  $\alpha$ -syn fibrils. The dimensions of the large structure grew at a similar rate as that of fibril elongation and could be clearly distinguished already after 3 h (Figure 6.3). Due to the limitation of the confocal method used for 3D imaging, it was not possible to resolve the morphology of the large structure with the same level of detail as was achieved by TIRF imaging of the part that was in contact with the surface.

It has been shown previously that upon binding to SLB,  $\alpha$ -syn monomer adopts an  $\alpha$ -helical conformation [46–49]. Presumably, this conformation is less prone to aggregation on the 100% POPC made SLB surface, although the experiments by Rabe et al. [43] show that aggregates are readily formed on negatively charged surfaces even at low  $\alpha$ -syn concentration. In particular, we show that once seeds are formed, their interaction with charged surfaces appears to promote the formation of large, three-dimensional aggregates.

The large amyloid structures are often observed *in vivo* [50] and linked to a variety of neurodegenerative disorders. For example, similar morphologies have been observed in the images of amyloid deposits in brain plaques of the Alzheimer's disease patients [51]. It raises the question about the role of membrane surfaces in the formation of these amyloid deposits. The results presented here show that, at least *in vitro*, large aggregates can form in a relatively short time compared to that of the development of the disease. Why do the large structures not form in all individuals? A question like this leads to speculation about a cellular mechanism that prohibits amyloid aggregate formation, but more experiments are needed to substantiate such a conjecture.

So far the presence of larger  $\alpha$ -syn aggregated structures has been connected to a pH value that is close to the isoelectric point of  $\alpha$ -syn at 4.6, and to higher salt concentrations [52,53]. Hoyer and coworkers [52] had imaged the final stage of the  $\alpha$ -syn aggregation process, where the larger  $\alpha$ -syn aggregated structure has already been formed. The morphological information they acquired was limited because of the techniques they used [52]. We have observed the formation of the large  $\alpha$ -syn aggregated structure in real-time under pH close to physiological. The formation of higher-ordered  $\alpha$ -syn structures at neutral pH was highlighted in a recent paper by Buell and coworkers [38]. Structural details of the observed higher-ordered  $\alpha$ -syn structures were lacking, however, due to the limited imaging resolution.

Buell and coworkers pointed out that the assembly of higher ordered structures might be important in the context of the spreading of aggregates to neighboring cells in PD [54].

Here, we showed that the aggregate morphology is related to the substrate-surface properties. It has been already reported that the aggregation of membrane-bound  $\alpha$ -syn plays a key role in the protein's neurotoxicity in PD [55], yet the real-time information on aggregate formation *in vivo* is still missing. Application of the same method we used might be helpful to understand the aggregation process *in vivo* and its relation to membranes.

## 6.5. Conclusion

The application of real-time two-color TIRF has been demonstrated to be a powerful tool for the visualization of  $\alpha$ -syn fibril growth from seeds. The growth of  $\alpha$ -syn was followed on a zwitterionic SLB, on a hydrophilic, negatively charged and positively charged glass coverslip, and in solution, using real-time total internal reflection microscopy. Our results show a different morphology of aggregates depending on the kind of surface used for the experiments. The formation of extended three-dimensional, aggregated structures composed of micrometer-long  $\alpha$ -syn fibrils on charged glass surfaces in real time, but on SLB and in solution we observed only the growth of linear amyloid fibrils. These findings strongly suggest a significant effect of surface properties on the growth and morphology of  $\alpha$ -syn aggregates.

## Acknowledgements

We thank Ms. N. Schilderink from University of Twente for  $\alpha$ -synuclein expression and purification and MSc. B. Pradhan from Leiden University for the assistance in supporting lipid bilayer preparation. This work was performed in the framework of research program ‘‘A Single Molecule View on Protein Aggregation’’, supported by the Foundation for Fundamental Research on Matter (FOM), which is part of the Netherlands Organization for Scientific Research (NWO).

## 6.6. References

- [1] M. Goedert, M.G. Spillantini, K. Del Tredici, H. Braak, 100 years of Lewy pathology, *Nat. Rev. Neurol.* 9 (2012) 13–24. doi:10.1038/nrneurol.2012.242.
- [2] D.G. Healy, M. Falchi, S.S. O’Sullivan, V. Bonifati, A. Durr, S. Bressman, A. Brice, J. Aasly, C.P. Zabetian, S. Goldwurm, J.J. Ferreira, E. Tolosa, D.M. Kay, C. Klein, D.R. Williams, C. Marras, A.E. Lang, Z.K. Wszolek, J. Berciano, A.H. Schapira, T. Lynch, K.P. Bhatia, T. Gasser, A.J. Lees, N.W. Wood, Phenotype, genotype, and worldwide genetic penetrance of LRRK2-associated Parkinson’s disease: a case-control study, *Lancet Neurol.* 7 (2008) 583–590. doi:10.1016/S1474-4422(08)70117-0.
- [3] D.J. Moore, A.B. West, V.L. Dawson, T.M. Dawson, Molecular pathophysiology of Parkinson’s disease., *Annu. Rev. Neurosci.* 28 (2005) 57–87. doi:10.1146/annurev.neuro.28.061604.135718.
- [4] M.H. Polymeropoulos, C. Lavedan, E. Leroy, S.E. Ide, A. Dehejia, A. Dutra, B. Pike, H. Root, J. Rubenstein, R. Boyer, E.S. Stenroos, S. Chandrasekharappa, A. Athanassiadou, T. Papapetropoulos, W.G. Johnson, A.M. Lazzarini, R.C. Duvoisin, G. Di Iorio, L.I. Golbe, R.L. Nussbaum, Mutation in the  $\alpha$ -Synuclein Gene Identified in Families with Parkinson’s Disease, *Science* (80-. ). 276 (1997) 2045–2047. doi:10.1126/science.276.5321.2045.
- [5] M.G. Spillantini, R.A. Crowther, R. Jakes, M. Hasegawa, M. Goedert,  $\alpha$ -Synuclein in filamentous inclusions of Lewy bodies from Parkinson’s disease and dementia with Lewy bodies, *Proc. Natl. Acad. Sci.* 95 (1998) 6469–6473. doi:10.1073/pnas.95.11.6469.
- [6] D.D. Murphy, S.M. Rueter, J.Q. Trojanowski, V.M. Lee, Synucleins are developmentally expressed, and alpha-synuclein regulates the size of the presynaptic vesicular pool in primary hippocampal neurons., *J. Neurosci.* 20 (2000) 3214–3220.
- [7] A. Sidhu, C. Wersinger, P. Vernier,  $\alpha$ -Synuclein regulation of the dopaminergic transporter: A possible role in the pathogenesis of Parkinson’s disease, *FEBS Lett.* 565 (2004) 1–5. doi:10.1016/j.febslet.2004.03.063.
- [8] G. Fusco, A. De Simone, T. Gopinath, V. Vostrikov, M. Vendruscolo, C.M. Dobson, G. Veglia, Direct observation of the three regions in  $\alpha$ -synuclein that determine its membrane-bound behaviour., *Nat. Commun.* 5 (2014) 3827. doi:10.1038/ncomms4827.
- [9] V.V. Shvadchak, D.A. Yushchenko, R. Pievo, T.M. Jovin, The mode of  $\alpha$ -synuclein binding to membranes depends on lipid composition and lipid to protein ratio, *FEBS Lett.* 585 (2011) 3513–3519. doi:10.1016/j.febslet.2011.10.006.
- [10] A.J. Baldwin, T.P.J. Knowles, G.G. Tartaglia, A.W. Fitzpatrick, G.L. Devlin, S.L. Shammass, C.A. Waudby, M.F. Mossuto, S. Meehan, S.L. Gras, J. Christodoulou, S.J. Anthony-cahill, P.D. Barker, M. Vendruscolo, C.M. Dobson, Metastability of native proteins and the phenomenon of amyloid formation.pdf, (2011) 14160–14163.
- [11] A.T. Sabareesan, J.B. Udgaonkar, Amyloid fibril formation by the chain B subunit of monellin occurs by a nucleation-dependent polymerization mechanism., *Biochemistry.* 53 (2014) 1206–17. doi:10.1021/bi401467p.
- [12] V.V. Shvadchak, M.M.A.E. Claessens, V. Subramaniam, Fibril Breaking Accelerates  $\alpha$ -Synuclein Fibrillization, *J. Phys. Chem. B.* 119 (2015) 1912–1918. doi:10.1021/jp5111604.

- [13] S.R. Collins, A. Douglass, R.D. Vale, J.S. Weissman, Mechanism of prion propagation: Amyloid growth occurs by monomer addition, *PLoS Biol.* 2 (2004) doi:10.1371/journal.pbio.0020321.
- [14] C. Galvagnion, A.K. Buell, G. Meisl, T.C.T. Michaels, M. Vendruscolo, T.P.J. Knowles, C.M. Dobson, Lipid vesicles trigger  $\alpha$ -synuclein aggregation by stimulating primary nucleation, *Nat. Chem. Biol.* 11 (2015) 229–234. doi:10.1038/nchembio.1750.
- [15] S.I.A. Cohen, S. Linse, L.M. Luheshi, E. Hellstrand, D.A. White, L. Rajah, D.E. Otzen, M. Vendruscolo, C.M. Dobson, T.P.J. Knowles, Proliferation of amyloid-42 aggregates occurs through a secondary nucleation mechanism, *Proc. Natl. Acad. Sci.* 110 (2013) 9758–9763. doi:10.1073/pnas.1218402110.
- [16] S.M. Butterfield, H.A. Lashuel, Amyloidogenic protein-membrane interactions: Mechanistic insight from model systems, *Angew. Chemie - Int. Ed.* 49 (2010) 5628–5654. doi:10.1002/anie.200906670.
- [17] N.B. Cole, D.D. Murphy, T. Grider, S. Rueter, D. Brasaemle, R.L. Nussbaum, Lipid Droplet Binding and Oligomerization Properties of the Parkinson's Disease Protein  $\alpha$ -Synuclein, *J. Biol. Chem.* 277 (2002) 6344–6352. doi:10.1074/jbc.M108414200.
- [18] H.A. Lashuel, B.M. Petre, J. Wall, M. Simon, R.J. Nowak, T. Walz, P.T. Lansbury,  $\alpha$ -Synuclein, Especially the Parkinson's Disease-Associated Mutants, Forms Pore-Like Annular and Tubular Protofibrils, *J. Mol. Biol.* 322 (2002) 1089–1102. doi:10.1016/S0022-2836(02)00735-0.
- [19] T. Ban, Y. Goto, Direct Observation of Amyloid Growth Monitored by Total Internal Reflection Fluorescence Microscopy, *Methods Enzymol.* 413 (2006) 91–102. doi:10.1016/S0076-6879(06)13005-0.
- [20] C.B. Andersen, H. Yagi, M. Manno, V. Martorana, T. Ban, G. Christiansen, D.E. Otzen, Y. Goto, C. Rischel, Branching in amyloid fibril growth, *Biophys. J.* 96 (2009) 1529–1536. doi:10.1016/j.bpj.2008.11.024.
- [21] S.M. Patil, A. Mehta, S. Jha, A.T. Alexandrescu, Heterogeneous amylin fibril growth mechanisms imaged by total internal reflection fluorescence microscopy, *Biochemistry.* 50 (2011) 2808–2819. doi:10.1021/bi101908m.
- [22] H. Yagi, Y. Abe, N. Takayanagi, Y. Goto, Elongation of amyloid fibrils through lateral binding of monomers revealed by total internal reflection fluorescence microscopy, *Biochim. Biophys. Acta - Proteins Proteomics.* 1844 (2014) 1881–1888. doi:10.1016/j.bbapap.2014.06.014.
- [23] M.M. Wördehoff, O. Bannach, H. Shaykhalishahi, A. Kulawik, S. Schiefer, D. Willbold, W. Hoyer, E. Birkmann, Single Fibril Growth Kinetics of  $\alpha$ -Synuclein, *J. Mol. Biol.* 427 (2015) 1428–1435. doi:10.1016/j.jmb.2015.01.020.
- [24] S. Nath, J. Meunier, J. Hendrix, S.A. Carl, Y. Engelborghs, Early aggregation steps in  $\alpha$ -synuclein as measured by FCS and FRET: Evidence for a contagious conformational change, *Biophys. J.* 98 (2010) 1302–1311. doi:10.1016/j.bpj.2009.12.4290.
- [25] L. Tosatto, M.H. Horrocks, A.J. Dear, T.P.J. Knowles, M. Dalla Serra, N. Cremades, C.M. Dobson, D. Klenerman, Single-molecule FRET studies on alpha-synuclein oligomerization of Parkinson's disease genetically related mutants, *Sci. Rep.* 5 (2015) 16696. doi:10.1038/srep16696.
- [26] D. Pinotsi, A.K. Buell, C. Galvagnion, C.M. Dobson, G.S. Kaminski Schierle, C.F. Kaminski, Direct observation of heterogeneous amyloid fibril growth kinetics via two-

- color super-resolution microscopy, *Nano Lett.* 14 (2014) 339–345.  
doi:10.1021/nl4041093.
- [27] S.L. Shammass, G.A. Garcia, S. Kumar, M. Kjaergaard, M.H. Horrocks, N. Shivji, E. Mandelkow, T.P.J. Knowles, E. Mandelkow, D. Klenerman, A mechanistic model of tau amyloid aggregation based on direct observation of oligomers., *Nat. Commun.* 6 (2015) 7025. doi:10.1038/ncomms8025.
- [28] M. Mučibabić, M.M. Apetri, G.W. Canters, T.J. Aartsma, The effect of fluorescent labeling on  $\alpha$ -synuclein fibril morphology, *Biochim. Biophys. Acta - Proteins Proteomics.* (2016). doi:10.1016/j.bbapap.2016.07.007.
- [29] C.N. Pace, F. Vajdos, L. Fee, G. Grimsley, T. Gray, How to measure and predict the molar absorption coefficient of a protein., *Protein Sci.* 4 (1995) 2411–2423.  
doi:10.1002/pro.5560041120.
- [30] A.N.D. Stefanovic, M.T. Stöckl, M.M.A.E. Claessens, V. Subramaniam,  $\alpha$ -Synuclein oligomers distinctively permeabilize complex model membranes, *FEBS J.* 281 (2014) 2838–2850. doi:10.1111/febs.12824.
- [31] A. Gupta, T.J. Aartsma, G.W. Canters, One at a Time : Intramolecular Electron Transfer Kinetics in Small Laccase observed during Turnover, (2014).  
doi:10.1021/ja411078b.
- [32] B. Pradhan, S. Khatua, A. Gupta, T.J. Aartsma, G.W. Canters, M. Orrit, Gold-Nanorod-Enhanced FCS of Fluorophores with High Quantum Yield in Lipid Bilayers, *J. Phys. Chem. C.* (2016) acs.jpcc.6b07875. doi:10.1021/acs.jpcc.6b07875.
- [33] L.C. Serpell, J. Berriman, R. Jakes, M. Goedert, R.A. Crowther, Fiber diffraction of synthetic alpha-synuclein filaments shows amyloid-like cross-beta conformation., *Proc. Natl. Acad. Sci. U. S. A.* 97 (2000) 4897–4902. doi:10.1073/pnas.97.9.4897.
- [34] S.J. Wood, J. Wypych, S. Steavenson, J. Louis, M. Citron, A.L. Biere,  $\alpha$ -Synuclein Fibrillogenesis is Nucleation-dependent, *Biochemistry.* (1999) 19509–19512.
- [35] F. Chiti, C.M. Dobson, Protein misfolding, functional amyloid, and human disease., *Annu. Rev. Biochem.* 75 (2006) 333–366.  
doi:10.1146/annurev.biochem.75.101304.123901.
- [36] R. Khurana, C. Coleman, C. Ionescu-Zanetti, S.A. Carter, V. Krishna, R.K. Grover, R. Roy, S. Singh, Mechanism of thioflavin T binding to amyloid fibrils, *J. Struct. Biol.* 151 (2005) 229–238. doi:10.1016/j.jsb.2005.06.006.
- [37] A. Iyer, N.O. Petersen, M.M.A.E. Claessens, V. Subramaniam, Amyloids of alpha-synuclein affect the structure and dynamics of supported lipid bilayers, *Biophys. J.* 106 (2014) 2585–2594. doi:10.1016/j.bpj.2014.05.001.
- [38] A.K. Buell, C. Galvagnion, R. Gaspar, E. Sparr, M. Vendruscolo, T.P.J. Knowles, S. Linse, C.M. Dobson, Solution conditions determine the relative importance of nucleation and growth processes in  $\alpha$ -synuclein aggregation., *Proc. Natl. Acad. Sci. U. S. A.* 111 (2014) 7671–7676. doi:10.1073/pnas.1315346111.
- [39] M. Vilar, H.-T. Chou, T. Lührs, S.K. Maji, D. Riek-Loher, R. Verel, G. Manning, H. Stahlberg, R. Riek, The fold of  $\alpha$ -synuclein fibrils, *105* (2008) 8637–8642.  
doi:10.1073/pnas.0712179105.
- [40] T. Ha, Amyloid Fibrils: Formation, Polymorphism, and Inhibition, (2014).
- [41] K.I.M. Sweers, Nanoscale structural and mechanical properties of alpha-synuclein amyloid fibrils, 2012.



- [42] S.H. Behrens, D.G. Grier, The charge of glass and silica surfaces, *J. Chem. Phys.* 115 (2001) 6716–6721. doi:10.1063/1.1404988.
- [43] M. Rabe, A. Soragni, N.P. Reynolds, D. Verdes, E. Liverani, R. Riek, S. Seeger, On-surface aggregation of  $\alpha$ -synuclein at nanomolar concentrations results in two distinct growth mechanisms, *ACS Chem. Neurosci.* 4 (2013) 408–417. doi:10.1021/cn3001312.
- [44] T. Ruckstuhl, D. Verdes, Supercritical angle fluorescence (SAF) microscopy., *Opt. Express.* 12 (2004) 4246–4254. doi:10.1364/OPEX.12.004246.
- [45] Y. Ma, A. Benda, P.R. Nicovich, K. Gaus, Measuring membrane association and protein diffusion within membranes with supercritical angle fluorescence microscopy, *Biomed. Opt. Express.* 7 (2016) 1561. doi:10.1364/BOE.7.001561.
- [46] T.S. Ulmer, A. Bax, N.B. Cole, R.L. Nussbaum, Structure and Dynamics of Micelle-bound Human  $\alpha$ -Synuclein, *J. Biol. Chem.* 280 (2005) 9595–9603. doi:10.1074/jbc.M411805200.
- [47] M. Drescher, F. Godschalk, G. Veldhuis, B.D. van Rooijen, V. Subramaniam, M. Huber, Spin-label EPR on  $\alpha$ -synuclein reveals differences in the membrane binding affinity of the two antiparallel helices, *ChemBioChem.* 9 (2008) 2411–2416. doi:10.1002/cbic.200800238.
- [48] M. Drescher, G. Veldhuis, B.D. Van Rooijen, S. Milikisyants, V. Subramaniam, M. Huber, Antiparallel arrangement of the helices of vesicle-bound  $\alpha$ -synuclein, *J. Am. Chem. Soc.* 130 (2008) 7796–7797. doi:10.1021/ja801594s.
- [49] E.R. Georgieva, T.F. Ramlall, P.P. Borbat, J.H. Freed, D. Eliezer, Membrane-bound alpha-synuclein forms an extended helix: Long-distance pulsed ESR measurements using vesicles, bicelles, and rodlike micelles, *J. Am. Chem. Soc.* 130 (2008) 12856–12857. doi:10.1021/ja804517m.
- [50] H. Welander, S.V. Bontha, T. Näsström, M. Karlsson, F. Nikolajeff, K. Danzer, M. Kostka, H. Kalimo, L. Lannfelt, M. Ingelsson, J. Bergström, Gelsolin co-occurs with Lewy bodies in vivo and accelerates  $\alpha$ -synuclein aggregation in vitro, *Biochem. Biophys. Res. Commun.* 412 (2011) 32–38. doi:10.1016/j.bbrc.2011.07.027.
- [51] L.-W. Jin, K.A. Claborn, M. Kurimoto, M.A. Geday, I. Maezawa, F. Sohraby, M. Estrada, W. Kaminsky, B. Kahr, Imaging linear birefringence and dichroism in cerebral amyloid pathologies., *Proc. Natl. Acad. Sci. U. S. A.* 100 (2003) 15294–15298. doi:10.1073/pnas.2534647100.
- [52] W. Hoyer, T. Antony, D. Cherny, G. Heim, T.M. Jovin, V. Subramaniam, Dependence of  $\alpha$ -synuclein aggregate morphology on solution conditions, *J. Mol. Biol.* 322 (2002) 383–393. doi:10.1016/S0022-2836(02)00775-1.
- [53] M. Zhu, P.O. Souillac, C. Ionescu-Zanetti, S.A. Carter, A.L. Fink, Surface-catalyzed amyloid fibril formation, *J. Biol. Chem.* 277 (2002) 50914–50922. doi:10.1074/jbc.M207225200.
- [54] J.H. Kordower, Y. Chu, R.A. Hauser, T.B. Freeman, C.W. Olanow, Lewy body-like pathology in long-term embryonic nigral transplants in Parkinson’s disease., *Nat. Med.* 14 (2008) 504–506. doi:10.1038/nm1747.
- [55] D. Ysselstein, M. Joshi, V. Mishra, A.M. Griggs, J.M. Asiago, G.P. McCabe, L.A. Stanciu, C.B. Post, J.C. Rochet, Effects of impaired membrane interactions on  $\alpha$ -synuclein aggregation and neurotoxicity, *Neurobiol. Dis.* 79 (2015) 150–163.

doi:10.1016/j.nbd.2015.04.007.

## Summary & Prospects

Neurodegenerative diseases like Alzheimer's, Parkinson's (PD), Huntington's disease, and the prion disease are accompanied by the formation of protein aggregates in the brain. Recent insights point to an essential role for early stage aggregates (oligomers) of many amyloid-forming proteins in cell-death. Yet, the molecular architecture and plasticity of the early aggregates, the dynamics of initial protein aggregation, and the detailed mechanisms by which these aggregates cause cell damage remain a mystery. It has been suggested that some oligomeric species may disrupt or permeabilize cellular membranes by forming pores, analogous to the bacterial pore-forming toxins, leading to disruption of calcium regulation and cell-death. For these reasons the properties of amyloid-forming proteins and the underlying mechanisms of this process are subject of close research.

In this thesis we report on the intricacies of  $\alpha$ -synuclein ( $\alpha$ -syn) aggregation, a protein which is characteristic of PD. Modifications of the protein, including mutations, truncations, and phosphorylation, as well as interactions with metal ions and other cellular components modify the (free) energy landscape for aggregation. The intrinsically disordered nature of  $\alpha$ -syn gives rise to a remarkable conformational plasticity that appears to play a crucial role in the initial steps of aggregation, in the adoption of different structures, and in its interactions with membranes and other cellular components.

Aggregation of  $\alpha$ -syn is often monitored using the assay based on the fluorescence enhancement of Thioflavin T (ThT). This is a dye which specifically binds to  $\beta$ -sheet structures. A typical aggregation curve has a sigmoidal shape reflecting three stages: nucleation (lag phase), growth (exponential phase) and saturation (plateau phase). Initiation of aggregation occurs in the lag or nucleation phase, followed by the growth phase with an exponential increase of the ThT fluorescence by fibril elongation and secondary nucleation. In the saturation phase ThT fluorescence reaches a plateau, where most of the monomer pool has been depleted by incorporation into aggregates and the rate of the monomer addition to the fibril ends is equal to the dissociation rate. The time scale for primary nucleation of  $\alpha$ -syn aggregation is highly variable and this process is still not very well understood. Concerning

the overall mechanism of  $\alpha$ -syn aggregation, the rate-limiting steps, the role and nature of intermediates still remain not well elucidated. The lag phase that represents the primary nucleation can be largely eliminated by using preformed fibrils (seeds) which provides a convenient way to focus specifically on the elongation reaction of  $\alpha$ -syn fibrils.

In addition to the ThT assay we have employed fluorescence labeling techniques to study  $\alpha$ -syn aggregation. Fluorescent labeling of biomolecules facilitates detailed detection of numerous features of their role and function *in vitro* and *in vivo* with high sensitivity. In principle, fluorescent labeling of  $\alpha$ -syn could be a very effective tool not only for the observation of the very onset of the aggregation *in vitro*, *e.g.*, by single-molecule techniques, but also to follow the role of the aggregation process in live cells. This approach requires suitable labeling of the protein, which was achieved by replacing one of the residues of  $\alpha$ -syn with a cysteine so that maleimide-functionalized dyes could be used for labeling. Whether the functionality and intrinsic properties of  $\alpha$ -syn after attaching a fluorescent probe would be preserved used to be largely unknown. Specifically, the presence of the dye may affect the propensity of  $\alpha$ -syn for aggregation.

In **Chapter 2** we describe the effects of fluorescent probes on the  $\alpha$ -syn aggregate morphology which was studied by means of atomic force microscopy. We determined  $\alpha$ -syn fibril characteristics such as fibrillar height, length and twisting, where the fibrils were formed starting from a solution of monomeric  $\alpha$ -syn of which a quantified fraction was fluorescently labeled. The effect of various fluorophores was examined. Although the overall charge of the fluorophores we used and their chemical structure varied significantly, the morphology of  $\alpha$ -syn fibrils changed in a similar way in all cases. The increase in the fraction of labeled  $\alpha$ -syn in solution led to shortening of the fibrils as compared to those from WT-only  $\alpha$ -syn, whereas the height of the fibrils remained mainly unaffected. The observed decrease of the fibrillar length with the increase in the fraction of labeled protein was ascribed to a change of elongation kinetics, probably caused by a reduced affinity of  $\alpha$ -syn monomer to the fibril end. The twisted fibril morphology observed in the WT and A140C  $\alpha$ -syn mutant completely disappeared when the A140C  $\alpha$ -syn mutant was 100% fluorescently labeled.

The results obtained in this study clearly confirm that fluorescent dyes do exert a pronounced effect on the morphology of  $\alpha$ -syn aggregates. Labeling at the C-terminus – as performed in

this work – is probably least disruptive, but our results show that even this case imposes a significant limitation on the use of fluorescent labeling techniques in the study of  $\alpha$ -syn aggregation, both, *in vivo* and *in vitro*, by restrictions on the fraction of labeled  $\alpha$ -syn. This limitation may be prohibitive, for example, for the application of super resolution methods for fluorescence imaging of  $\alpha$ -syn aggregates since they require high labeling densities in order to reconstruct a high-resolution image.

It has been shown that soluble oligomeric species of  $\alpha$ -syn are the most potent toxic species in neuronal cells. Although a characterization of  $\alpha$ -syn monomers and fibrils has been investigated in detail, the nature of the species derived from monomer aggregation and the dynamics of their formation still remain mysterious. In **Chapter 3** we document the early events in  $\alpha$ -syn aggregation by gel electrophoresis and by fluorescence correlation spectroscopy (FCS). In particular, we observed the formation of stable dimers and tetramers of  $\alpha$ -syn by sensitive gel imaging based on fluorescence detection. The presence and the stoichiometry of these early species were confirmed by FCS and mass spectrometry. Moreover, we tracked the accumulation of these early oligomeric species in time which suggests their conversion to or incorporation into larger aggregates. The time profile of the formation of  $\alpha$ -syn dimer and tetramer species suggests a sequential process, certainly in case of WT. Apparently the dimer is a precursor for the formation of the tetramer. We further conclude from these time profiles that the dimers and tetramers we observe are incorporated in, or even initiate, the formation of larger oligomers and fibrils. If it is the dominant pathway, then dimer formation is certainly the critical rate-limiting step for fibril formation.

Detailed information about the kinetics of fibrillar growth from seeds as a function of pH and salt concentration, respectively, is still incomplete. For this reason we aimed to determine the effect of solution conditions on the growth of  $\alpha$ -syn fibrils by the use of a ThT fluorescence assay in **Chapter 4**. The effect of ionic strength and pH on  $\alpha$ -syn elongation kinetics was studied, and a detailed analysis presented in terms of a kinetic model. The elongation kinetics of preformed  $\alpha$ -syn fibrils as a function of pH and of salt concentration deviate significantly from their effect on the lag phase, suggesting that the mechanisms for  $\alpha$ -syn nucleation and fibril elongation are different. An explanation may be that the  $\alpha$ -syn fibrils are stabilized by a change of conformation of the constituent initial aggregate, *i.e.*, the fibrillar template is formed in a secondary step after nucleation. Such a conformational change may lead to a different reactivity for binding of  $\alpha$ -syn monomers to the fibril end compared to primary

nucleation. Alternatively, the  $\alpha$ -syn monomer addition to the fibril end involves a different molecular conformation than the one which promotes nucleation.

In **Chapter 5** we focused on the elongation of  $\alpha$ -syn fibrils from seeds using total internal reflection fluorescence microscopy. From the length distribution of fibrils and the average fibrillar length increase in time we concluded that the elongation of  $\alpha$ -syn fibrils proceeds in highly discontinuous pattern. This observation was corroborated by single fibril measurements that showed intermittent periods of halted elongation. Moreover, our results show that the increase of fibril length slowed down in time, despite the presence of monomeric  $\alpha$ -syn in the solution. Assuming that fibril elongation requires the addition of  $\alpha$ -syn in a more or less specific conformation to achieve continuous growth, it is concluded that the discontinuous elongation pattern probably results from monomer binding to fibril ends in a mismatched conformation for proper fibril elongation, blocking temporarily or even permanently further growth of the fibril. Fibrillar growth can continue if the mismatched  $\alpha$ -syn dissociates from the fibril or if it adopts the proper conformation for further elongation.

In **Chapter 6** we probed the influence of a substrate surface on  $\alpha$ -syn aggregation using real-time two-color total internal reflection fluorescence microscopy. Understanding the interaction of  $\alpha$ -syn with the surface is important to elucidate its possible functional or pathological role. Our results show different morphologies of aggregates depending on the kind of surface used for experiments. The formation of extended three-dimensional aggregated structures, composed of micrometer-long  $\alpha$ -syn fibrils in real time was observed on charged glass surfaces, but on supported lipid bilayers and in solution we observed only the growth of linear amyloid fibrils. It is remarkable that these structures can form on a time scale of hours, much shorter than is usually associated with the pathology of PD. These findings strongly suggest a significant effect of surface properties on the growth and morphology of  $\alpha$ -syn aggregates.

Based on our conclusions and the latest developments in the field, some prospects for future work are the following:

- The physiological relevance of isolated small-sized  $\alpha$ -syn species, including dimers and tetramers, for understanding the mechanism of PD is very high. In case they represent on-pathway species, further examination of mechanism of their cytotoxicity would be even more important.

- Aging has been confirmed to cause a change in the cell membrane composition, so it would be highly beneficial to study the possible effect of different ratios of relevant lipids in supported lipid bilayers on the mechanism of  $\alpha$ -syn aggregate formation. To this end real-time dual-color total internal fluorescence microscopy can be employed.
- One more important aspect in better understanding the intricacy of the aggregation process would be to study the aggregation of disease mutants on different substrate surfaces and to unravel if the individual processes of  $\alpha$ -syn aggregation and the aggregate morphology of different mutants are affected by substrate surface properties.
- Fibrils of  $\alpha$ -syn are highly ordered nanoscale assemblies, which combine relatively high stability with elasticity, self-assembly and even self-healing. That qualifies them for many bio- and nano-applications, so further studies of their stabilizing mechanisms would be important for understanding their pathological function and biomedical application, as well as possible application in material science.





# Samenvatting

---

Neurodegeneratieve ziekten zoals Alzheimer, Parkinson, Huntington, en de prion ziekten gaan gepaard met de aggregatie van amyloïde-vormende eiwitten wat leidt tot het afsterven van aangetaste neuronen in de hersenen. Recente inzichten wijzen op een belangrijke rol voor met name die aggregaten (oligomeren) welke worden gevormd in een vroeg stadium van oligomerisatie. Echter, de moleculaire architectuur en de plasticiteit van deze vroeg-gevormde aggregaten, de dynamiek van eiwitaggregatie in dit stadium, en de gedetailleerde mechanismen waardoor deze aggregaten celschade veroorzaken zijn tot dusver een mysterie. Verondersteld wordt dat dergelijke oligomeren leiden tot verstoring of tot permeabiliteit door porievorming (analoog aan bacteriële porievormende toxinen) van cellulaire membranen, wat leidt tot verstoring van calciumregulatie en celdood. Om deze redenen zijn de eigenschappen van amyloïde vormende eiwitten en de onderliggende mechanismen onderwerp van intensief onderzoek. In dit proefschrift wordt verslag gedaan van een onderzoek naar de vroege stadia van  $\alpha$ -synucleïne ( $\alpha$ -syn) aggregatie *in vitro*, het eiwit dat kenmerkend is voor de ziekte van Parkinson.

Aggregatie van  $\alpha$ -syn wordt veelal onderzocht door de fluorescentie intensiteit te meten van Thioflavine T (ThT) dat aan de eiwitoplossing wordt toegevoegd. Dit is een kleurstof die specifiek bindt aan eiwitstructuren die bestaan uit  $\beta$ -sheets, wat leidt tot een sterke fluorescentietoename van ThT. Een typische aggregatiecurve heeft een sigmoïdale vorm waarin drie fasen zijn te onderscheiden: nucleatie of kiemvorming (aanlooptijd), groei (exponentiële fase) en verzadiging (plateau fase). De fase waarin kiemvorming optreedt wordt gevolgd door de groeifase die gepaard gaat met een exponentiële toename van de fluorescentie van ThT doordat de lengte van de fibrillen toeneemt en door secundaire kiemvorming. In de verzadigde fase bereikt de ThT fluorescentie een plateau omdat een evenwicht wordt bereikt in de reactie van  $\alpha$ -syn monomeren met de uiteinden van de fibrillen. De tijdschaal voor de primaire nucleatie van  $\alpha$ -syn aggregatie is zeer variabel, en dit is een proces dat nog steeds niet goed wordt begrepen. Onze kennis van het mechanisme van  $\alpha$ -syn aggregatie, de snelheidsbeperkende stappen, en de rol en de aard van de tussenproducten is zeer onvolledig. De aanlooptijd, die geassocieerd is met primaire nucleatie, kan grotendeels worden geëlimineerd door vooraf gevormde fibrillen (zaden) aan de eiwitoplossing toe te

voegen. Dit biedt de mogelijkheid om specifiek de lengtetoeename van  $\alpha$ -syn fibrillen te meten in de loop van de tijd.

In dit project hebben we ons gericht op de vorming van  $\alpha$ -syn aggregaten in een vroeg stadium van het aggregatieproces. Modificaties van het eiwit, waaronder mutaties, inkorting, en fosforylatie, en interacties met metaalionen en andere cellulaire componenten beïnvloeden het (vrije) energielandschap van aggregatie.  $\alpha$ -Syn heeft in oplossing geen specifieke secundaire of tertiaire structuur, en deze structurele flexibiliteit speelt ongetwijfeld een cruciale rol bij de eerste stappen van aggregatie, en is bepalend voor de structuur van de gevormde oligomeren en de interactie met membranen en andere cellulaire componenten.

Naast de ThT fluorescentie bepaling hebben we ook gebruik gemaakt van fluorescente labeling technieken om  $\alpha$ -syn aggregatie bestuderen. Fluorescente labeling van biomoleculen maakt het vaak mogelijk om gedetailleerde waarnemingen te verrichten met hoge gevoeligheid van hun specifieke kenmerken en van hun rol en functie, zowel *in vitro* als *in vivo*. In principe kan fluorescente labeling van  $\alpha$ -syn een zeer effectieve methode zijn om niet alleen het begin van eiwit aggregatie te volgen *in vitro*, bijvoorbeeld door “single-molecule” technieken toe te passen, maar ook de rol en het effect van het aggregatieproces in levende cellen. Deze benadering vereist specifiek aanpassingen van het eiwit, onder andere door het vervangen van één van de residuen van  $\alpha$ -syn met cysteïne zodat maleïmide gefunctionaliseerde kleurstoffen kunnen worden gebruikt voor het labelen. Voorwaarde is dat de functionaliteit en de intrinsieke eigenschappen van  $\alpha$ -syn na labeling met een fluorescente probe niet worden aangetast. De binding met de kleurstof zou met name de vorming van  $\alpha$ -syn aggregaten kunnen beïnvloeden.

In **Hoofdstuk 2** worden de effecten beschreven van fluorescerende probes op de morfologie van  $\alpha$ -syn aggregaten zoals waargenomen door middel van atomaire krachtmicroscopie. De kenmerken van hoogte, lengte en draaiing rond de lengte-as van de  $\alpha$ -syn fibrillen werden gemeten als functie van de fractie van gelabeld eiwit in de oplossing van  $\alpha$ -syn monomeren waarmee het experiment aanving. De effecten die verschillende fluoroforen teweegbrachten werden met elkaar vergeleken. In alle gevallen was hun effect op de morfologie van de  $\alpha$ -syn fibrillen niet significant verschillend, alhoewel de lading van de fluoroforen en hun chemische structuur aanzienlijk variëerden. Een verhoging van de fractie van gelabeld  $\alpha$ -syn in oplossing leidde tot steeds kortere fibrillen in vergelijking met die welke werden gevormd

met alleen wild type (WT)  $\alpha$ -syn, terwijl de hoogte van de fibrillen onveranderd bleef. Dit effect wordt toegeschreven aan een verandering van de reactiviteit van de fibrillen, waarschijnlijk veroorzaakt door een verminderde affiniteit van gelabelde  $\alpha$ -syn monomeren voor binding aan het uiteinde van de  $\alpha$ -syn fibrillen. De draaiing van de fibrillen rond de lengte-as, zowel voor WT  $\alpha$ -syn als voor de A140C  $\alpha$ -syn mutant, werd niet waargenomen in het geval dat het eiwit voor 100% was gelabeld.

De in dit onderzoek verkregen resultaten bevestigen dat binding van fluorescente kleurstoffen een uitgesproken effect heeft op de morfologie van  $\alpha$  syn aggregaten. Labeling van de C-terminus - zoals hier uitgevoerd – is waarschijnlijk minimaal storend, maar onze resultaten laten zien dat zelfs in dit geval ernstig rekening moet worden gehouden met een beperkte toepasbaarheid van fluorescente labelingtechnieken in de studie van  $\alpha$ -syn aggregatie, zowel *in vivo* als *in vitro*. Alleen bij lage fracties van gelabeld  $\alpha$  syn is het effect daarvan op de morfologie van de aggregaten verwaarloosbaar. Deze beperking is onder andere relevant voor de toepassing van superresolutiemethoden voor fluorescentie microscopie van  $\alpha$  syn aggregaten vanwege de hoge label-dichtheden die nodig zijn om afbeeldingen met een hoge resolutie te kunnen reconstrueren.

Alhoewel  $\alpha$ -syn monomeren en uitgegroeide fibrillen in toenemend detail worden beschreven in de literatuur vormen de aard, de eigenschappen, en het ontstaan van oligomere tussenvormen nog steeds een mysterie. Het is bekend dat juist deze oplosbare, oligomere tussenvormen van  $\alpha$ -syn het meest toxisch zijn voor neuronale cellen. In **hoofdstuk 3** documenteren we de beginfase van  $\alpha$ -syn aggregatie met behulp van gel-elektroforese, massa-spectrometrie en fluorescentie correlatie spectroscopie (FCS). Hierbij ontdekten we de vorming van stabiele dimeren en tetrameren van  $\alpha$ -syn door gebruik te maken van hooggevoelige fluorescentie detectie van gelabelde  $\alpha$ -syn componenten in de gel. De aanwezigheid en de stoichiometrie van deze vroege multimeren werden bevestigd door FCS en massaspectrometrie (MS). Bovendien konden de vorming van deze multimeren en het concentratieverloop in de tijd worden gemeten. Het tijdsprofiel van dit verloop suggereert een sequentieel proces, zeker in het geval van WT, waarbij eerst de dimeren worden gevormd en daarna de tetrameren. Blijkbaar zijn de dimeren een precursor voor de vorming van de tetrameren. We concluderen verder uit deze tijdprofielen dat de dimeren en tetrameren worden opgenomen in - of zelfs leiden tot de vorming van - grotere oligomeren en fibrillen.

Als deze multimeren inderdaad precursors zijn in het dominante pad in de vorming van  $\alpha$ -syn fibrillen, dan is dimeervorming zeker de snelheidsbepalende stap in dit proces.

De informatie over de groeifase van  $\alpha$ -syn fibrillen in de literatuur is nog onvolledig, met name wat betreft het effect van de pH en de zoutconcentratie van de oplossing. In **Hoofdstuk 4** worden daarom resultaten beschreven van het effect van pH en ionsterkte op de groei en ontwikkeling van  $\alpha$ -syn fibrillen met behulp van de ThT fluorescentie assay. De reactiesnelheden werden geanalyseerd in termen van een kinetisch model. De snelheid van de lengtetoeename van voorgevormde  $\alpha$ -syn fibrillen werd gemeten als functie, respectievelijk, van de pH en de zoutconcentratie. De reactiesnelheden blijken aanzienlijk af te wijken van vergelijkbare metingen in de nucleatiefase, wat suggereert dat de mechanismen voor  $\alpha$ -syn nucleatie en de lengtetoeename van fibrillen verschillend zijn. Een verklaring kan zijn dat de  $\alpha$ -syn fibrillen worden gestabiliseerd door een verandering van de eiwitconformatie nadat het desbetreffende  $\alpha$ -syn molecuul zich heeft gehecht aan het uiteinde van de fibril, waarbij dit  $\alpha$ -syn molecuul zich aanpast aan de structurele mal van de fibril. Een dergelijke conformatieverandering kan leiden tot een andere reactiviteit voor binding van  $\alpha$ -syn monomeren aan het fibril uiteinde dan voor primaire nucleatie. Anders gezegd, de binding van een  $\alpha$ -syn monomeer aan het fibril uiteinde betreft een andere moleculaire conformatie dan die welke kiemvorming bevordert.

**Hoofdstuk 5** is gericht op het verloop van de lengtetoeename van voorgevormde  $\alpha$ -syn fibrillen, gemeten met behulp van totale interne reflectie fluorescentiemicroscopie. Uit de lengteverdeling van de fibrillen en de gemiddelde snelheid waarmee de lengte toeneemt in de tijd kan worden geconcludeerd dat dit proces een discontinu verloop kent. Deze waarneming werd bevestigd door metingen aan individuele fibrillen die afwisselende periodes lieten zien waarin de groei stopte. Bovendien tonen onze resultaten aan dat de toename van de gemiddelde lengte van de fibrillen vertraagde in de tijd, ondanks de aanwezigheid van voldoende  $\alpha$ -syn monomeren in de oplossing. Een redelijke aanname is dat de fibrillen in lengte toenemen door de binding van een  $\alpha$ -syn molecuul in een min of meer specifieke conformatie. Het discontinue verloop van dit proces betekent vermoedelijk dat  $\alpha$ -syn monomeren kunnen binden in een niet-passende conformatie, waardoor verdere groei tijdelijk of zelfs permanent wordt geblokkeerd. De mogelijkheid voor groei wordt hersteld als het niet-passende eiwit dissocieert of alsnog de juiste conformatie aanneemt.

In **hoofdstuk 6** wordt de invloed onderzocht van een substraatoppervlak op  $\alpha$ -syn aggregatie waarvan het tijdverloop werd gevolgd middels twee-kleuren totale interne reflectie fluorescentiemicroscopie (TIRF). De effecten van de interactie van  $\alpha$ -syn met het oppervlak op het aggregatieproces zijn belangrijk om een mogelijk functionele of pathologische rol te kunnen vaststellen. Onze resultaten tonen aan dat  $\alpha$ -syn aggregaten meerdere vormen kunnen aannemen, afhankelijk van het soort oppervlak. Op negatief geladen, glazen oppervlakken werd de vorming waargenomen op een tijdschaal van uren van grote, driedimensionale structuren, bestaande uit micrometer-lange  $\alpha$ -syn fibrillen. Op een oppervlak bestaande uit een lipide-dubbellaag en in oplossing zagen we alleen de groei van lineaire amyloïde fibrillen. Opmerkelijk is dat deze structuren zich kunnen vormen op een tijdschaal van uren, veel korter dan gewoonlijk wordt geassocieerd met de pathologie van de ziekte van Parkinson. Deze bevindingen suggereren een significant effect van oppervlakte-eigenschappen op de groei en morfologie van  $\alpha$ -syn aggregaten.

Op basis van onze conclusies en de laatste ontwikkelingen in het veld kunnen enkele vooruitzichten voor toekomstige onderzoek als volgt worden geschetst:

- De fysiologische relevantie van relatief kleine  $\alpha$ -syn oligomeren, waaronder dimeren en tetrameren, voor het begrijpen van het mechanisme van de ziekte van Parkinson is hoog. Het mechanisme van hun cytotoxiciteit is een belangrijk thema voor verder onderzoek.
- Veroudering gaat gepaard met een verandering in de samenstelling van celmembranen. Het is daarom van belang om de invloed te onderzoeken die de samenstelling van een lipide-dubbellaag heeft op de vorming van  $\alpha$ -syn aggregaten en het mechanisme daarvan. Twee-kleuren totale interne reflectie fluorescentiemicroscopie (TIRF) is hiervoor een geschikte methode.
- Een belangrijk aspect bij het beter begrijpen van de complexiteit van  $\alpha$ -syn aggregatie en de rol daarvan in de ontwikkeling van de ziekte van Parkinson is het onderzoek van  $\alpha$ -syn mutanten. Het is daarom zinvol om de aggregatie-eigenschappen van deze mutanten nader te bestuderen en de effecten die verschillende substraatoppervlakken daarop hebben.
- Fibrillen van  $\alpha$ -syn zijn sterk geordende nanostructuren die een relatief hoge stabiliteit combineren met elasticiteit, zelf-assemblage en zelf-reparatie. Daardoor ontstaan mogelijkheden voor toepassingen in de bio- en nanotechnologie. Verder onderzoek van stabiliserende factoren in de vorming van deze aggregaten is van belang, niet alleen voor het

begrijpen van hun pathologische functie en voor biomedische toepassingen, maar ook voor mogelijke toepassing in de materiaalwetenschap.

# Zaključak

---

Neurodegenerativne bolesti kao što su Alchajmerova, Parkinsonova (PB), Hantingtonova i prionska uključuju formiranje agregata proteina u mozgu. Nedavna istraživanja ukazuju na to da suštinsku ulogu u ćelijskoj smrti ima formiranje ranih agregata (oligomera) brojnih proteina sklonih formiranju amiloida. Ipak, molekulska građa i plastičnost ranih agregata, dinamika početnog agregiranja proteina i pojedinosti mehanizama po kojima ti agregati oštećuju ćelije, ostaju zagonetni. Neke vrste oligomera mogu da poremete ćelijske membrane ili ih učine propustljivim obrazovanjem pora, analognih bakterijskom formiranju toksičnih pora, što vodi prestanku regulisanja kalcijuma i ćelijskoj smrti. Zato su osobine proteina koji formiraju amiloide i osnovni mehanizmi tog procesa predmet opsežnih istraživanja. U ovoj disertaciji iznosimo svu složenost agregiranja  $\alpha$ -sinukleina ( $\alpha$ -sin).

Agregiranje  $\alpha$ -sin obično se posmatra primenom metode na bazi povećanja fluorescentnog signala tioflavina T (ThT), to jest boje koja se posebno vezuje za  $\beta$ -ploče (ravni) i tom prilikom fluorescira. Tipična kriva agregiranja ima sigmoidni oblik što pokazuje tri faze: nukleacija (lag faza), rast (eksponencijalna faza) i saturacija (plato faza). Iniciranje agregacije nastaje u fazi lag ili u fazi nukleacije, a prate je faza rasta sa eksponencijalnim porastom ThT fluorescencije izduživanjem fibrila i sekundarna nukleacija. U fazi saturacije ThT fluorescencija dostiže plato, gde se većina monomera inkorporira u agregate, a brzina inkorporiranja monomera na krajeve fibrila izjednačuje se sa brzinom njegove disocijacije. Vreme događanja primarne nukleacije  $\alpha$ -sin veoma varira i taj proces i dalje ostaje nerazjašnjen. Što se tiče čitavog mehanizma agregiranja  $\alpha$ -sin, vremenski ograničavajućih faza, uloga i priroda intermedijera i dalje ostaju nedovoljno rasvetljeni. Faza lag, koja predstavlja primarnu nukleaciju, mogla bi se umnogome eliminisati pomoću pripremljenih fibrila (semena), što omogućava fokusiranje posebno na izduživanje fibrila  $\alpha$ -sin.

U ovom projektu fokusirali smo se na formiranje ranih agregata  $\alpha$ -sin, karakterističnog za PB. Modifikacije proteina, uključujući mutacije, skraćivanje i fosforilaciju, kao i međureakcije sa jonima metala i drugih ćelijskih komponenti utiču na promenu (slobodne) energije za agregiranje.

Osim ThT metode, za proučavanje agregiranja  $\alpha$ -sin koristili smo i fluorescentno obeležavanje. Fluorescentno obeležavanje biomolekula olakšava detaljno utvrđivanje njihove uloge i funkcije *in vivo* i *in vitro* uz visoku osetljivost. U principu, fluorescentno obeležavanje  $\alpha$ -sin moglo bi biti veoma efektivno ne samo za opažanje samog početka agregiranja *in vitro*, npr. tehnikama za praćenje jednog molekula, već i za praćenje uloge procesa agregiranja u živim ćelijama. Ovaj pristup, međutim, zahteva odgovarajuće obeležavanje proteina, što smo postigli zamenom jedne od amino kiselina  $\alpha$ -sin cisteinom, tako da su mogle da se koriste maleimid-funkcionalizovane boje. To da li će funkcionalnost i prirodna svojstva  $\alpha$ -sin biti očuvani posle priključivanja fluorescentne probe bilo je nepoznato, posebno zbog toga što prisustvo boje može uticati na sklonost  $\alpha$ -sin agregiranju.

U Poglavlju 2 opisujemo uticaje fluorescentnih proba na morfologiju agregata  $\alpha$ -sin, koje smo proučavali primenom mikroskopije atomskih sila. Utvrdili smo karakteristike fibrila  $\alpha$ -sin kao što su visina, dužina, periodičnost, kada su se fibrili obrazovali počevši od monomera  $\alpha$ -sin od kojeg je fluorescentno obeležena kvantifikovana frakcija. Ispitali smo i uticaj različitih fluorofora. Iako je ukupno primenjeno naelektrisanje fluorofora znatno variralo, morfologija fibrila  $\alpha$ -sin slično se promenila u svim slučajevima. Porast frakcije obeleženog  $\alpha$ -sin u rastvoru doveo je do skraćivanja fibrila u poređenju sa WT  $\alpha$ -sin, dok je visina fibrila ostala uglavnom nepomenjena. Primećeno smanjivanje dužine fibrila sa povećanjem frakcije obeleženog proteina pripisali smo promeni kinetike produžavanja, verovatno izazvane afinitetom monomera  $\alpha$ -sin za krajevima fibrila. Uvijena morfologija fibrila koju smo zapazili kod WT i A140C mutanta  $\alpha$ -sin potpuno je nestala kada smo A140C mutant  $\alpha$ -sin 100% fluorescentno obeležili.

Rezultati koje smo dobili u ovoj studiji jasno potvrđuju da fluorescentne boje vrše veliki uticaj na morfologiju fibrila  $\alpha$ -sin. Obeležavanje na C-terminusu – kao što je urađeno u ovoj studiji – verovatno je najmanje disruptivno, međutim, naši rezultati pokazuju da čak i ovo znatno ograničava primenu tehnika fluorescentnog obeležavanja za istraživanje agregiranja  $\alpha$ -sin *in vitro* i *in vivo*, tako što ograničava frakciju obeleženog  $\alpha$ -sin. Ovo ograničenje moglo bi biti prohibitivno, na primer, za primenu metoda super rezolucije za fluorescentno snimanje agregata  $\alpha$ -sin, jer oni iziskuju visoke gustine obeležavanja da bi se rekonstruisala slika visoke rezolucije.

Pokazano je da su rastvorljive vrste oligomera  $\alpha$ -sin najtoksičnije u neuronima. Iako je karakterizacija monomera i fibrila  $\alpha$ -sin detaljno proučavana, priroda vrsta nastalih



agregiranjem monomera i dinamika njihovog formiranja još uvek ostaje zagonetna. U Poglavlju 3 dokumentujemo rane događaje u agregiranju  $\alpha$ -sin primenom gel elektroforeze i fluorescentne korelacione spektroskopije (FCS). Naročito, pomoću osetljivog snimanja gela koje se zasniva na fluorescentnoj detekciji, zapazili smo formiranje stabilnih dimera i tetramera  $\alpha$ -sin. Prisustvo i stehiometriju ovih ranih vrsta potvrdili smo pomoću FCS i masene spektrometrije. Osim toga, ušli smo u trag nagomilavanju ovih ranih vrsta oligomera s vremenom, što ukazuje na njihovu konverziju u, ili inkorporaciju u veće agregate. Vremenski profil formiranja dimera i tetramera  $\alpha$ -sin ukazuje na sekvencijalni proces, svakako u slučaju WT. Očigledno je da je dimer prekursor formiranja tetramera. Prema ovim vremenskim profilima, dalje zaključujemo da su dimeri i tetrameri inkorporirani u, ili čak iniciraju formiranje većih oligomera i fibrila. Ako je to dominantni put, onda je formiranje dimera svakako kritična vremenski-ograničavajuća faza formiranja fibrila.

Podaci o kinetici i rastu fibrila od semena u zavisnosti od pH i koncentracije soli još su nepotpuni. Stoga je naš cilj bio da utvrdimo uticaj uslova rastvora na rast fibrila  $\alpha$ -sin pomoću fluorescentne ThT metode (Poglavlje 4). Proučavali smo uticaj jonske jačine i pH na kinetiku izduživanja  $\alpha$ -sin, a detaljnu analizu prikazali smo kroz kinetički model. Kinetika preformiranih fibrila  $\alpha$ -sin u funkciji pH i koncentracije soli znatno odstupaju od njihovog uticaja na lag fazu, ukazujući da su mehanizmi nukleacije  $\alpha$ -sin i izduživanja fibrila različiti. To bi se moglo objasniti time što se fibrili  $\alpha$ -sin stabilizuju promenom konformacije konstituentnog početnog agregata, t.j. šablon fibrila formira se u fazi posle nukleacije. Ovakva promena konformacije može dovesti do različite reaktivnosti vezivanja monomera  $\alpha$ -sin za kraj fibrila u poređenju sa primarnom nukleacijom. Alternativno, vezivanje monomera  $\alpha$ -sin za kraj fibrila uključuje drugačiju konformaciju molekula od one koja podržava nukleaciju.

U Poglavlju 5 usmereni smo na izduživanje fibrila  $\alpha$ -sin od semena primenom interne refleksione fluorescentne mikroskopije. Na osnovu distribucije dužine fibrila i prosečnog rasta dužine tokom vremena zaključili smo da se izduživanje fibrila  $\alpha$ -sin nastavlja diskontinualno. Ovo zapažanje potvrdili smo merenjem na nivou jednog fibrila, što je pokazalo periode zastoja izduživanja. Osim toga, naši rezultati pokazuju da se povećanje dužine fibrila vremenom usporava, uprkos prisustvu monomera  $\alpha$ -sin u rastvoru. Ako pretpostavimo da izduživanje fibrila zahteva dodavanje  $\alpha$ -sin specifične konformacije za postizanje kontinualnog rasta, zaključuje se da je diskontinualno izduživanje verovatno rezultat vezivanja monomera pogrešne konformacije za krajeve fibrila za pravilno

izduživanje fibrila, što privremeno ili čak trajno blokira dalji rast fibrila. Rast fibrila može se nastaviti ako se  $\alpha$ -sin sa pogrešnom konformacijom odvoji od fibrila, ili ako poprimi pravilnu konformaciju za dalje izduživanje.

Poglavlje 6 govori o ispitivanju uticaja površine supstrata na agregiranje  $\alpha$ -sin primenom dvobojne totalne interne refleksione fluorescentne mikroskopije u realnom vremenu. Razumevanje interakcije  $\alpha$ -sin sa površinom veoma je značajno za rasvetljavanje moguće funkcionalne ili patološke uloge. Naši rezultati pokazuju različite morfologije agregata u zavisnosti od tipa površine uzete za istraživanje. Formiranje produženih trodimenzionalnih agregiranih struktura, sastavljenih od fibrila  $\alpha$ -sin mikrometarske dužine u realnom vremenu, primećeno je na naelektrisanj staklenoj površini, ali smo na podržanim lipidnim dvoslojevima i u rastvoru zapazili samo rast linearnih fibrila amiloida. Veoma je značajno što se te strukture mogu da formiraju tokom nekoliko sati, mnogo pre no što se misli u vezi sa patologijom PB. Ovi rezultati snažno ukazuju na važan uticaj karakteristika površine na rast i morfologiju agregata  $\alpha$ -sin.

Na osnovu naših zaključaka i najnovijih prodora u ovoj oblasti, dajemo predloge za dalje istraživanje:

- Fiziološki značaj izolovanih oligomera – dimera i tetramera – veoma je veliki za razumevanje mehanizama nastanka PB. U slučaju da su oni glavni, dalje istraživanje mehanizama njihove citotoksičnosti bilo bi još značajnije.
- Potvrđeno je da starenje izaziva promene sastava ćelijske membrane, te bi bilo veoma korisno proučavanje mogućih uticaja različitih odnosa važnih lipida kod podržanih dvoslojeva lipida na mehanizme formiranja agregata  $\alpha$ -sin. Za ovo istraživanje korisna je dvobojna totalna interna fluorescentna mikroskopija u realnom vremenu.
- Još jedan važan aspekt boljeg shvatanja složenosti procesa agregiranja bio bi proučavanje agregiranja mutanata bolesti na različitim površinama supstrata da bi se otkrilo da li su pojedinačni procesi agregiranja  $\alpha$ -sin i morfologija agregata različitih mutanata pod uticajem površine supstrata.
- Fibrili  $\alpha$ -sin su visokouređeni nanosistemi u kojima se kombinuju relativno visoka stabilnost i elastičnost, samoformiranje i, čak, samorepariranje. To ih kvalifikuje za mnoge biološke i nanoprime, tako da bi dalje proučavanje mehanizama njihovog

stabilizovanja bilo važno za shvatanje njihove patološke funkcije i biomedicinske primene, kao i moguće primene u nauci o materijalima.



# Curriculum Vitae

---

## **Marija Mučibabić**

July 7, 1983 Born in Kruševac, Serbia

1990-2002 Primary and Secondary education, Primary Musical School, Belgrade, Serbia

2002-2007 University of Belgrade, Faculty of Biology, Department of Molecular Biology and Physiology, Belgrade, Serbia

Diploma Thesis: Isolation of VP2 gene from *Canine Parvovirus*  
(Thesis supervisor: Prof. Dr. Marina Stamenković-Radak)

2008-2011 Analyst development program, Check Mark, The Netherlands

A 3-years career program with placements in the research and development departments of Schering-Plough, Solvay Pharmaceuticals and DSM Biotechnology Centre, in each case for a term of one year.

2011-2016 PhD researcher at Leiden University, Leiden Institute of Physics, Biophysics Department

Thesis: Intricacies of  $\alpha$ -synuclein aggregation  
(Thesis supervisors: Prof. Dr. Thijs J. Aartsma and Prof. Dr. Gerard W. Canters)

Results of the project have been presented at national and international conferences

Teaching assistant for Biology for Physicists and Natuurkunde B

Thesis supervisor of one master, two bachelor and two high school students

2016- Postdoctoral researcher at Umeå University, Department of Molecular Medicine, Umeå, Sweden (Supervisor: Prof. Dr. Helena Edlund)



# List of publications

---

1. **M. Mučibabić**, G. Canters, T. Aartsma, Parkinson's disease – the hardship at old age, *Vojnosanit Pregl* 2016; 73(4): 303–305.
2. **M. Mučibabić**, M.M. Apetri, G.W. Canters, T.J. Aartsma, The effect of fluorescent labeling on  $\alpha$ -synuclein fibril morphology, *Biochim. Biophys. Acta - Proteins Proteomics*. (2016). doi:10.1016/j.bbapap.2016.07.007.
3. **M. Mučibabić**, D. Donato, D. Heinrich, G.W. Canters, and T.J. Aartsma, Substrate surface affects  $\alpha$ -synuclein aggregate morphology, manuscript in preparation.
4. **M. Mučibabić**, D. Vliegthart, H. van den Elst, H. Overkleeft, G.W. Canters, and T.J. Aartsma, Early events in  $\alpha$ -synuclein aggregation, manuscript in preparation.





# Acknowledgements

---

Approaching the end of this exciting PhD journey, I would like to thank a number of remarkable people that made every single step of it memorable. Every one of them was very important in various stages along the way. Some of them shaped my professional side, while others helped me privately, but I would not have succeeded in completing this thesis without them!

First and foremost I want to express my gratitude to my supervisors, Professor Thijs Aartsma and Professor Gerard Canters for giving me an opportunity to join the project. Your dedicated supervision during the project and scientific freedom I got from you at the same time were very precious to me. I was very fortunate to learn from you! I would like to thank Dr. Mihaela Apetri for her patient guidance into the world of  $\alpha$ -synuclein and atomic force microscopy and her friendly support in- and outside of the project.

I am thankful to our collaborators, Professor Vinod Subramaniam and his group, for inspiring discussions on protein aggregation we had during the whole project and allowing me to use the equipment in their lab. Especially I would like to thank Dr. Volodymyr Shvadchak for the expertise in kinetics of  $\alpha$ -synuclein he shared with me, and MSc Leffert Lanssink for his always motivating discussions on the experimental results.  $\alpha$ -Synuclein was always available and ready for experiments, thanks to Ing. Nathalie Schilderink who generously responded to my requests for material again and again.

Collaboration with Professor Doris Heinrich and Dr. Dominique Donato was very fruitful and resulted in more insights into substrate-surface effects on  $\alpha$ -synuclein aggregation. Careful guidance into TIRF microscopy by Dr. Dominique Donato and her dedication helped us a lot during this collaboration.

Also, I would like to thank the students who did their projects with me, namely Sander van Lidth de Jeude, Viktoria Trautner, Hanneke Leegwater and especially to Dirk Vliegenhart for their dedication and curiosity in conducting scientific research.

Assistance by Yvonne Kerkhof for administrative support, the staff of the Fine-Mechanical Department and the Electronic Department in solving technical problems, and Dr. Federica Galli regarding AFM experiments, is gratefully acknowledged.

Dr. Nemanja Markešević and Dr. Saptaswa Sen, my dear friends and paranymphs, made every day in the lab extraordinary with friendly chats and support. MSc Biswajit Pradhan, my office mate and friend, was always there for constructive discussions, not only scientifically, but also philosophically. Next to them I would like to thank all members of the LION Section on Biological and Soft Matter Physics. Meetings and discussions within the FOM programme ‘‘A single molecule view on protein aggregation’’ were always very inspirational thanks to Professor Mireille Claessens, Dr. Martina Huber, Dr. Ioana Ilie, Dr. Aditya Iyer and MSc Pravin Kumar. In the future I sincerely hope to work again with all of you.

I am incredibly grateful to Ger and Manon van Meel together with Sven Hemmink from Check Mark who are responsible for my move to The Netherlands and the unforgettable experiences and memories I had during the ADP program.

My last words go to my dearest friends and family. I am fortunate to have exceptional people for friends and I am thankful to all of them for the great memories I will never forget. My sister, Ksenija, I am so proud and happy of having you in my life. I am sure you know with how many emotions I am writing this, while thinking of our childhood and all funny adventures we had.

Especially thankful I am to Manas Sahoo for his genuine love and incredible support. I am happy we are accomplishing one more milestone together and looking forward to new challenges we will embrace in life.

Finally, words can hardly express the gratitude to my mother Dragana and my father Spasoje, to whom this book is dedicated. Thank you for unconditional love, everlasting support and precious memories. You are my true heroes!

